ADA178464

REPORT DOCUMENTATION PAGE

1a. REPORT SECURITY CLASSIFICATION		1b. RESTRICTIVE MARKINGS
UNCLASSIFIED		N/A

2a. SECURITY CLASSIFICATION AUTHORITY	3. DISTRIBUTION / AVAILABILITY OF REPORT
N/A	Approved for public release; distribution unlimited.
2b. DECLASSIFICATION / DOWNGRADING SCHEDULE	
N/A	

4. PERFORMING ORGANIZATION REPORT NUMBER(S)	5. MONITORING ORGANIZATION REPORT NUMBER(S)
UTEC MD-86-054	RADC-TR-86-129

6a. NAME OF PERFORMING ORGANIZATION	6b. OFFICE SYMBOL (If applicable)	7a. NAME OF MONITORING ORGANIZATION
University of Utah		Rome Air Development Center (OCTP)

6c. ADDRESS (City, State, and ZIP Code)	7b. ADDRESS (City, State, and ZIP Code)
Department of Electrical Engineering Microwave Device & Physical Electronics Lab Salt Lake City UT 84112	Griffiss AFB NY 13441-5700

8a. NAME OF FUNDING / SPONSORING ORGANIZATION	8b. OFFICE SYMBOL (If applicable)	9. PROCUREMENT INSTRUMENT IDENTIFICATION NUMBER
AFOSR	NE	F30602-82-C-0161

8c. ADDRESS (City, State, and ZIP Code)	10. SOURCE OF FUNDING NUMBERS			
Bolling AFB Wash DC 20332	PROGRAM ELEMENT NO.	PROJECT NO.	TASK NO.	WORK UNIT ACCESSION NO.
	61102F	2305	J9	16

11. TITLE (Include Security Classification)

WAVEGUIDE JUNCTION ANALYSIS INVOLVING ASYMMETRICAL MODES

12. PERSONAL AUTHOR(S)

Cyrus N. Tau

13a. TYPE OF REPORT	13b. TIME COVERED	14. DATE OF REPORT (Year, Month, Day)	15. PAGE COUNT
Final	FROM Sep 82 TO Sep 85	September 1986	116

16. SUPPLEMENTARY NOTATION

Research accomplished in conjunction with Air Force Thermionics Engineering Research Program (AFTER)

17.	COSATI CODES		18. SUBJECT TERMS (Continue on reverse if necessary and identify by block number)
FIELD	GROUP	SUB-GROUP	Modal Expansions Waveguide Design
09	03		Abrupt Junctions Numerical Solutions

19. ABSTRACT (Continue on reverse if necessary and identify by block number)

A modal expansion technique is applied to a system of uniform waveguides interconnected by abrupt junctions. Computer codes developed for the asymmetrical modes on-axis transition and all modes off-axis transition have been tested and verified through two separate experimental verifications.

The three main parts of this work are:

a. The tentative formulation for an abrupt transition from one waveguide to another, where each junction is restricted to having only one input and one output waveguide, while a conducting wall on each side of the junction is accounted for,

b. The development of convergence criteria for the selection of the important modes via symmetry used in each waveguide section, and

20. DISTRIBUTION / AVAILABILITY OF ABSTRACT	21. ABSTRACT SECURITY CLASSIFICATION
☒ UNCLASSIFIED/UNLIMITED ☐ SAME AS RPT ☐ DTIC USERS	UNCLASSIFIED

22a. NAME OF RESPONSIBLE INDIVIDUAL	22b. TELEPHONE (Include Area Code)	22c. OFFICE SYMBOL
Andrew E. Chrostowski	(315) 330-4381	RADC (OCTP)

DD FORM 1473, 84 MAR   83 APR edition may be used until exhausted.   SECURITY CLASSIFICATION OF THIS PAGE
All other editions are obsolete.

UNCLASSIFIED

c. The numerical implementation of the evaluation of the coupling co-
efficients for the coupling cases:

On-axis asymmetrical modes (circular to circular, circular to coaxial,
and coaxial to coaxial waveguide transitions). Off-axis for all modes (circular
to circular, circular to coaxial, and coaxial to coaxial waveguide transitions).

The implementation of this formulation requires modification of the structure of
the matrix equation of the existing code. To expand the capability and the
versatility of the code, future work should include the implementation of ridged
waveguide, dielectric loaded waveguide, and multiport junctions.

Accession For	
NTIS GRA&I	☒
DTIC TAB	☐
Unannounced	☐
Justification	

By	
Distribution/	
Availability Codes	
Dist	Avail and/or Special
A-1	

DTIC
COPY
INSPECTED
6

ACKNOWLEDGEMENTS

i

TABLE OF CONTENTS

LIST OF ILLUSTRATIONS

LIST OF ILLUSTRATIONS (Continued)

LIST OF ILLUSTRATIONS (Continued)

vi

LIST OF TABLES

I. INTRODUCTION

Waveguide discontinuity problems are very common to microwave engineering. Various approaches for different type of waveguide transitions have been developed including the conventional lumped equivalent circuits and field theory techniques[1,3]. Following the approach of Clarricoats[1] which is a field theory technique led to more detailed work and numerical applications by Mielke[4]. In brief, this technique involves matching the normal mode expansions in each waveguide section at the junction between sections. A large matrix equation is obtained which is then solved for mode amplitudes. Transmission coefficients, reflection coefficients, and power flow are calculated in terms of these amplitudes. Mielke's original work only allowed an abrupt transitions from one waveguide to another. Within this junction, two additional restrictions are imposed. One is that each junction can have only one input and one output waveguide. Second is that the smaller waveguide must lie entirely within the boundaries of the larger waveguide. Within this framework, the following coupling coefficient calculations have been obtained analytically and implemented in a computer code:

- on-axis symmetrical modes (circular to circular, circular to coaxial, and coaxial to coaxial waveguide transitions)
- on-axis and off-axis for all modes (rectangular to rectangular waveguide transition)

Subsequent work on circular to rectangular waveguide transition case has been implemented numerically by Palevsky[5].

The first part of the work presented is to introduce a tentative formulation which is able to handle the transition problem of the type that permits a conducting wall on each side of the junction. However, the junction is still restricted to be an abrupt transition from one waveguide to another. Also each junction is still allowed to have only one input and one output waveguide. The modal expansion technique is again applied here[1]. This formulation is not yet implemented and its derivation is described in Chapter II.

The second part of this work is the development of the convergence criteria. Accurate results depend critically upon judicious choice of the important modes via symmetry used in each waveguide section. Ideally, an infinite number of modes should be used. In practice, truncation errors caused by use of a finite number of modes can be reduced if these modes are wisely selected. Criteria for such selections are derived.

The third aspect of this thesis is to implement the evaluations of the coupling coefficients for the following cases:

- on-axis asymmetrical modes (circular to circular, circular to coaxial, and coaxial to coaxial waveguide transitions)

- off-axis for all modes (circular to circular, circular to coaxial, and coaxial to coaxial transitions)

The numerical implementation of the above cases is done following the technique developed for the circular to rectangular waveguide transition[5].

II. FORMULATION

The transition which has a transverse conducting wall on each side of the junction is investigated. The coaxial to coaxial transition as shown in Figure 2-1b which maintains the same characteristic impedance is a common transition that requires this extended formulation. A number of different geometries of a two-sided boundary transition is illustrated in Figure 2-1.

Adopt the definition of expressing the transverse electromagnetic fields in the expansion of an infinite number of vector mode functions found in Reference 3. For a junction which has an input guide 1 and an output guide 2, the fields in both guides are matched at the junction.

The boundary conditions require that:
in the common cross-sectional area (aperture)

$$\vec{E}_t'(1) = \vec{E}_t(2) \tag{2-1}$$

$$\vec{H}_t'(1) = \vec{H}_t(2) \tag{2-2}$$

and on the left side of the conducting wall

$$\vec{E}_t'(1) = 0 \tag{2-3}$$

and on the right side of the conducting wall

$$\vec{E}_t(2) = 0 \tag{2-4}$$
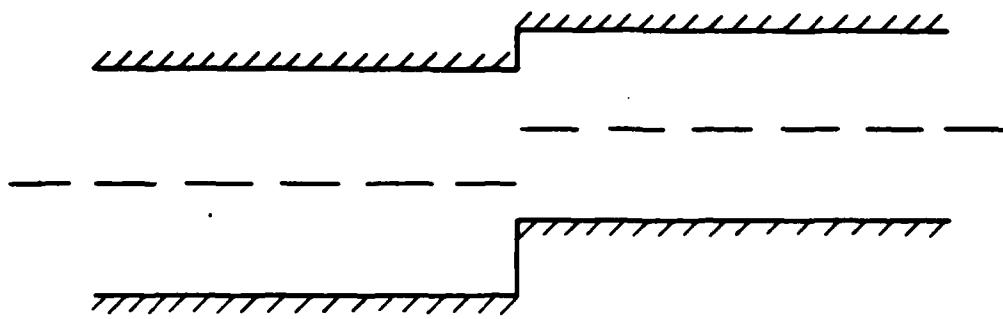
a - Circular to Circular Transition
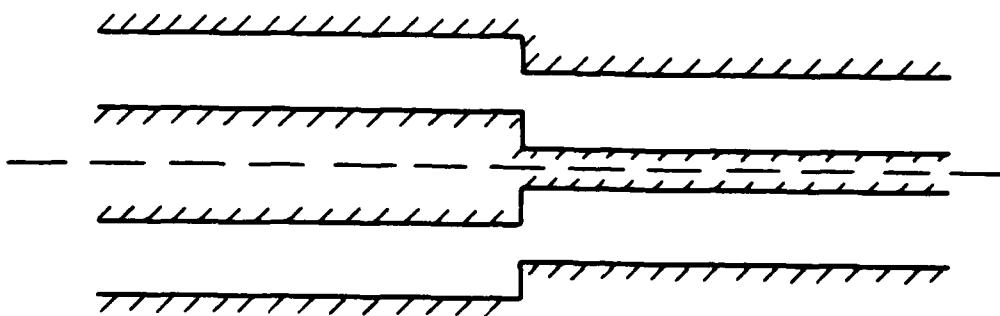
b - Coaxial to Coaxial Transition
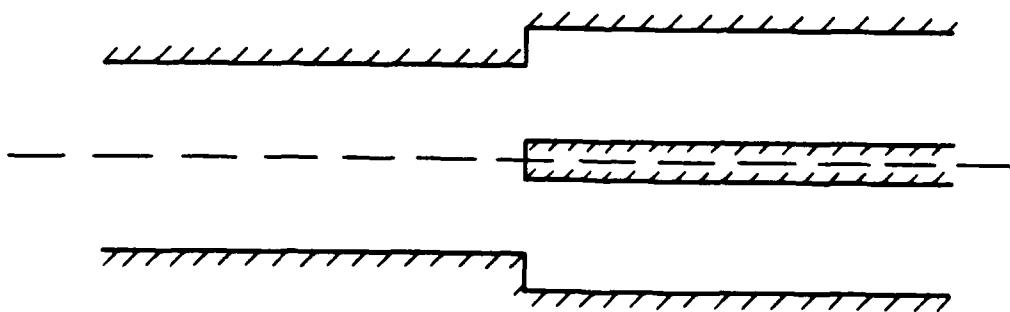
c - Circular to Coaxial Transition

Figure 2-1. Two-Sided Boundary Transitions.

Two useful pairs of equations may be derived from equations (2-1) and (2-2) by manipulating either (2-3) or (2-4).

First scalar multiply equations of (2-1) and (2-3) by

$$\sum_{k_1' = 1}^{N(1)} \overline{e}\,(k_1',\,1),$$

$$\vec{E}_t'\,(1) \cdot \sum_{k_1' = 1}^{N(1)} \overline{e}\,(k_1',\,1) = \vec{E}_t\,(2) \cdot \sum_{k_1' = 1}^{N(1)} \overline{e}\,(k_1',\,1) \qquad (2\text{-}5)$$

in the aperture

$$\vec{E}_t'\,(1) \cdot \sum_{k_1' = 1}^{N(1)} \overline{e}\,(k_1',\,1) = 0 \qquad (2\text{-}6)$$

on the left side of the conducting wall

Where $\overline{e}\,(k_1,\,1)$ are basis vector mode functions in region 1 and $N(1)$ is number of modes used in the expansion.

Secondly post vector multiply equation (2-2) by $\displaystyle\sum_{k_2' = 1}^{N(2)} \overline{e}\,(k_2',\,2),$

$$\vec{H}_t'\,(1) \times \sum_{k_2' = 1}^{N(2)} \overline{e}\,(k_2',\,2) = \vec{H}_t\,(2) \times \sum_{k_2' = 1}^{N(2)} \overline{e}\,(k_2',\,2) \qquad (2\text{-}7)$$

in the aperture

Where $\overline{e}\,(k_2',\,2)$ are basis vector mode functions in region 2 and $N(2)$ is number of modes used in the expansion.

Integrating (2-5) over the aperture, added to the integration of (2-6) over the left conducting wall gives:

$$\iint_{cs(1)} \vec{E}_t'\,(1) \cdot \sum_{k_1' = 1}^{N(1)} \overline{e}\,(k_1',\,1)\,ds = \iint_{A(1,2)} \vec{E}_t\,(2) \cdot \sum_{k_1' = 1}^{N(1)} \overline{e}\,(k_1',\,1)\,ds$$

$$(2\text{-}8a)$$

Integration of (2-7) over the aperture yields:

$$\iint_{A(1,2)} \left[\vec{H}_t'\,(1) \times \sum_{k_2' = 1}^{N(2)} \overline{e}\,(k_2',\,2) \right] \cdot d\overline{s} = \iint_{A(1,2)} \left[\vec{H}_t\,(2) \times \sum_{k_2' = 1}^{N(2)} \overline{e}\,(k_2',\,2) \right] \cdot d\overline{s}$$

$$(2\text{-}9a)$$

5

The use of the symmetric manipulations leads to the following dual
equations (2-8) and (2-9):

$$\iint\limits_{A(1,2)} \left[\vec{H}_t^{\,\prime}(1) \times \sum_{k_1^\prime = 1}^{N(1)} \bar{e}(k_1^\prime, 1) \right] \cdot d\bar{s} = \iint\limits_{A(1,2)} \left[\vec{H}_t(2) \times \sum_{k_1^\prime = 1}^{N(1)} \bar{e}(k_1^\prime, 1) \right] \cdot d\bar{s}$$

(2-8b)

$$\iint\limits_{A(1,2)} \vec{E}_t^{\,\prime}(1) \cdot \sum_{k_2^\prime = 1}^{N(2)} \bar{e}(k_2^\prime, 2)\, ds = \iint\limits_{cs(2)} \vec{E}_t(2) \cdot \sum_{k_2^\prime = 1}^{N(2)} \bar{e}(k_2^\prime, 2)\, ds$$

(2-9b)

Where cs(1), cs(2) are cross-sectional area of guides 1 and 2 and
A(1,2) the common cross-sectional area at the junction between guides
1 and 2. Since both sets of equations should give the same solutions
in the limit of an infinite number of modes, any linear combination
should also give the same solutions. How these two sets of equations
should be weighted in a linear combination is discussed in detail in
Appendix A. The combined equations (2-8a + 2-8b) and (2-9a + 2-9b)
form the matrix equation which is solved for the forward mode amplitudes
and the backward mode amplitudes. The size of the matrix will increase
as the number of modes per region and the number of regions increase.

To set up the large matrix equation, the coupling terms and the
propagation terms must be calculated. The one-sided boundary tran-
sition formulation contains coupling terms that are integrals of two
modes, one from each side of the junction, over the aperture (Overlap
Integrals). The two-sided boundary transition formulation contains
additional coupling terms that are integrals of two modes, both from
the same waveguide, over the aperture (Cross-Overlap Integrals).

Whereas the propagation terms are the same for both transitions. To include this type of transition into the existing system of equation of the one-sided boundary problem, the entries of the matrix structure as well as the entries of the known subvectors have to be modified. The very detailed structure of the matrix equation is given in Appendix A.

III. NUMERICAL CONVERGENCE CRITERIA

There are always solutions to the matrix equation. However, unless sufficient modes in both regions preceding and following any junction are considered, the solutions will be inaccurate. The accuracy can be estimated, in principle, by examining the transverse fields at the junction.

This is done by adding all the transverse fields in region preceding the junction to obtain the total field and substracting the summation of all the transverse fields following the junction. The result will indicate how close the fields in both regions are matched at the junction. However, this is a cumbersome process. Therefore, another technique is developed which provides a way of estimating the accuracy of the solutions.

Figure 3-1 illustrates the longitudinal view of a single junction.
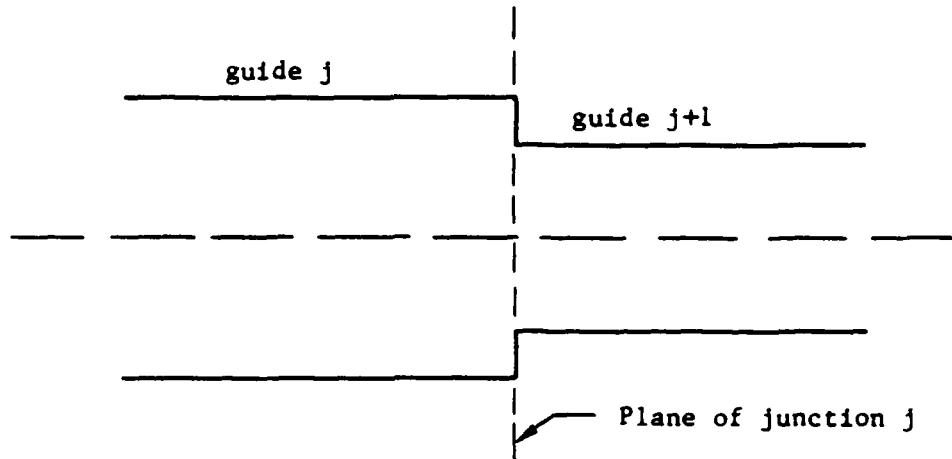
Figure 3-1. Longitudinal View of a Single Junction.

The transverse vector mode functions of guides j and j+1 are given by:

$$\bar{e}\ (k_j,\ j) \qquad \text{for guide } j$$

$$\bar{e}\ (k_{j+1},\ j+1) \quad \text{for guide } j+1$$

The overlap and self-overlap integrals are defined by:

$$\text{O.I. } (k_j,\ k_{j+1},\ j)\ = \iint\limits_{A(j,\ j+1)} \bar{e}\ (k_j,\ j)\ .\ \bar{e}\ (k_{j+1},\ j+1)\ ds \qquad (3-1)$$

$$\text{S.O.I. } (k_j,\ j)\ = \iint\limits_{A(j,\ j+1)} \bar{e}\ (k_j,\ j)\ .\ \bar{e}\ (k_j,\ j)\ ds \qquad (3-2)$$

$$\text{S.O.I. } (k_{j+1}\ j)\ = \iint\limits_{A(j,\ j+1)} \bar{e}\ (k_{j+1},\ j+1)\ .\ \bar{e}\ (k_{j+1},\ j+1)\ ds \qquad (3-3)$$

First consider a given single incident mode in larger guide j. Due to the discontinuity, an infinite number of modes in guide j+1 are excited. This incident mode over the smaller cross section can be represented at the junction by:

$$\bar{e}\ (k_j,\ j)\ = \lim_{N(j+1)\ \rightarrow\ \infty}\ \sum_{k'_{j+1}=1}^{N(j+1)}\ a\ (k'_{j+1},\ j+1)\ .\ \bar{e}\ (k'_{j+1},\ j+1) \qquad (3-4)$$

Where $a\ (k'_{j+1},\ j+1)$ is a weighting factor of each excited mode in guide j+1. Substitution of (3-4) into (3-1) yields:

$$\text{O.I. } (k_j,\ k_{j+1},\ j)\ = \lim_{N(j+1)\ \rightarrow\ \infty}\ \sum_{k'_{j+1}=1}^{N(j+1)}\ a\ (k'_{j+1},\ j+1)$$

$$.\ \iint\limits_{A(j,\ j+1)} \bar{e}\ (k'_{j+1},\ j+1)\ .\ \bar{e}\ (k_{j+1},\ j+1)\ ds \qquad (3-5)$$

9

Application of the orthogonality of the normal mode properties, (3-5) becomes:

$$O.I. \ (k_j, \ k_{j+1}, \ j) = \begin{cases} a \ (k_{j+1}, \ j+1) & \text{if} \quad k_{j+1} = k'_{j+1} \\ 0 & \text{if} \quad k_{j+1} \neq k'_{j+1} \end{cases} \qquad (3\text{-}6)$$

Hence, (3-4) becomes:

$$\overline{e} \ (k_j, \ j) = \lim_{N(j+1) \to \infty} \sum_{k_{j+1} = 1}^{N(j+1)} O.I. \ (k_j, \ k_{j+1}, \ j) \cdot \overline{e} \ (k_{j+1}, \ j+1) \qquad (3\text{-}7)$$

Substitution of (3-7) into (3-2) yields:

$$S.O.I. \ (k_j, \ j) = \lim_{N(j+1) \to \infty} \sum_{k_{j+1} = 1}^{N(j+1)} \left\{ O.I. \ (k_j, \ k_{j+1}, \ j) \right\}^2 \ \cdot$$

$$\iint_{A(j, \ j+1)} \overline{e} \ (k_{j+1}, \ j+1) \cdot \overline{e} \ (k_{j+1}, \ j+1) \ ds \qquad (3\text{-}8)$$

or,

$$S.O.I. \ (k_j, \ j) = \lim_{N(j+1) \to \infty} \sum_{k_{j+1} = 1}^{N(j+1)} \left\{ O.I. \ (k_j, \ k_{j+1}, \ j) \right\}^2 \qquad (3\text{-}9)$$

Secondly consider a single mode in the smaller guide $j+1$ incident on the junction, with an infinite number of modes are excited in guide j. This incident mode over the large cross section can be represented by:

$$\overline{e} \ (k_{j+1}, \ j+1) = \lim_{N(j) \to \infty} \sum_{k'_j = 1}^{N(j)} b \ (k'_j, \ j) \cdot \overline{e} \ (k'_j, \ j) \qquad (3\text{-}10)$$

Where $b \ (k'_j, \ j)$ is a weighting factor of each reflected mode in guide j. Substitution of (3-10) into (3-1) yields:

$$O.I. \ (k_j, \ k_{j+1}, \ j) = \lim_{N(j) \to \infty} \sum_{k'_j = 1}^{N(j)} b \ (k'_j, \ j) \cdot \iint_{A(j, \ j+1)} \overline{e} \ (k_j, \ j) \cdot \overline{e} \ (k'_j, \ j) \ ds \qquad (3\text{-}11)$$

or,

$$
\text{O.I. } (k_j, k_{j+1}, j) = \begin{cases} b(k_j, j) & \text{if } k_j' = k_j \\ 0 & \text{if } k_j' \neq k_j \end{cases} \tag{3-12}
$$

Hence, (3-10) becomes:

$$
\overline{e}(k_{j+1}, j+1) = \lim_{N(j) \to \infty} \sum_{k_j=1}^{N(j)} \text{O.I. } (k_j, k_{j+1}, j) \cdot \overline{e}(k_j, j) \tag{3-13}
$$

Substitution of (3-13) into (3-3) yields:

$$
\iint_{cs(j+1)} \overline{e}(k_{j+1}, j+1) \cdot \overline{e}(k_{j+1}, j+1) \, ds = \lim_{N(j) \to \infty} \sum_{k_j=1}^{N(j)} \left\{ \text{O.I. } (k_j, k_{j+1}, j) \right\}^2
$$
$$
\cdot \iint_{cs(j)} \overline{e}(k_j, j) \cdot \overline{e}(k_j, j) \, ds \tag{3-14}
$$

or,

$$
1 = \lim_{N(j) \to \infty} \sum_{k_j=1}^{N(j)} \left\{ \text{O.I. } (k_j, K_{j+1}, j) \right\}^2 \tag{3-15}
$$

Equations (3-9) and (3-15) are indicators for the completeness of the total representation of an infinite number of modes accountable for both transverse electromagnetic fields in guide j and j+1.

For the first case:

$$
0 \leq \frac{\displaystyle\sum_{k_{j+1}=1}^{N(j+1)} \left\{ \text{O.I. } (k_j, k_{j+1}, j) \right\}^2}{\text{S.O.I. } (k_j, j)} \leq 1.0 \tag{3-9}
$$

For the second case:

$$
0 \leq \sum_{k_j=1}^{N(j)} \left\{ \text{O.I. } (k_j, k_{j+1}, j) \right\}^2 \leq 1.0 \tag{3-15}
$$

11

Therefore the convergence can be verified by including a sufficient number of high order modes in both regions preceding and following the junction until the calculated value of equations (3-9) and (3-15) reaches roughly 95% or higher.

The knowledge of the field patterns of different modes for various geometries is helpful in choosing the correct modes for convergence. The number of modes required for convergence varies depending on the ratio of the cross-sectional areas of the two guides, the amount of offset, and the similarity of geometry. For example, two rectangular guides of only slightly different dimensions will require only a few modes to obtain good convergence. However, a rectangular to circular junction with offset axes and a large difference in cross-sectional area will take many modes to achieve good convergence.

IV. NUMERICAL EVALUATION OF OVERLAP AND SELF-OVERLAP INTEGRALS FOR CIRCULAR AND COAXIAL GEOMETRIES

For a one-sided boundary transition, the closed form solutions of the overlap and self-overlap integrals for the symmetrical modes on-axis transition are available in Reference 4, whereas for the asymmetrical modes on-axis and for all the modes off-axis transition have not yet been obtained analytically. Therefore, they must be evaluated numerically. The overlap and self-overlap integrals for the asymmetrical modes on-axis transition which are dependent only on the radial coordinate are evaluated in one dimension, while the overlap and self-overlap integrals for all the modes off-axis transition are evaluated in two dimensions.

The IMSL[6] routines DCADRE and DBLIN are used for one and two dimension integrations respectively. DCADRE is a routine of one dimension numerical integration of a function using cautious adaptive Romberg extrapolation; where DBLIN is a two dimensional version of DCADRE applying the same numerical approach. The routines require as inputs the limits of integration and the value of the integrand as a function of position. The remainder of this chapter describes how these two items are calculated.

Since the radial dependent part of the mode vector functions are expressed in terms of Bessel functions, an explicit evaluation of the functions in the integrands is computationally expensive. Therefore, a spline routine is used to fit the radial dependent part of the mode vector functions, and spline interpolation is used to evaluate it in the integrand. The IMSL[6] routines ICSICU and ICSEVU are used for the fitting and interpolation. Eight steps (radial increment) per wavelength plus four steps at each end point are used in the spline fit to guarantee a smooth interpolation.

13

The center of the input guide is adopted as a reference frame for the evaluation of the integral.

A.   <u>Overlap Integral of an On-Axis Transition</u>

The following derivation is valid for the on-axis circular/coaxial transitions.   The transitions for various geometries are shown in Figure 4-1.

The overlap integral is given by:

$$O.I. \; (k_j, \; k_{j+1}, \; j) \; = \iint_{A(j, \; j+1)} \bar{e} \; (k_j, \; j) \cdot \bar{e} \; (k_{j+1}, \; j+1) \; ds \qquad (4-1)$$

Substituting the mode functions listed in Appendix C into the above integral, it yields:

$$O.I. \; (k_j, \; k_{j+1}, \; j) = \iint_{A(j, \; j+1)} \Big\{ E_r \; (k_j, \; j, \; r) \cdot E_r \; (k_{j+1}, \; j+1, \; r) \cdot P_r \; (k_j, \; k_{j+1} \; \psi)$$

$$(4-2)$$

$$+ \; E_\psi \; (k_j, \; j, \; r) \cdot E_\psi \; (k_{j+1}, \; j+1, \; r)$$

$$\cdot \; P_\psi \; (k_j, \; k_{j+1}, \; \psi) \Big\} \cdot rdr \cdot d\psi$$

Where $E_r \; (k_j, \; j, \; r)$, $E_r \; (k_{j+1}, \; j+1, \; r)$ are radial dependent parts of the radial electric fields, and $E_\psi \; (k_j, \; j, \; r)$, $E_\psi \; (k_{j+1}, \; j+1, \; r)$ are radial dependent parts of the azimuthal electric fields. Since the integral of the product of polarization terms for radial electric fields is the same as the integral of the product of polarization terms for azimuthal electric fields, the integral is represented by $P \; (k_j, \; k_{j+1}, \; \psi)$.

Upon factoring the r and ψ components, (4-2) becomes:

$$O.I. \; (k_j, \; k_{j+1}, \; j) = \Big\{ \int [E_r \; (k_j, \; j, \; r) \cdot E_r \; (k_{j+1}, \; j+1, \; r) \; +$$

$$E_\psi \; (k_j, \; j, \; r) \cdot E_\psi \; (k_{j+1} \; j+1, \; r)] \cdot r \; dr \Big\} \cdot$$

$$\Big\{ P \; (k_j, \; k_{j+1}, \; \psi) \Big\} \qquad (4-3)$$

14

guide j

guide j+1

a - Circular - Circular.

guide j

guide j+1
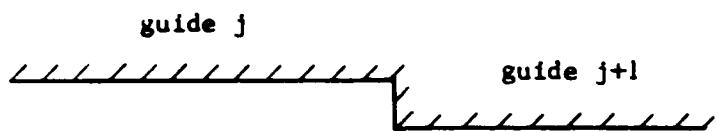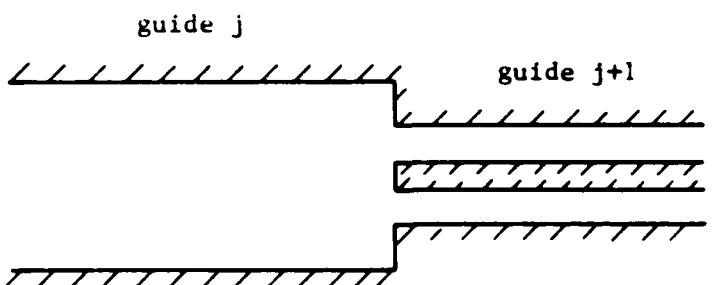
b - Circular - Coaxial.

guide j   guide j+1
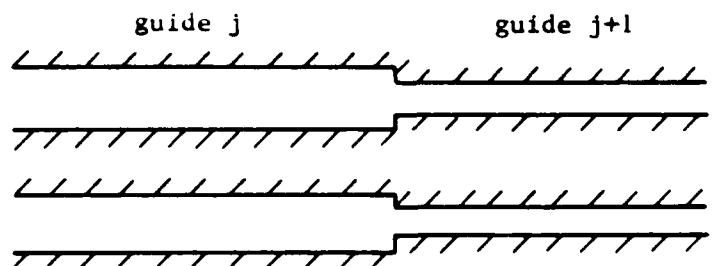
c - Coaxial - Coaxial.

Figure 4-1. One-Sided Boundary On-Axis Transition.

The integral $P\ (k_j,\ k_{j+1},\ \psi)$ is evaluated for different modes coupling
and the results are listed in Table 4-1. Obviously, the polarization
factors for mode couplings of the different azimuthal mode number are
equal to zero. The remaining task is to numerically integrate the
radial part of integrand. The limits for the radial integral are
simply the extreme boundaries of the common cross-sectional area at
the junction.

Table 4-1. Polarization Factors for Various Mode Coupling of the Same Azimuthal Mode Number m

Polarization	Mode Coupling			
	TE - TE	TE - TM	TM - TE	TM - TM
Parallel - Parallel	$+\pi\cos(m.\Delta\theta)$	$-\pi\sin(m.\Delta\theta)$	$+\pi\sin(m.\Delta\theta)$	$+\pi\cos(m.\Delta\theta)$
Parallel - Perpendicular	$-\pi\sin(m.\Delta\theta)$	$-\pi\cos(m.\Delta\theta)$	$+\pi\cos(m.\Delta\theta)$	$-\pi\sin(m.\Delta\theta)$
Perpendicular - Parallel	$+\pi\sin(m.\Delta\theta)$	$+\pi\cos(m.\Delta\theta)$	$-\pi\cos(m.\Delta\theta)$	$+\pi\sin(m.\Delta\theta)$
Perpendicular - Perpendicular	$+\pi\cos(m.\Delta\theta)$	$-\pi\sin(m.\Delta\theta)$	$+\pi\sin(m.\Delta\theta)$	$+\pi\cos(m.\Delta\theta)$

$\Delta\theta$ is an angular rotation of the secondary axes relative to the main
frame axes.

B.   Overlap Integral of an Off-Axis Transition

The off-axis transition involves the integration of a
function of two variables. The integration is always performed in
the cartesian coordinate system of the first region j. The relation-
ship between the two coordinate systems is illustrated in Figure 4-2.
Δx, Δy, and $\Delta\theta$ are the offset of the guide j+1 relative to the guide
j, and $\Delta\theta$ is applied after Δx and Δy.
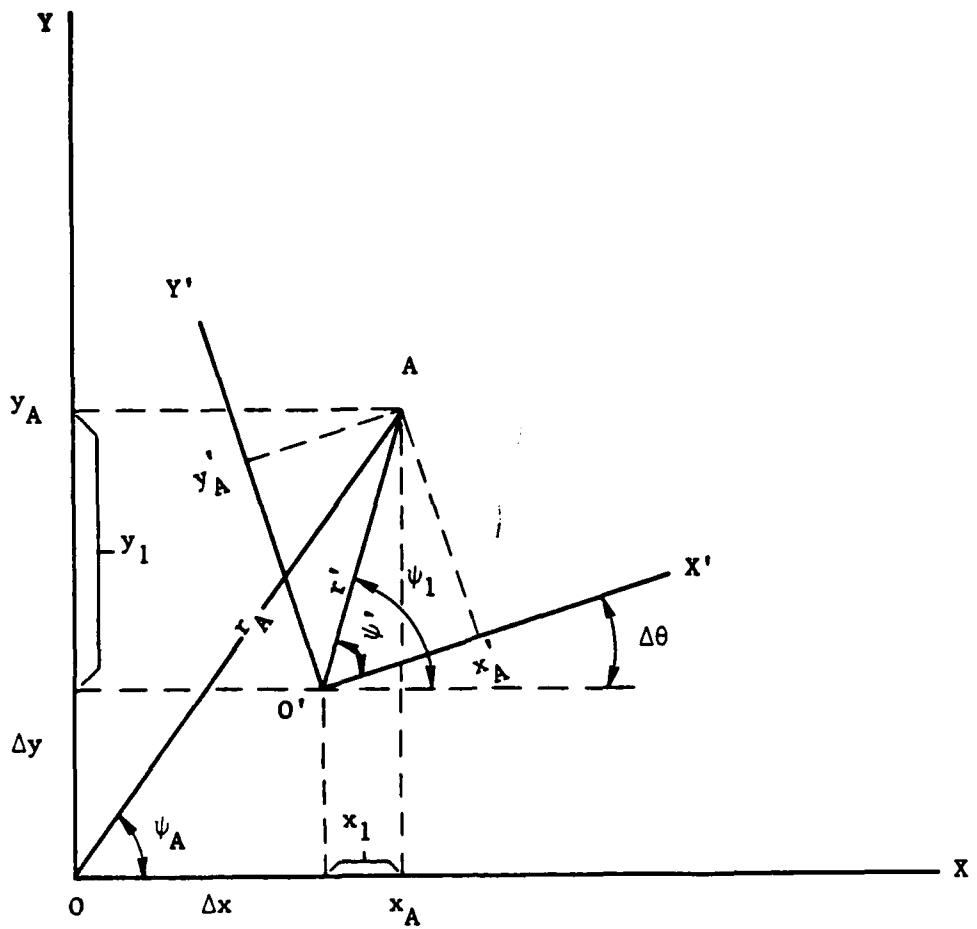
Figure 4-2. Cross Section View of the Two Coordinate Systems.

The vector mode functions in guides j and $j+1$ can be written in terms of their cylindrical coordinates as:

$$\overline{e}(k_j, j) = E_r(k_j, j, r) \cdot p(k_j, j, \psi) \cdot \hat{r}_0 +$$
$$E_\psi(k_j, j, r) \cdot q(k_j, j, \psi) \cdot \hat{\psi}_0$$

$$\overline{e}(k_{j+1}, j+1) = E_{r'}(k_{j+1}, j+1, r') \cdot p(k_{j+1}, j+1, \psi') \cdot \hat{r}_0' + \tag{4-4}$$
$$E_{\psi'}(k_{j+1}, j+1, r') \cdot q(k_{j+1}, j+1, \psi') \cdot \hat{\psi}_0'$$

Where $\hat{r}_0$, $\hat{\psi}_0$ are unit vectors along r and ψ directions; and $\hat{r}_0'$, $\hat{\psi}_0'$ are unit vectors along r' and ψ' directions. The expressions $p(k_j, j, \psi)$, $q(k_j, j, \psi)$ and $p(k_{j+1}, j+1, \psi')$, $q(k_{j+1}, j+1, \psi')$ are polarization terms of guides j and $j+1$ respectively.

Using the following coordinate transformation,

$$x = r \cdot \cos \psi - \psi \cdot \sin \psi$$
$$y = r \cdot \sin \psi - \psi \cdot \cos \psi \tag{4-5}$$

the transverse fields of guide j evaluated at a local point A are given in the cartesian coordinate system (reference frame) as:

$$E_x(k_j, j)\Big|_A = \Big\{E_r(k_j, j, r) \cdot p(k_j, j, \psi)\Big\}\Big|_A \cdot \cos \psi_A -$$
$$\Big\{E_\psi(k_j, j, r) \cdot q(k_j, j, \psi)\Big\}\Big|_A \cdot \sin \psi_A$$

$$\tag{4-6}$$

$$E_y(k_j, j)\Big|_A = \Big\{E_r(k_j, j, r) \cdot p(k_j, j, \psi)\Big\}\Big|_A \cdot \sin \psi_A +$$
$$\Big\{E_\psi(k_j, j, r) \cdot q(k_j, j, \psi)\Big\}\Big|_A \cdot \cos \psi_A$$

Where at point A, r_A and ψ_A are given by:

$$r_A = \sqrt{x_A^2 + y_A^2}$$

$$\psi_A = \tan^{-1} \frac{y_A}{x_A} \tag{4-7}$$

At the same point A, the coordinate transformation from the second guide to the first guide is given by:

$$x_1 = x_A - \Delta x$$

$$y_1 = y_A - \Delta y$$

$$r' = \sqrt{x_1^2 + y_1^2}$$

$$= \sqrt{x_A'^2 + y_A'^2} \tag{4-8}$$

$$\psi_1 = \tan^{-1} \frac{y_1}{x_1}$$

$$\psi' = \psi_1 - \Delta\theta$$

$$= \tan^{-1} \frac{y_A'}{x_A'}$$

Applying the coordinate transformation of (4-5), the transverse fields of guide j+1 expressed in terms of the reference coordinate system are:

$$E_x (k_{j+1}, j+1) \bigg|_A = \left\{ E_{r'} (k_{j+1}, j+1, r') \cdot p (k_{j+1}, j+1, \psi') \right\} \bigg|_A \cdot \cos \psi_1 -$$

$$\left\{ E_{\psi'} (k_{j+1}, j+1, r') \cdot q (k_{j+1}, j+1, \psi') \right\} \bigg|_A \cdot \sin \psi_1$$

$$\tag{4-9}$$

$$E_y (k_{j+1}, j+1) \bigg|_A = \left\{ E_{r'} (k_{j+1}, j+1, r') \cdot p (k_{j+1}, j+1, \psi') \right\} \bigg|_A \cdot \sin \psi_1 +$$

$$\left\{ E_{\psi'} (k_{j+1}, j+1, r') \cdot q (k_{j+1}, j+1, \psi') \right\} \bigg|_A \cdot \cos \psi_1$$

19

Equation (4-1) becomes:

$$\text{O.I.} (k_j, k_{j+1}, j) = \iint\limits_{A(j, j+1)} \left\{ E_x (k_j, j) \cdot E_x (k_{j+1}, j+1) + E_y (k_j, j) \cdot \right.$$

$$\left. E_y (k_{j+1}, j+1) \right\} \cdot dx \, dy \qquad (4\text{-}10)$$

The limits of the integration of the above integral are derived below for various transitions and geometries.

B1.   **Circular to Circular Transistion**

Figure 4-3 illustrates the cross section view of the junction.
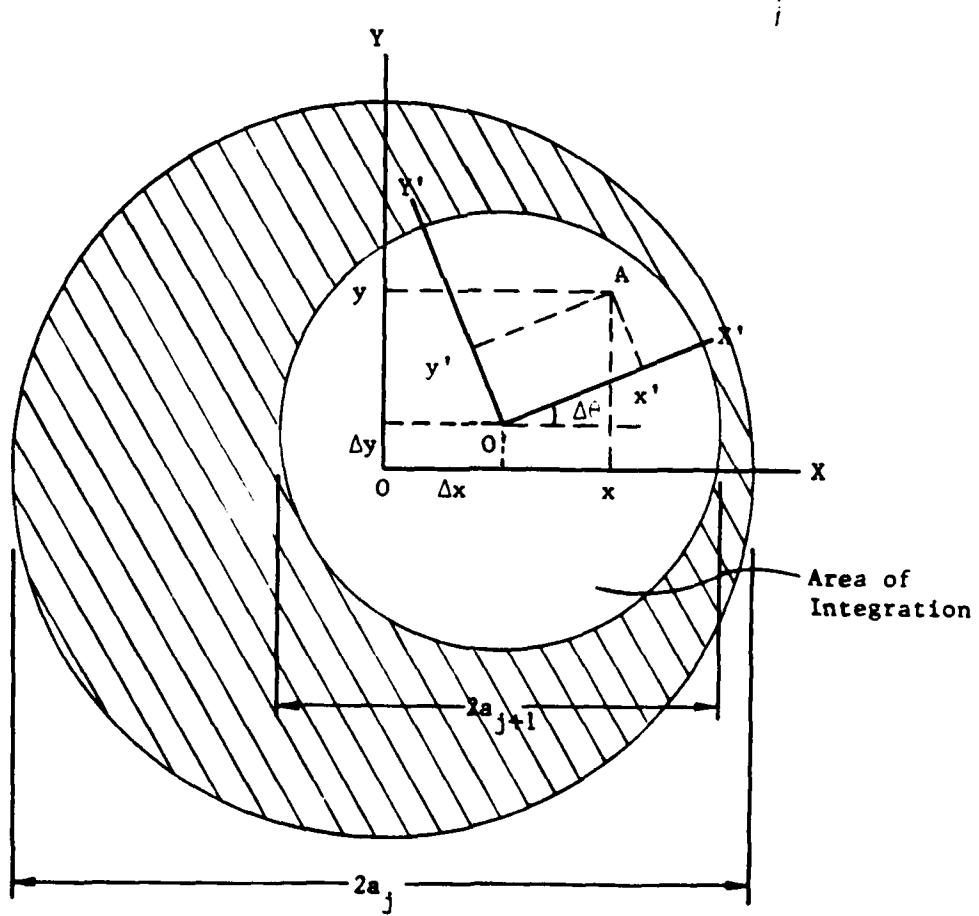
Figure 4-3.   Cross Section View of Circular to Circular Transition.

The lower and upper limits of the horizontal end points are found to be:

$$x_{lower} = - a_{j+1} + \Delta x$$
$$x_{upper} = + a_{j+1} + \Delta x \qquad (4-11)$$

While the limits of the vertical end points are given by:

$$y_{lower}(x) = \Delta y - \sqrt{a_{j+1}^2 - (x - \Delta x)^2}$$
$$y_{upper}(x) = \Delta y + \sqrt{a_{j+1}^2 - (x - \Delta x)^2} \qquad (4-12)$$

B2. Coaxial to Coaxial Transition

The cross section view of the junction is depicted in Figure 4-4. The limits of the horizontal end points are:

$$x_{lower} = - a_{j+1} + \Delta x$$
$$x_{upper} = + a_{j+1} + \Delta x \qquad (4-13)$$

The common cross-sectional area is exactly the area bounded by the inner and the outer walls of guide j+1. For simplicity, the annular aperture is divided into two regions of integration. Figure 4-5 shows the top half annular ring, where the dashed line indicates the upper bound and the solid line indicates the lower bound of the region of integration.
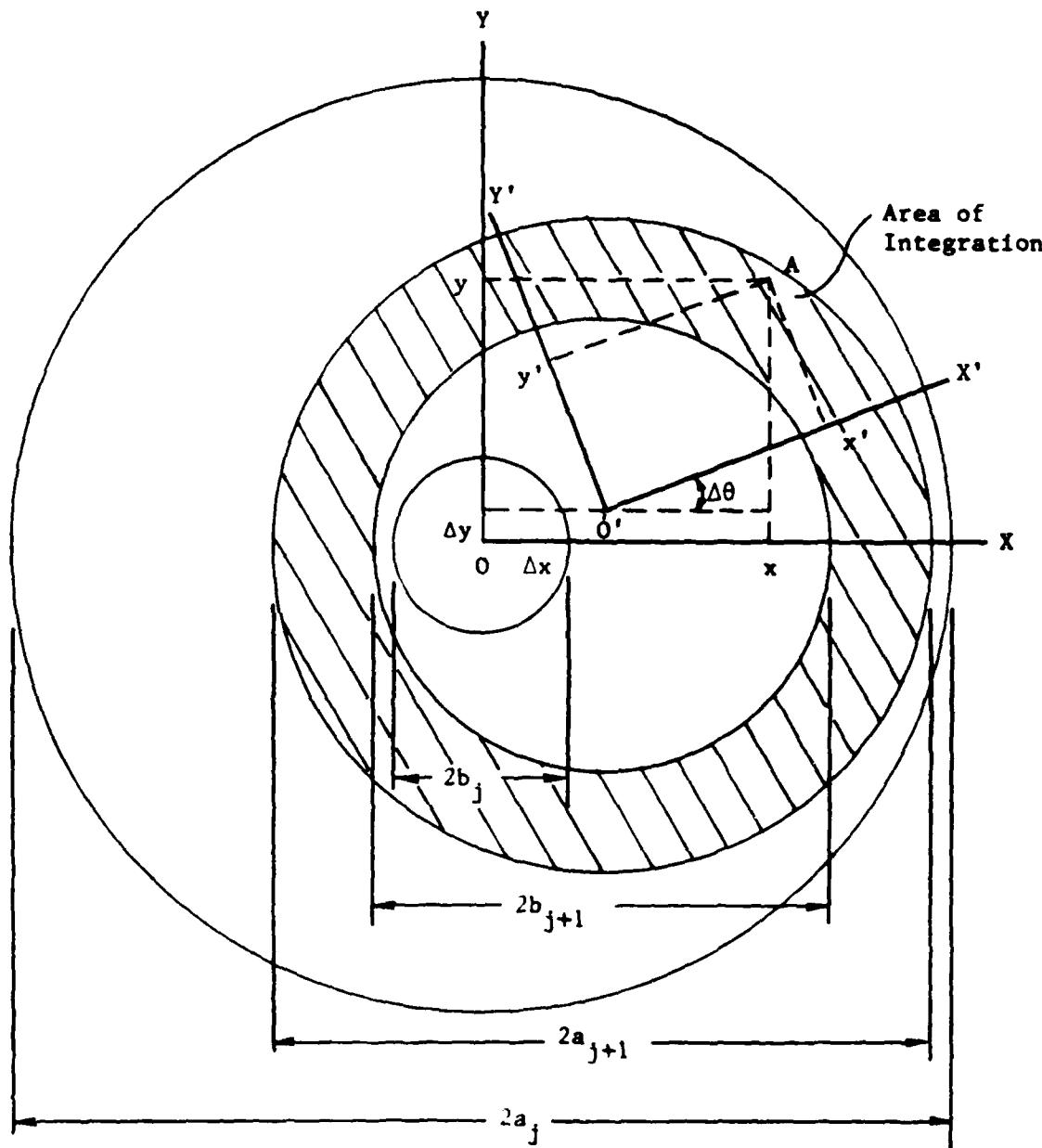
Figure 4-4. Cross Section View of Coaxial to Coaxial Transition.
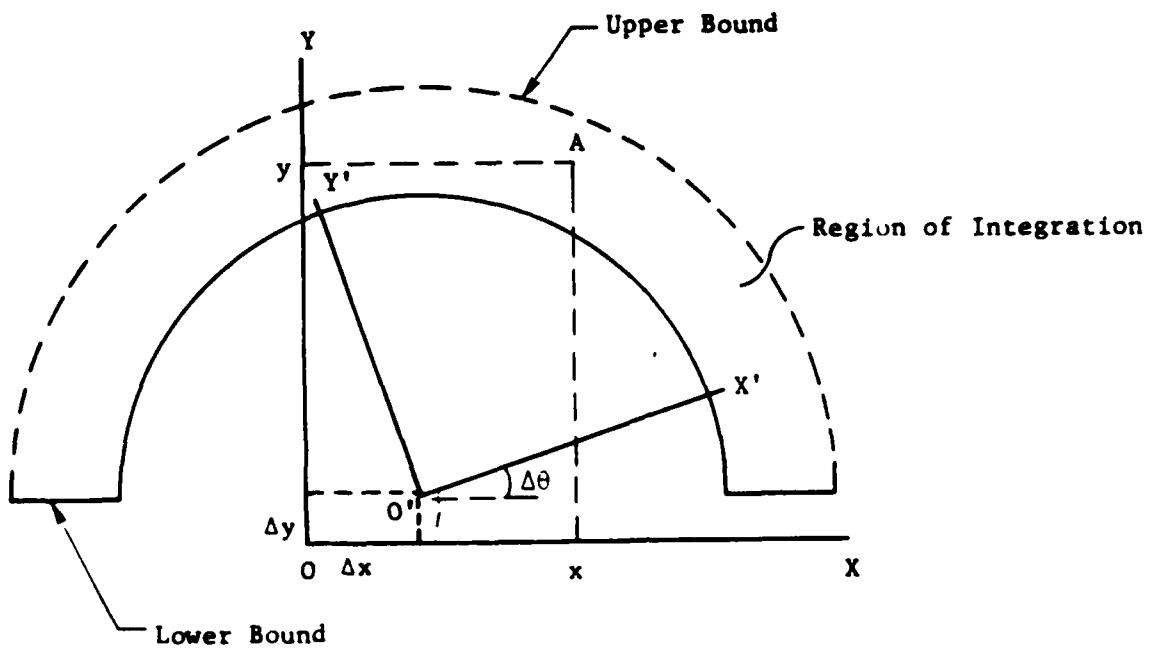
Figure 4-5. Top Half Annular Aperture.

For the top half:

$$y_{lower}(x) = \begin{cases} \Delta y & \text{for } |x - \Delta x| \geq b_{j+1} \\ \Delta y + \sqrt{b_{j+1}^2 - (x - \Delta x)^2} & \text{for } |x - \Delta x| < b_{j+1} \end{cases}$$

$$(4-14)$$

$$y_{upper}(x) = \Delta y + \sqrt{a_{j+1}^2 - (x - \Delta x)^2}$$

The bottom half annular aperture is illustrated in Figure 4-6.
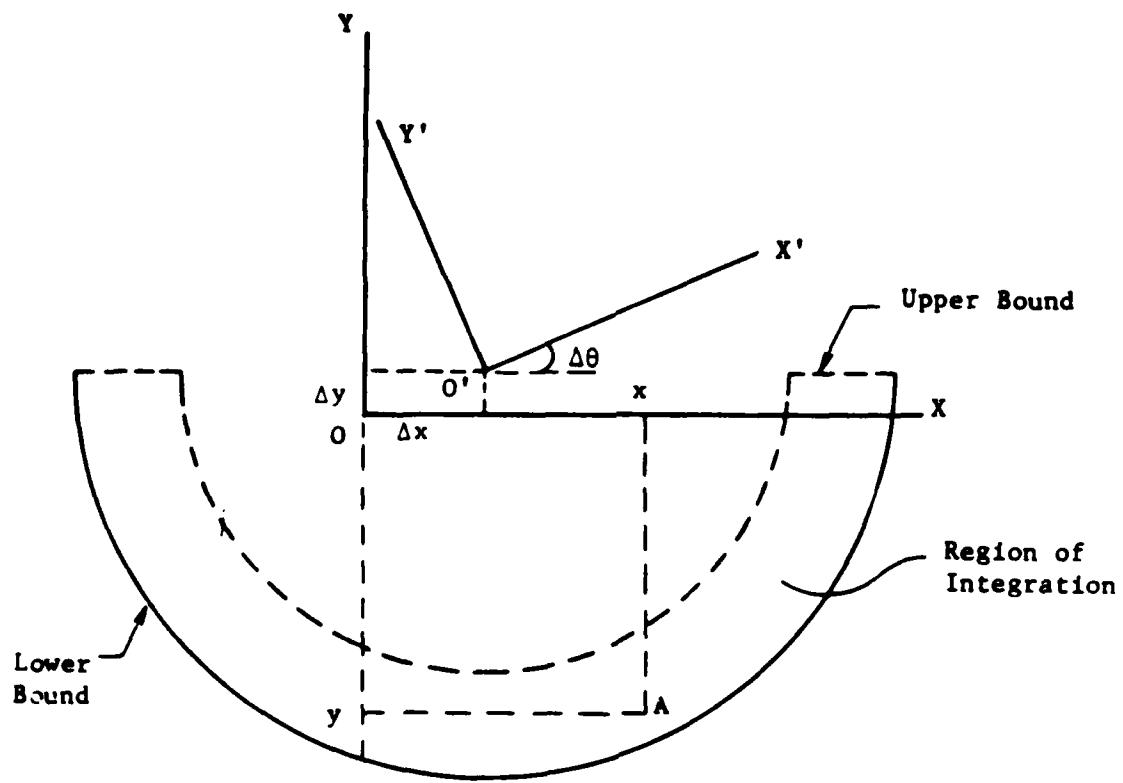
Figure 4-6.   Bottom Half Annular Aperture.

For the bottom half:

$$y_{lower}(x) = \Delta y - \sqrt{a_{j+1}^2 - (x - \Delta x)^2}$$

$$(4-15)$$

$$y_{upper}(x) = \begin{cases} \Delta y & \text{for} \quad |x - \Delta x| \geq b_{j+1} \\ \\ \Delta y - \sqrt{b_{j+1}^2 - (x - \Delta x)^2} & \text{for} \quad |x - \Delta x| < b_{j+1} \end{cases}$$

B3.   Circular to Coaxial Transition

Since the area of integration is bounded by the inner and outer walls of coaxial guide, the limits for both horizontal and vertical end points are the same as the previous case. The same techniques are used to numerically evaluate the self-overlap integrals.

V. EXPERIMENTAL VERIFICATION

The computer code developed for asymmetrical modes of the on-axis and the off-axis transitions has been tested with two separate configurations. The two dimension numerical integration code was tested by verifying the measured return loss (reflection) of an off-axis transition. The one dimension numerical integration code was tested by comparing the experimental results of the return loss of a centered circular aperture of finite thickness (obtained from Reference 3) to the numerical results.

The ratio of the cross-sectional areas of the two guides at the junction determines the preliminary guess of the ratio of the number of modes considered in each guide at that junction. Mode selection for limiting the choices of modes in the expansion to those which strongly affect the wave solution was done by observing the strength of the coupling between each higher order mode and the dominant mode. The convergence criteria was satisfied in all cases. Violation of this criteria yielded inaccurate results.

A.   Three Regions Off-Axis Circular to Circular Transition

An illustration of the three regions transition is depicted in Figure 5-1. Two units of the transition were fabricated. The dimensions for each unit are listed in Table 5-1. Notice that the only difference between the two units is that the length of the middle region which is of 11.0 mm for unit A, and 15.0 mm for unit B.

A block diagram of the experimental arrangements for the reflection measurement is illustrated in Figure 5-2. The equipment used for the setup is listed in Table 5-2. Calibration for 100% reflection was done by placing the shorting plate at the output of

26
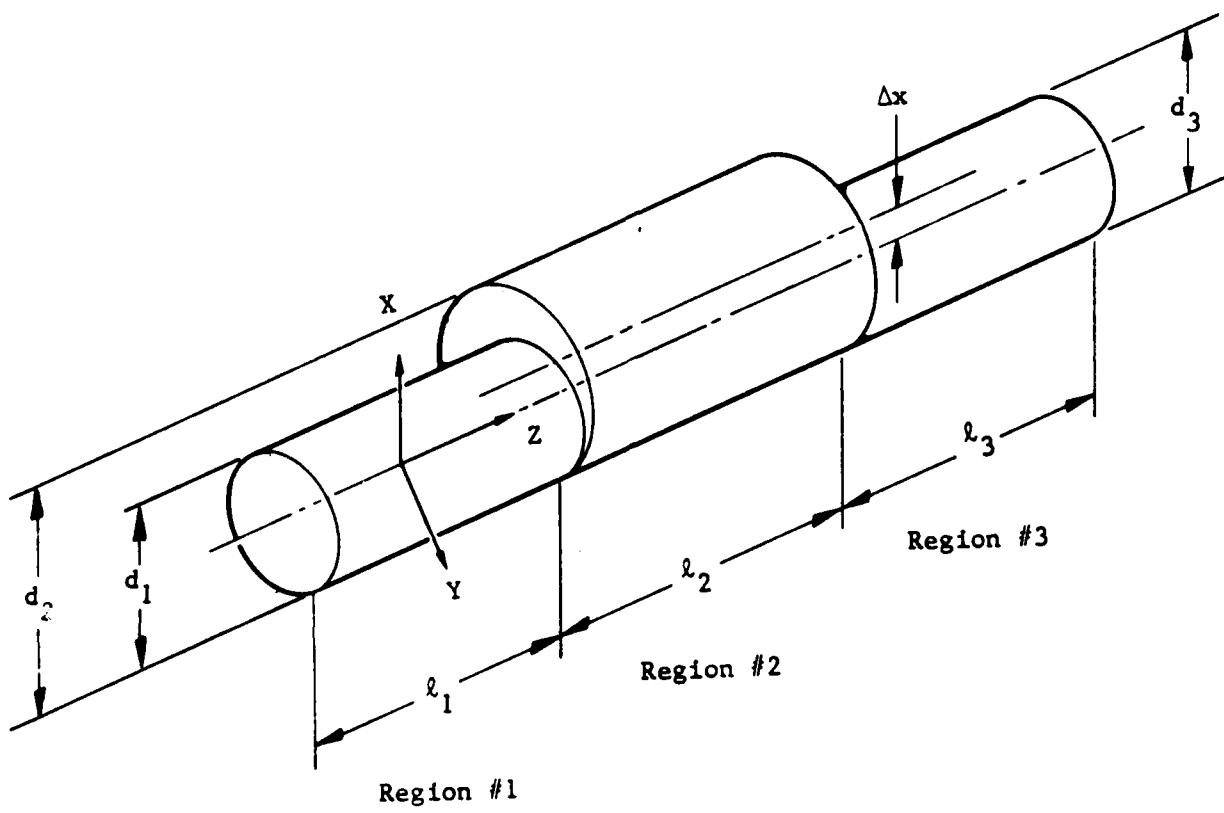
Figure 5-1. Three Regions Off-Axis Circular to Circular Transition.
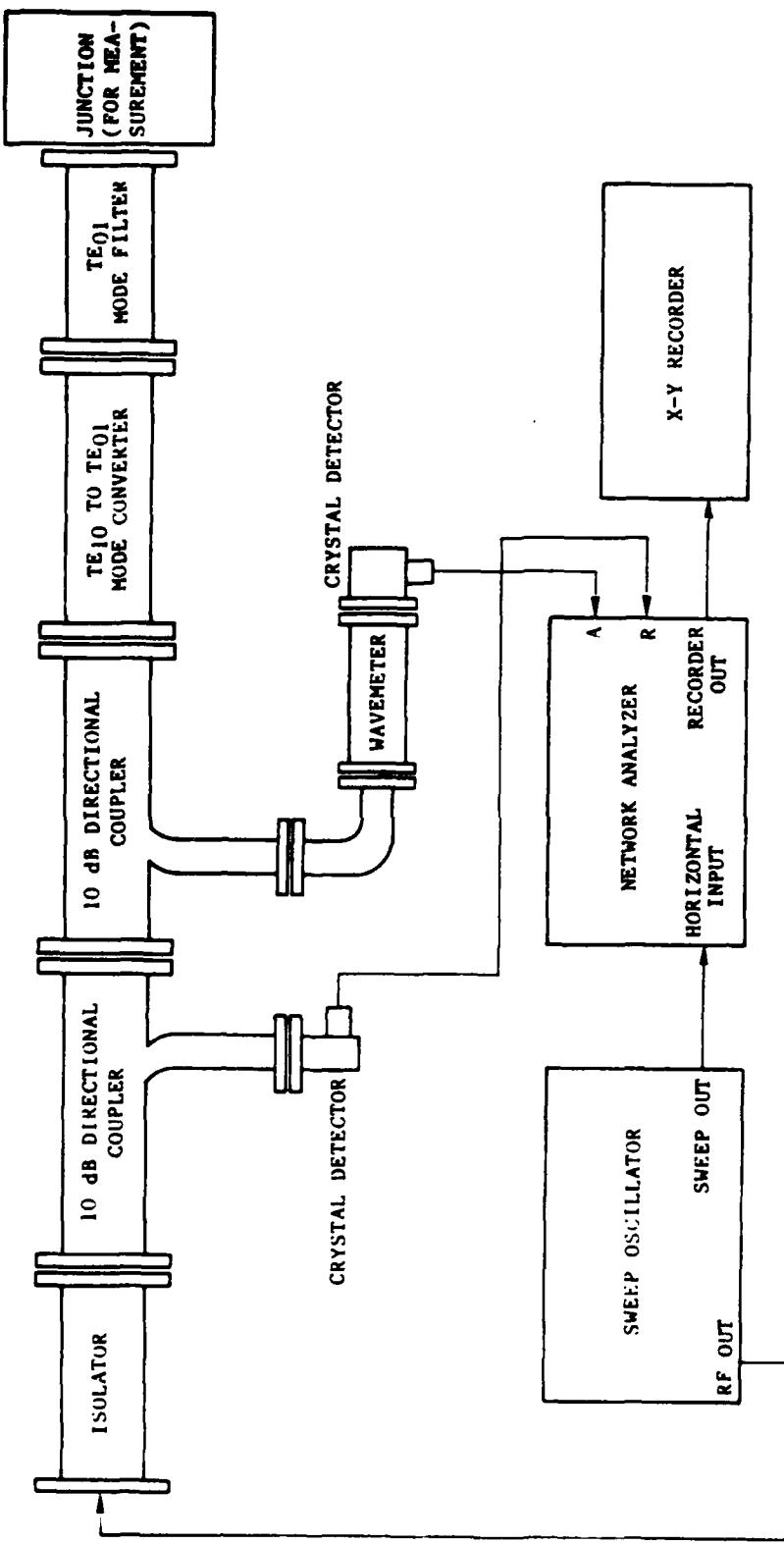
Figure 5-2. 28 GHz to 36 GHz Band Reflection Measurement Setup.

28

Table 5-1.

Dimensions List of Units A and B

Dimensions (mm)	Unit	
	A	B
d_1	15.90	15.90
ℓ_1	30.28	30.28
d_2	24.0	24.0
ℓ_2	11.0	15.0
d_3	15.90	15.90
ℓ_3	30.28	30.28
Δx	4.064	4.064

Table 5-2. Equipment List for Reflection Measurement

(1) HP 8690B Sweep Oscillator

(1) Wiltron Model 560A Scalar Network Analyzer

(1) HP 7035B X-Y Recorder

(2) HP R422A Crystal Detector

(1) HP Model R532A Wavemeter

(2) HP Model R752C 10 dB Directional Coupler

(1) TRG Model 340-634 Mode Filter

(1) TE_{10} to TE_{01} Mode Converter

(1) Shorting Plate

the mode filter. Since a high quality matched load was not available, the reflection measurement was performed by leaving the output end of the transition open to air. This was treated as an 18 dB of return loss in the code since the average measured return loss of the unterminated transition was approximately 18 dB across the entire frequency band.

The first calculated return losses which are obtained with no input reflections considered are not in good agreement with the measured results. They are shown in Figure 5-3 for Unit A, and in Figure 5-4 for Unit B. We theorized that this might be due to the mode filter not absorbing higher order reflected modes excited at the junction between the mode filter and mode converter. To take this into account, the overall length of the first region preceding the transition was adjusted and an input reflection of 50% was added in the computer code after a number of runs. The results of the measured and the calculated return losses of the two units are shown in Figures 5-5 and 5-6 respectively. The calculated curves for both units follow the measured curves closely across the frequency band. At the lowest end of the band which is near the cutoff frequency of the dominant mode (TE_{11} mode), the calculated return loss is higher than the measured return loss for Unit A. The ripples observed across the midband for Unit A and uniformly across the entire band for Unit B are probably caused by the imperfection of the mode filter.

B.   Centered Circular Aperture of Finite Thickness in Circular
      Guide

A small centered circular aperture in a transverse metallic plate of finite thickness (TE_{11} mode in circular guide) in circular

30
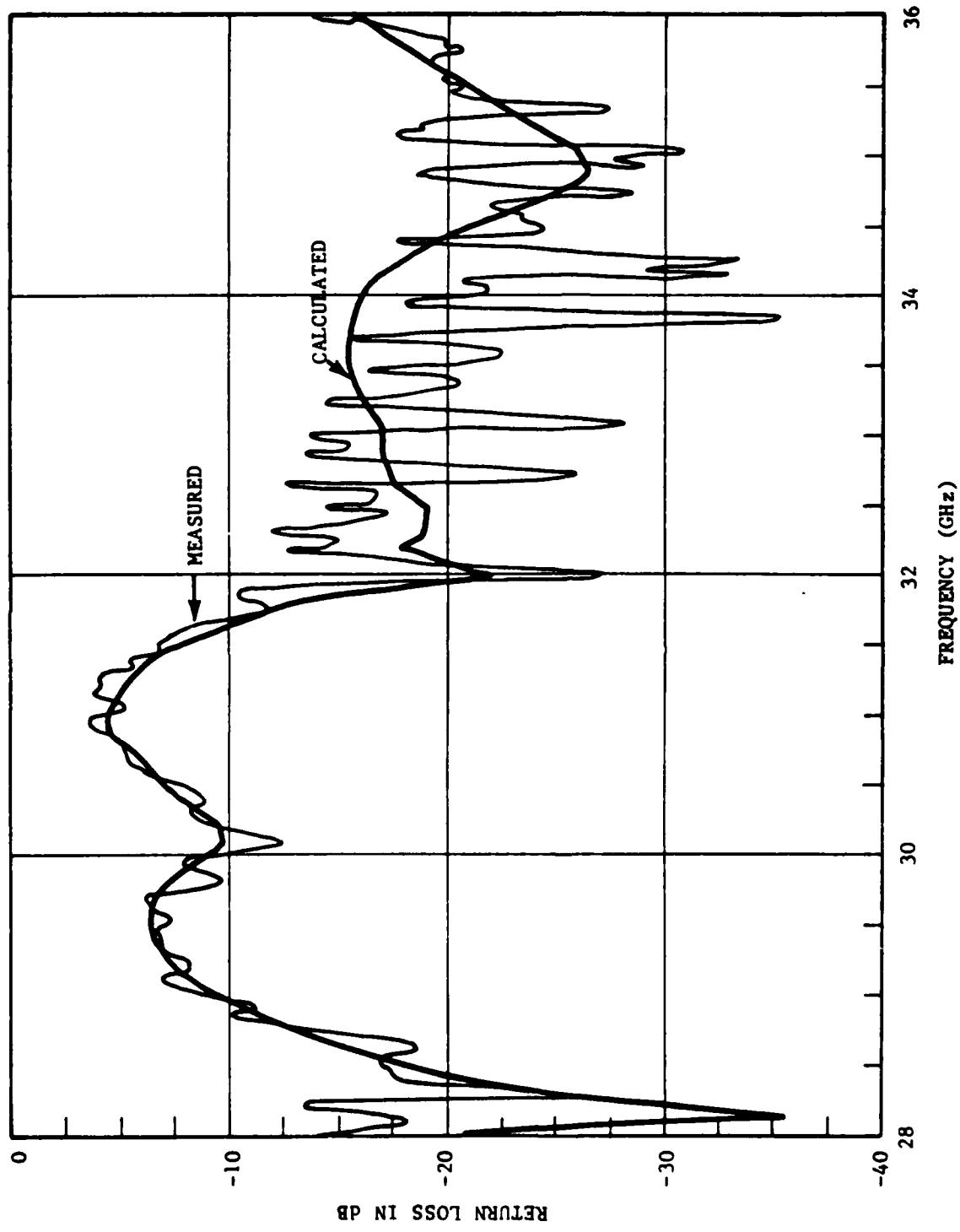
Figure 5-3. Measured and Calculated Reflection for Unit A (with No Input Reflection).

31
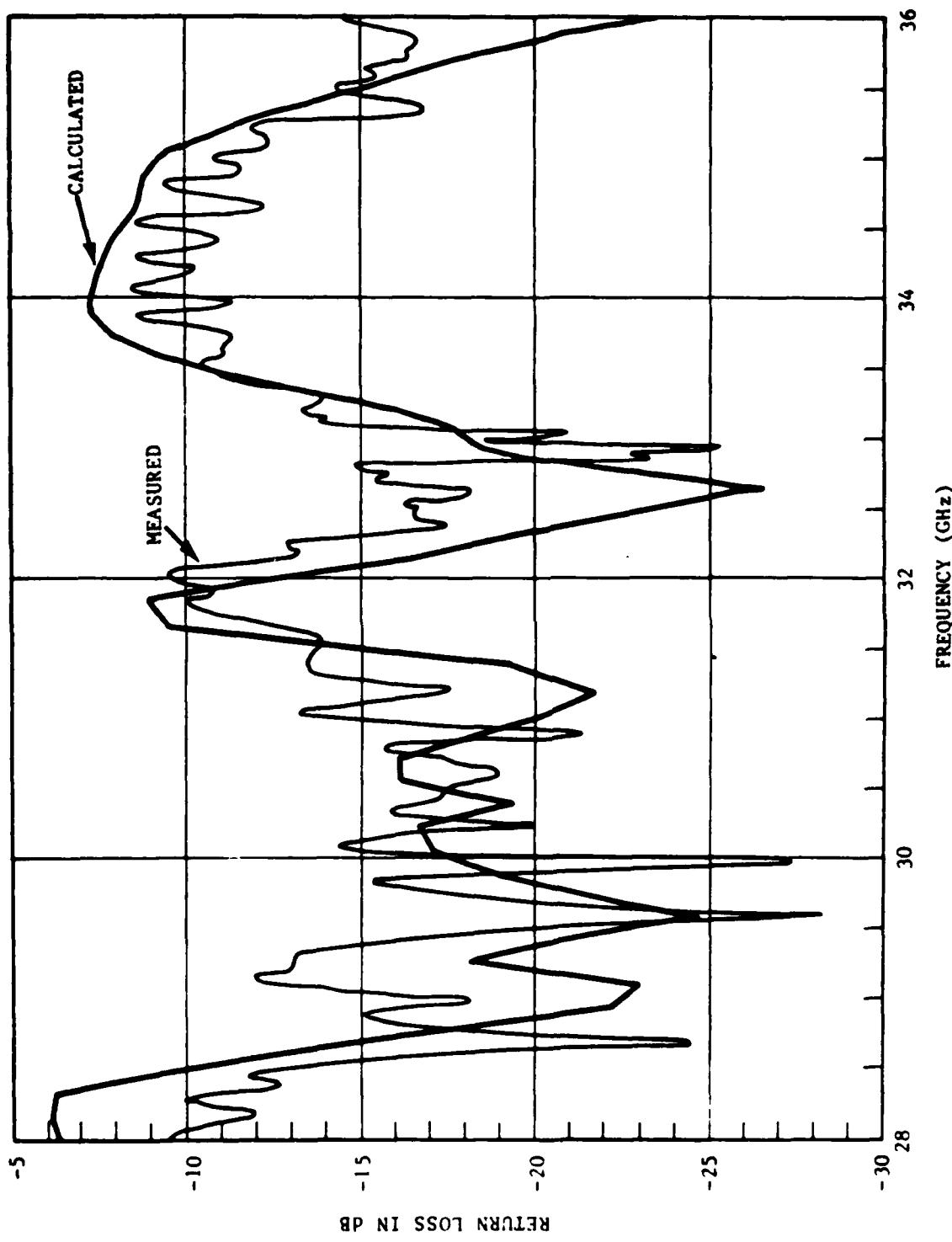
Figure 5-4. Measured and Calculated Reflection for Unit B (with 13% Input Reflection).
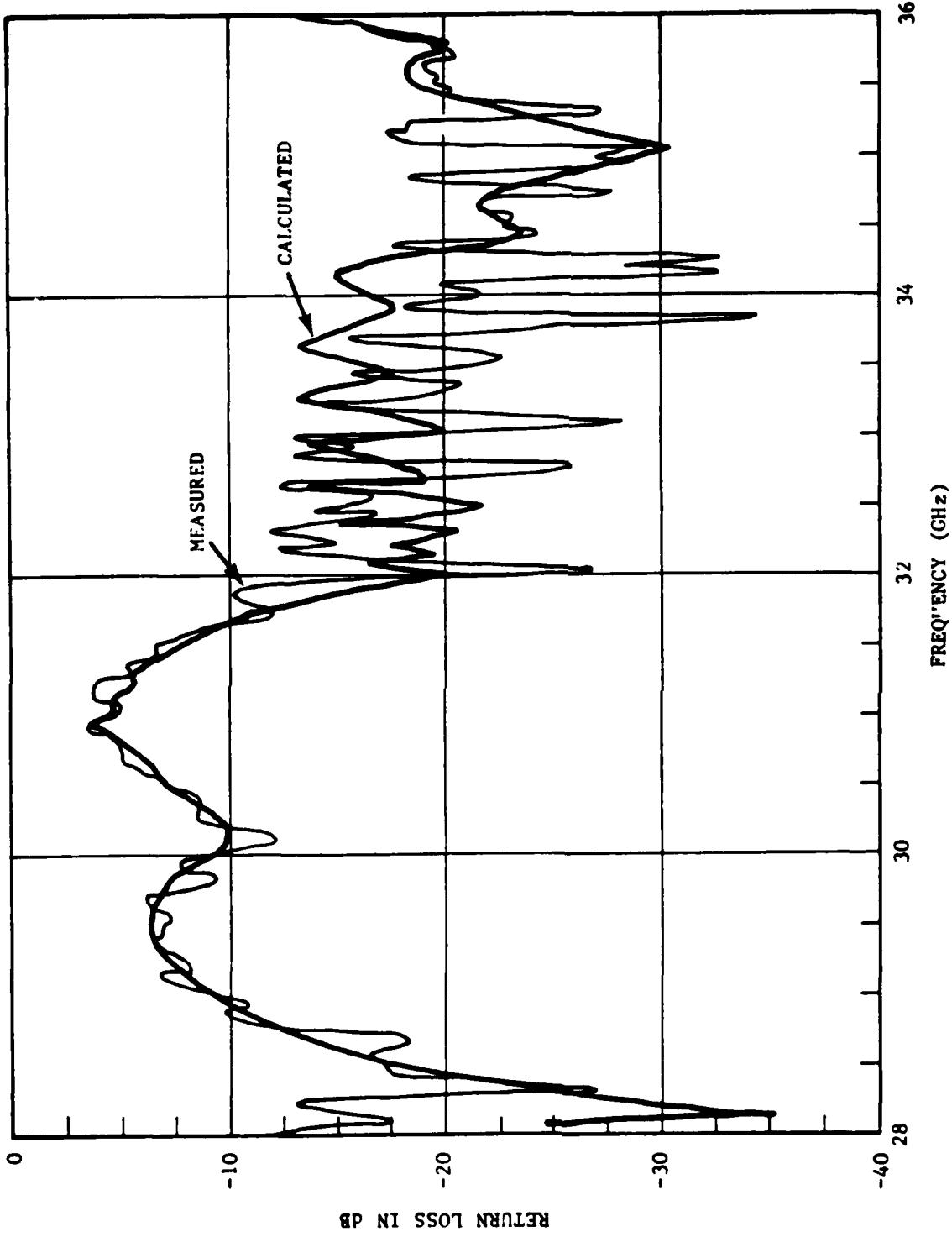
Figure 5-5. Measured and Calculated Reflection for Unit A (with 50% Input Reflection).

33
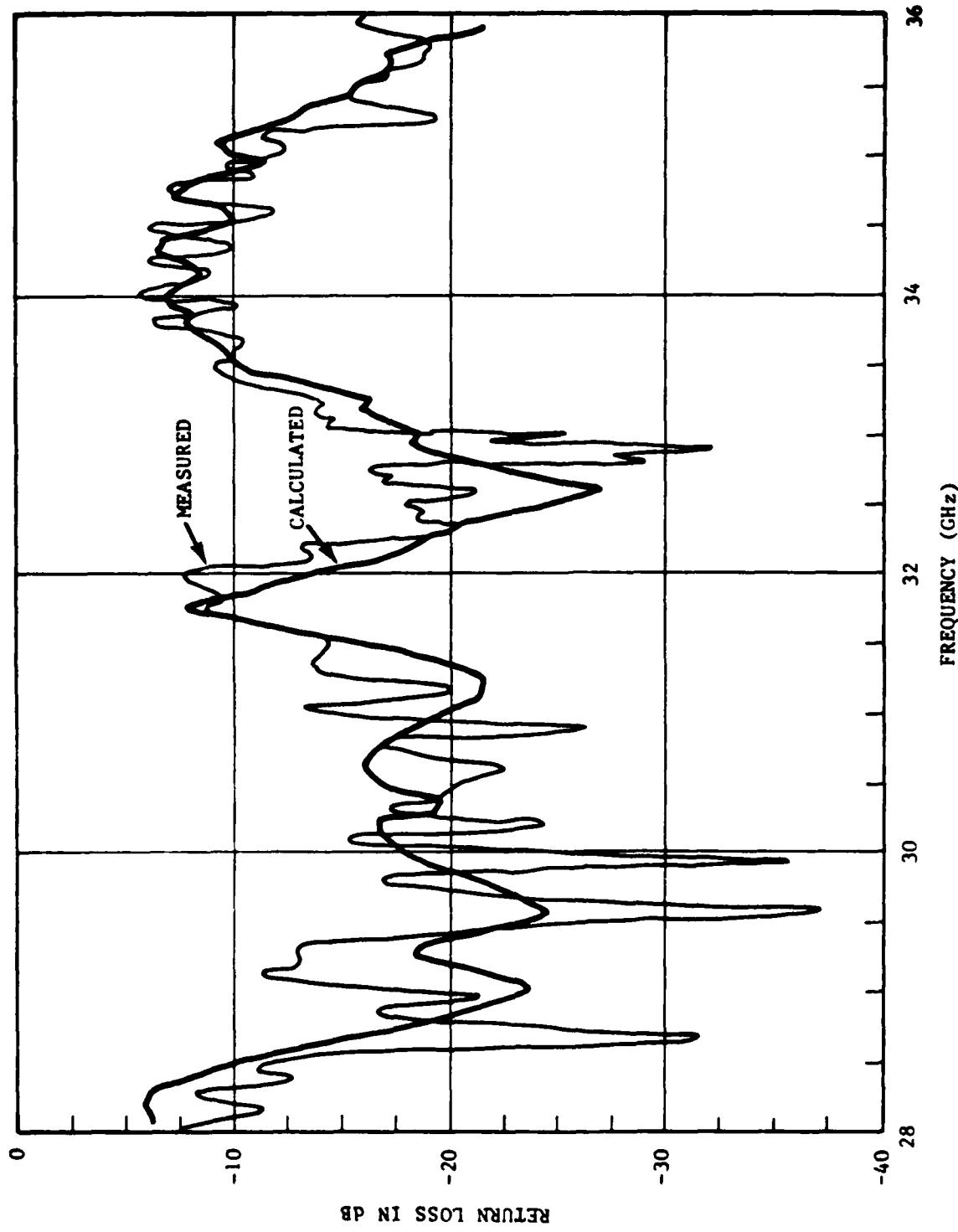
Figure 5-6. Measured and Calculated Reflection for Unit B (with 50% Input Reflection).

34

guide may be interpreted as a shunt inductance[3]. The cross sectional view, the side view, and the equivalent circuit are illustrated in Figure 5-7. At the reference plane T for a centered circular aperture, the normalized inductive susceptance is given by

$$\frac{B}{Y_o} = \frac{\lambda_g}{4R} \left\{ \frac{(2R)^3}{8.40\ M} - 2.344 \right\} \qquad (5-1)$$

where

$$M = \frac{d^3}{6} \qquad (5-2)$$

$$\lambda_g = \frac{\lambda}{\left\{ 1 - \left(\frac{\lambda}{3.412R} \right)^2 \right\}^{1/2}} \qquad (5-3)$$

the reflection coefficient can be expressed in term of $\frac{B}{Y_o}$ as:

$$\rho = \frac{\frac{1}{2} \left| \frac{B}{Y_o} \right|}{\left\{ 1 + \left(\frac{B}{2Y_o} \right)^2 \right\}^{1/2}} \qquad (5-4)$$

and the return loss in dB is,

$$\text{return loss} = -20 \log_{10} (\rho) \qquad (5-5)$$

Measurements of the return loss taken at $\lambda = 3.20$ cm in a circular guide of $\frac{15}{16}$ in. diameter and the centered aperture metallic plate of $\frac{1}{32}$ in. thickness with various sizes of diameter of the aperture are shown in Figure 5.5-3 in Reference 3, Section 5.5 page 243 to 246 in term of $\frac{B}{Y_o}$. In the computer code, the circular aperture of finite thickness is modeled as a circular guide with smaller diameter than the main guide, and its length is the thickness of the aperture. This is a three regions on-axis circular to circular transition. The

35

Cross Sectional View   Side View   Equivalent Circuit
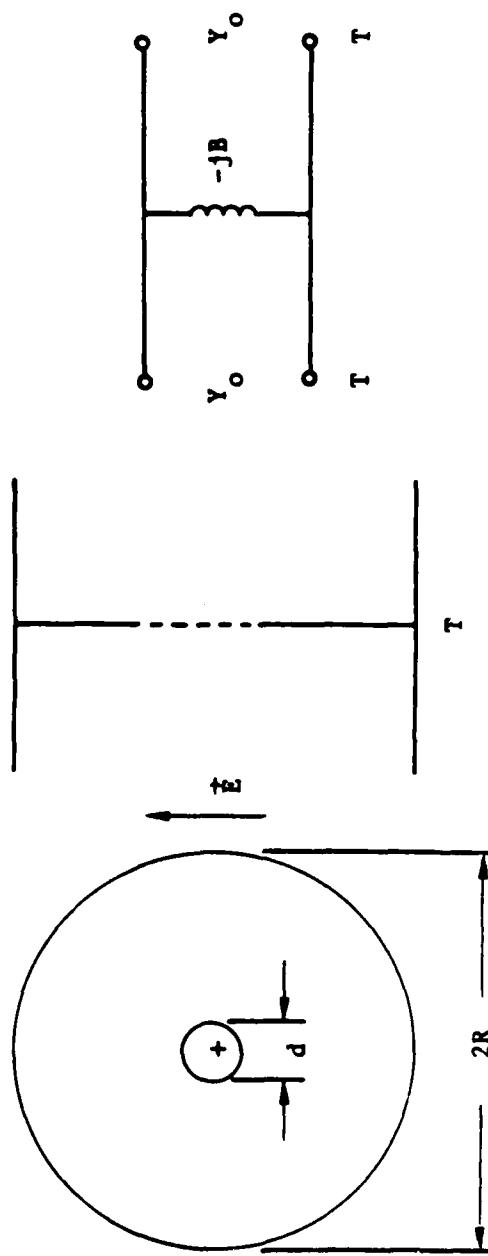
Figure 5-7. Centered Circular Aperture of Finite Thickness in Circular Guide.

diameter of 23.812 mm and the length of 100.0 mm are the dimensions
of the first and the last regions. The length of the middle region
is 0.794 mm, and the diameter varies from 6.35 mm to 23.019 mm. The
model of the transition is depicted in Figure 5-8. The theoretical
and the experimental results extrapolated from the graphs (Figure
5.5-3) in Reference 3 are compared to the numerical results and
listed in Table 5-3.

Disregarding the results at the point size aperture and at the
limit of the size of the aperture approaching the size of the main
guide, the experimental and the numerical results agree very well
within the average of +2.5 dB and −0.04 dB. Where at the point size
aperture, it is seen that the numerical result is about 0.009 dB less
than the experimental result. The probable cause is an insufficient
number of higher order modes in the modal expansion. It can be
explained that a point size aperture which can be interpreted as a
Dirac delta function has a spatial Fourier representation of an
infinite sum of harmonic components where the modal expansion technique
starts to break down. Likewise, at the limit of the size of the
aperture approaching the size of the guide, the numerical result is
roughly 11 dB higher than the experimental result. It suggested that
for this low scale of VSWR's reading, the measured data obtained from
Reference 3 was inaccurate. This is perhaps due to the insensitivity
of the equipment available at that time. Also 36 dB and 47 dB are
equivalent to 1.6% and 0.45% reflection coefficient respectively.
This error is less than 1.2% in absolute terms.

37
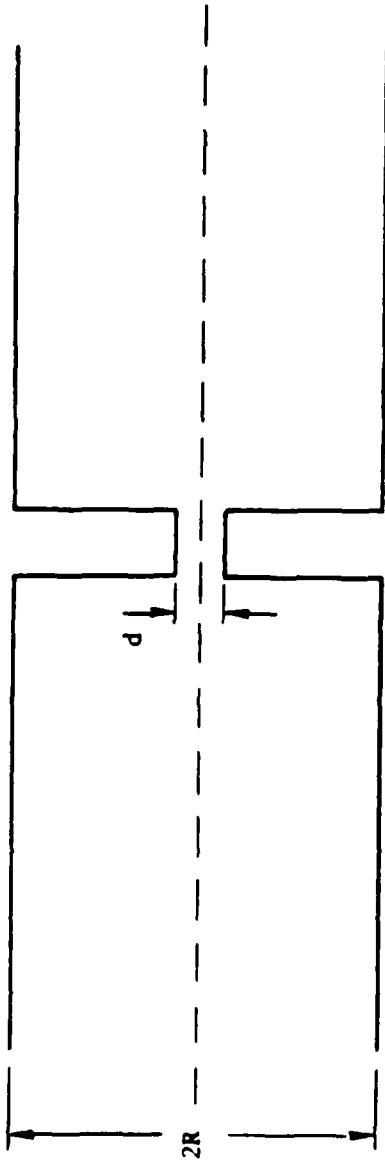
Figure 5-8. Three Regions On-Axis Circular to Circular Transition (Model of a Centered Circular Aperture of Finite Thickness in Circular Guide).

Table 5-3. Return Loss of a Circular Aperature in a Circular Guide of 15/16 in. Diameter

Return Loss (dB)

16 d (in)	Theoretical	Experimental	Numerical	Ratio in dB
4	0.0117	0.0141	0.0049	− 0.0092
5	0.0506	0.0180	0.0260	+ 0.0080
6	0.1837	0.1097	0.1067	− 0.0030
7	0.6189	0.4299	0.3644	− 0.0655
8	2.0437	1.1682	1.0820	− 0.0862
9	6.6540	2.8036	2.7454	− 0.0582
10		5.5145	5.8259	+ 0.3114
11		9.6205	10.0786	+ 0.4581
12		14.6900	15.5396	+ 0.8496
13		22.2399	22.7566	+ 0.5167
14		28.6419	33.3532	+ 4.7113
14.5		35.9187	46.9358	+11.0171

Note that the ratio in dB is defined as $-20 \log_{10} \dfrac{\rho_{Numerical}}{\rho_{Experimental}}$

VI. CONCLUSION

The modal expansion technique was found to be capable of handling any system of uniform waveguides interconnected by abrupt junctions. The computer codes developed for the asymmetrical modes on-axis transition and all modes off-axis transition have been tested and verified through two separate experimental verifications. The results obtained are satisfactory. Also, the numerical convergence criteria has been tested. Violation of the criteria has been shown of giving inaccurate solutions. Formulation of the two-sided boundary transition has been derived. The implementation of this formulation requires modification of the structure of the matrix equation of the existing code. To expand the capability and the versatility of the code, future work should also include the implementation of ridged waveguide, dielectric loaded waveguide and multiport junctions.

Appendix A: Derivation of the Matrix Equation

A very detailed derivation of matrix equations of a two-sided
boundary junction is presented in this appendix. This generalized
transition has conducting boundary on both sides of the junction.
The transition discussed in Reference 4 was restricted to only one
side of having a conducting wall.

A single junction of two-sided boundary is illustrated in Figure
A-1.
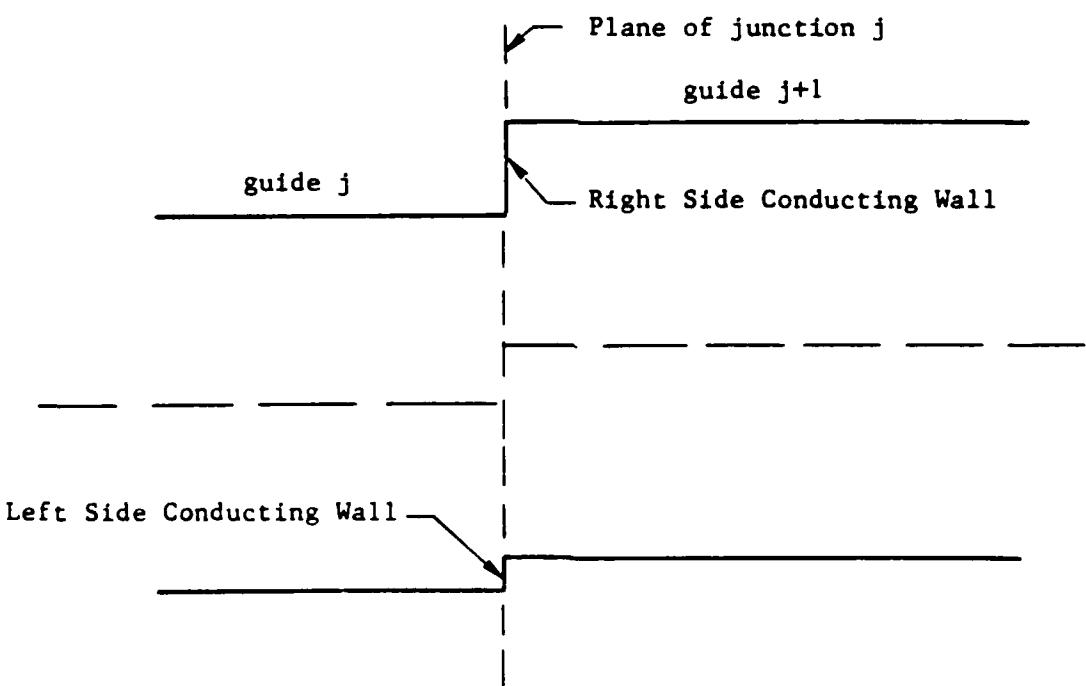
Figure A-1. Longitudinal View of a Two-Sided Boundary Off-Axis
Transition.

The guide j represents the input guide and the guide j+1 is the output guide. The junction is viewed as one transition of possibly many transitions preceding the guide j and following the guide j+1. In general, one source term per mode is allowed anywhere along the length of each section. Figure A-2 shows the forward going wave, the backward going wave, and the source term of a single region j.
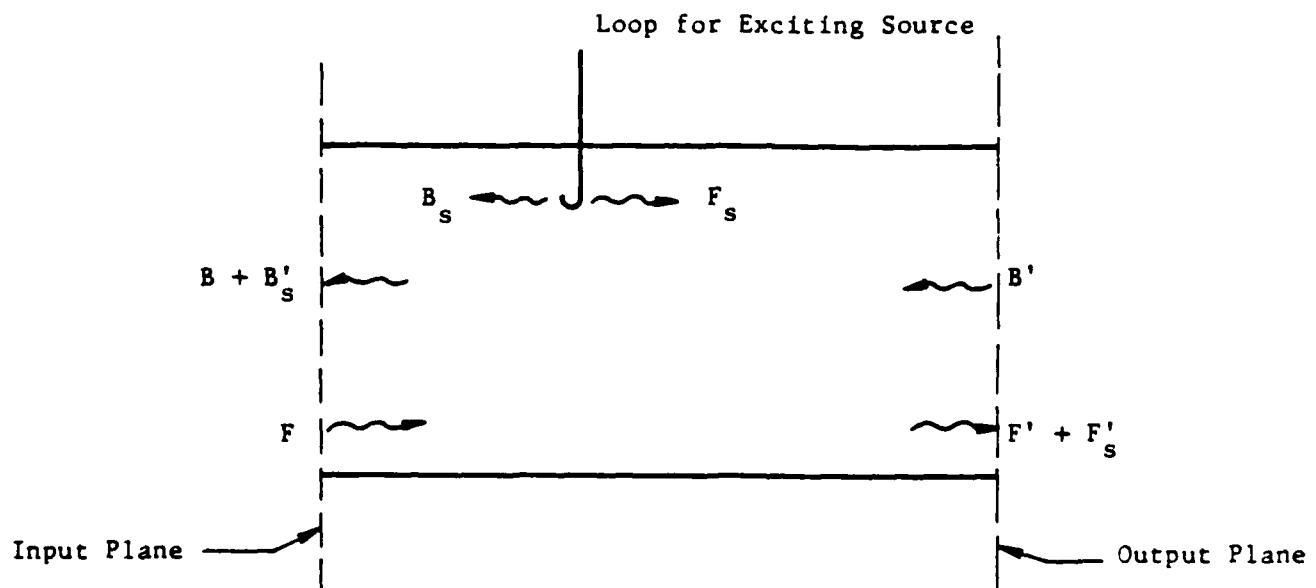
Figure A-2. A Single Region j Showing the Forward Going Wave, the Backward Going Wave, and the Source.

42

The forward mode amplitude, F, and the backward mode amplitude, B',
are the response of this cavity to the defined source terms F_s and
B_s. These terms F and B' are the solutions to the matrix equation
discussed in Chapter II.

The fields at any location along any waveguide region can be
expressed in terms of the sum of orthogonal functions weighed by
their respective mode amplitudes and propagation terms.

For a single junction as shown in Figure A-1, the total transverse
electromagnetic fields are given,

At the input plane of guide j+1:

$$\vec{E}_t\,(j+1) = \sum_{k_{j+1}=1}^{N(j+1)} \left\{ F\,(k_{j+1},\ j+1) + B\,(k_{j+1},\ j+1) + B_s'\,(k_{j+1},\ j+1) \right\} \cdot$$

$$\overline{e}\,(k_{j+1},\ j+1) \qquad\qquad (A-1)$$

$$\vec{H}_t\,(j+1) = \sum_{k_{j+1}=1}^{N(j+1)} \frac{1}{Z(k_{j+1},\ j+1)} \left\{ F\,(k_{j+1},\ j+1) - B\,(k_{j+1},\ j+1) - \right.$$

$$\left. B_s'\,(k_{j+1},\ j+1) \right\} \cdot \overline{h}\,(k_{j+1},\ j+1) \qquad (A-2)$$

At the output plane of guide j:

$$\vec{E}_t'\,(j) = \sum_{k_j=1}^{N(j)} \left\{ F'\,(k_j,j) + B'\,(k_j,j) + F_s'\,(k_j,j) \right\} \cdot \overline{e}\,(k_j,j) \quad (A-3)$$

$$\vec{H}_t'\,(j) = \sum_{k_j=1}^{N(j)} \frac{\overline{h}\,(k_j,j)}{Z\,(k_j,j)} \left\{ F'\,(k_j,j) - B'\,(k_j,j) + F_s'\,(k_j,j) \right\}$$

$$(A-4)$$

Where K_j, K_{j+1} are mode indicies for an arbitrary set of N(j), N(j+1)
modes.

At the junction, the transverse fields of the two regions must be matched at various areas. Let cs(j) and cs(j+1) be the cross-sectional area of regions j and j+1 respectively. And A(j, j+1) is the common cross-sectional area at the junction j between regions j and j+1. In the common cross-sectional area:

$$\vec{E}_t^{\,'}(j) = \vec{E}_t(j+1) \tag{A-5}$$

$$\vec{H}_t^{\,'}(j) = \vec{H}_t(j+1) \tag{A-6}$$

On the left side of the conducting wall:

$$\vec{E}_t^{\,'}(j) = 0 \tag{A-7}$$

On the right side of the conducting wall:

$$\vec{E}_t(j+1) = 0 \tag{A-8}$$

Two possible pairs of equations may be derived from equations (A-5) and (A-6) by using either (A-7) or (A-8). To cast the equations in a more useful form, the following manipulations are used. First consider the use of (A-7). Scalar vector multiplication of equations (A-5) and (A-7) by $\displaystyle\sum_{k_j'=1}^{N(j)} \bar{e}\,(k_j',j)$ yields:

$$\vec{E}_t^{\,'}(j) \cdot \sum_{k_j'=1}^{N(j)} \bar{e}\,(k_j',j) = \vec{E}_t(j+1) \cdot \sum_{k_j'=1}^{N(j)} \bar{e}\,(k_j',j) \tag{A-9}$$

(in the aperture)

$$\vec{E}_t^{\,'}(j) \cdot \sum_{k_j'=1}^{N(j)} \bar{e}\,(k_j',j) = 0 \tag{A-10}$$

(on the left conducting wall)

Post vector multiplication of equation (A-6) by $\sum\limits_{k'_{j+1}=1}^{N(j+1)} \overline{e}\,(k'_{j+1},\,j+1)$

yields:

$$\vec{H}_t'\,(j) \times \sum_{k'_{j+1}=1}^{N(j+1)} \overline{e}\,(k'_{j+1},\,j+1) = \vec{H}_t\,(j+1) \times \sum_{k'_{j+1}=1}^{N(j+1)} \overline{e}\,(k'_{j+1},\,j+1) \quad (A-11)$$

(in the aperture)

The integration of equation (A-9) over the common cross-sectional area, added to the integration of equation (A-10) over the left conducting wall gives:

$$\iint\limits_{cs(j)} \vec{E}_t'\,(j) \cdot \sum_{k'_j=1}^{N(j)} \overline{e}\,(k'_j,j)\, ds = \iint\limits_{A(j,\,j+1)} \vec{E}_t\,(j+1) \cdot \sum_{k'_j=1}^{N(j)} \overline{e}\,(k'_j,j)\, ds \quad (A-12)$$

The integration of equation (A-11) over the common cross-sectional area yields:

$$\iint\limits_{A(j,\,j+1)} \left[\vec{H}_t'\,(j) \times \sum_{k'_{j+1}=1}^{N(j+1)} \overline{e}\,(k'_{j+1},\,j+1)\right] \cdot d\overline{s} = \iint\limits_{A(j,\,j+1)} \left[\vec{H}_t\,(j+1) \times \sum_{k'_{j+1}=1}^{N(j+1)} \right.$$

$$\left. \overline{e}\,(k'_{j+1},\,j+1)\right] \cdot d\overline{s} \quad (A-13)$$

Substituting (A-1), (A-2), (A-3), and (A-4) into (A-12) and (A-13) gives:

$$\sum_{k_j=1}^{N(j)} \sum_{k'_j=1}^{N(j)} \left\{F'\,(k_j,\,j) + B'\,(k_j,j) + F_s'\,(k_j,j)\right\} \cdot$$

$$\iint\limits_{cs(j)} \overline{e}\,(k_j,j) \cdot \overline{e}\,(k'_j,j)\, ds =$$

$$\sum_{k'_j=1}^{N(j)} \sum_{k_{j+1}=1}^{N(j+1)} \left\{F\,(k_{j+1},\,j+1) + B\,(k_{j+1},\,j+1) + B_s'\,(k_{j+1},\,j+1)\right\} \cdot$$

$$\iint\limits_{A(j,\,j+1)} \overline{e}\,(k'_j,j) \cdot \overline{e}\,(k_{j+1},\,j+1)\, ds \quad (A-12)$$

45

$$\sum_{k_j = 1}^{N(j)} \sum_{k'_{j+1} = 1}^{N(j+1)} \frac{1}{Z(k_j,j)} \left\{ F'(k_j,j) - B'(k_j,j) + F'_s(k_j,j) \right\} \cdot$$

$$\iint_{A(j,\ j+1)} \left[\overline{h}(k_j,j) \times \overline{e}(k'_{j+1},\ j+1) \right] \cdot d\overline{s} =$$

$$\sum_{k_{j+1}}^{N(j+1)} \sum_{k'_{j+1} = 1}^{N(j+1)} \frac{1}{Z(k_{j+1},\ j+1)}$$

$$\cdot \left\{ F(k_{j+1},\ j+1) - B(k_{j+1},\ j+1) - B'_s(k_{j+1},\ j+1) \right\} \cdot$$

$$\iint_{A(j,\ j+1)} \left[\overline{h}(k_{j+1},\ j+1) \times \overline{e}(k'_{j+1},\ j+1) \right] \cdot d\overline{s} \qquad (A-13)$$

Applying the orthogonality conditions of the eigen modes,

$$\iint_{A(j,\ j+1)} \left[\overline{h}(k_j,j) \times \overline{e}(k'_{j+1},\ j+1) \right] \cdot d\overline{s} = - \iint_{A(j,\ j+1)} \overline{e}(k_j,j) \cdot \overline{e}(k'_{j+1},\ j+1) ds$$

$$\iint_{A(j,\ j+1)} \left[\overline{h}(k_{j+1},\ j+1) \times \overline{e}(k'_{j+1},\ j+1) \right] \cdot d\overline{s} = - \iint_{A(j,\ j+1)} \overline{e}(k_{j+1},\ j+1) \cdot$$

$$\overline{e}(k'_{j+1},\ j+1)\ ds$$

And using the definition for the overlap and cross-overlap integrals found in Table A-1, (A-12) and (A-13) become:

$$\sum_{k_j = 1}^{N(j)} \left\{ F'(k_j,j) + B'(k_j,j) + F'_s(k_j,j) \right\} =$$

$$\sum_{k_j = 1}^{N(j)} \sum_{k_{j+1} = 1}^{N(j+1)} \left\{ F(k_{j+1},\ j+1) + B(k_{j+1},\ j+1) + \right.$$

$$\left. B'_s(k_{j+1},\ j+1) \right\} O.I.\ (k_j,\ k_{j+1},j) \qquad (A-12a)$$

$$\sum_{k_j=1}^{N(j)} \sum_{k_{j+1}=1}^{N(j+1)} \frac{O.I. \ (k_j, \ k_{j+1}, j)}{Z \ (k_j, \ j)} \left\{ F^{'} \ (k_j, j) - B^{'} \ (k_j, j) + F_s^{'} \ (k_j, j) \right\} =$$

$$\sum_{k_{j+1}=1}^{N(j+1)} \sum_{k_{j+1}^{'}=1}^{N(j+1)} \frac{C.O.I. \ (k_{j+1}, \ k_{j+1}^{'}, \ j)}{Z \ (k_{j+1}, \ j+1)} \left\{ F \ (k_{j+1}, \ j+1) - B \ (k_{j+1}, \ j+1) - \right.$$
$$\left. B_s^{'} \ (k_{j+1}, \ j+1) \right\} \qquad \text{(A-13a)}$$

Second consider the use of (A-8). Using completely the symmetric

manipulations, the following dual to equations (A-12a) and (A-13a)

are obtained.

$$\sum_{k_j=1}^{N(j)} \sum_{k_j^{'}=1}^{N(j)} \frac{C.O.I. \ (k_j, \ k_j^{'}, \ j)}{Z \ (k_j, k)} \left\{ F^{'} \ (k_j, j) - B^{'} \ (k_j, \ j) + F_s^{'} \ (k_j, j) \right\} =$$

$$\sum_{k_j=1}^{N(j)} \sum_{k_{j+1}=1}^{N(j+1)} \frac{O.I. \ (k_j, \ k_{j+1}, \ j)}{Z \ (k_{j+1}, \ j+1)} \left\{ F \ (k_{j+1}, \ j+1) - B \ (k_{j+1}, \ j+1) - \right.$$
$$\left. B_s^{'} \ (k_{j+1}, \ j+1) \right\} \qquad \text{(A-12b)}$$

$$\sum_{k_j=1}^{N(j)} \sum_{k_{j+1}=1}^{N(j+1)} \left\{ F^{'} \ (k_j, j) + B^{'} \ (k_j, j) + F_s^{'} \ (k_j, j) \right\} O.I. \ (k_j, \ k_{j+1}, \ j) =$$

$$\sum_{k_{j+1}=1}^{N(j+1)} \left\{ F \ (k_{j+1}, \ j+1) + B \ (k_{j+1}, \ j+1) + B_s^{'} \ (k_{j+1}, \ j+1) \right\} \qquad \text{(A-13b)}$$

Both pair of the equations (A-12a), (A-13a), and (A-12b), (A-13b) can

be written in matrix form as:

$$M_\alpha \ \overline{x} \ = \ \overline{b}_\alpha \qquad \text{(A-14)}$$

Where α = a or b

47

The matrix M_α, vectors $\bar{x}$ and $\bar{b}_\alpha$ are shown in Figure A-3. Where the submatrices and subvectors are shown in Figures A-4 through A-16. For the case of single, two, and J junctions, the structures of the matrix equations are shown in Figures A-17 through A-19.

Both these sets of equations should have the same solution in the limit of an infinite number of modes. The similarity of these equations to the single sided boundary equations derived in Reference 4 is demonstrated. First examine the equations (A-12a) and (A-13a) in the limit of the area of the right wall going to zero.

Since,

$$\begin{aligned} &\text{limit} \\ &\text{area of right wall} \to 0 \end{aligned} \iint\limits_{A(j,\,j+1)} \bar{e}\,(k_{j+1},\,j+1) \cdot \bar{e}\,(k'_{j+1},\,j+1)\,ds =$$

$$\iint\limits_{cs(j+1)} \bar{e}\,(k_{j+1},\,j+1) \cdot \bar{e}\,(k'_{j+1},\,j+1)\,ds =$$

$$\begin{cases} 1 & \text{if } k_{j+1} = k'_{j+1} \\ 0 & \text{if } k_{j+1} \neq k'_{j+1} \end{cases} \qquad (A-15)$$

Then, equations (A-12a) and (A-13a) become a pair of equations derived for larger-to-smaller transition defined in Reference 4. Similarly, it can be shown that in the limit of the area of the left wall going to zero, the equations (A-12b) and (A-13b) are equivalent to another pair of equations derived for smaller-to-larger transition in Reference 4.

Since both sets of equations should yield the same result, any linear combination should also yield the same result. It is expected that the solutions to the equations (A-12a) and (A-13a) should converge

48

$$(\alpha = a \text{ or } b)$$

Equation (A12 α) in Matrix Form:

$$\begin{bmatrix} M_{j,j} \end{bmatrix} - \begin{bmatrix} M_{j,\,j+1} \end{bmatrix} \begin{bmatrix} x_j \\ x_{j+1} \end{bmatrix} = \begin{bmatrix} b_j \end{bmatrix}$$

Equation (A13 α) in Matrix Form:

$$\begin{bmatrix} M_{j+1,\,j} \end{bmatrix} - \begin{bmatrix} M_{j+1,\,j+1} \end{bmatrix} \begin{bmatrix} x_j \\ x_{j+1} \end{bmatrix} = \begin{bmatrix} b_{j+1} \end{bmatrix}$$

Figure A-3. Equations (A12 α) and (A13 α) in Matrix Form.

49

$$
\begin{bmatrix} M_{j,j} \end{bmatrix} \; = \; \begin{matrix} k_j \downarrow \end{matrix} \; \begin{bmatrix} G_f \; (k_j,j) & & \vdots & +1 & & 2N(j) \\ & & \bigcirc & & & & \bigcirc \\ & \bigcirc & & & \bigcirc & & \\ & & & & & & \\ N(j) & & & & & & \end{bmatrix}
$$
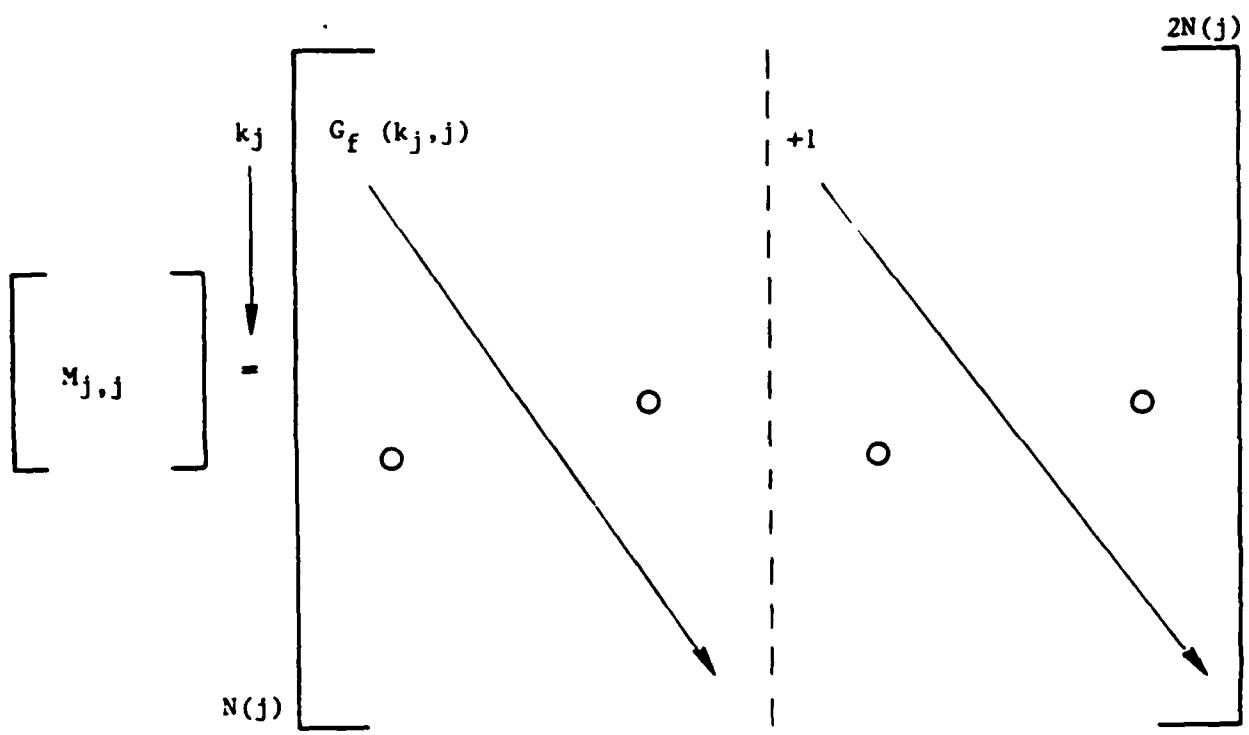
Figure A-4. Equation (A12a).
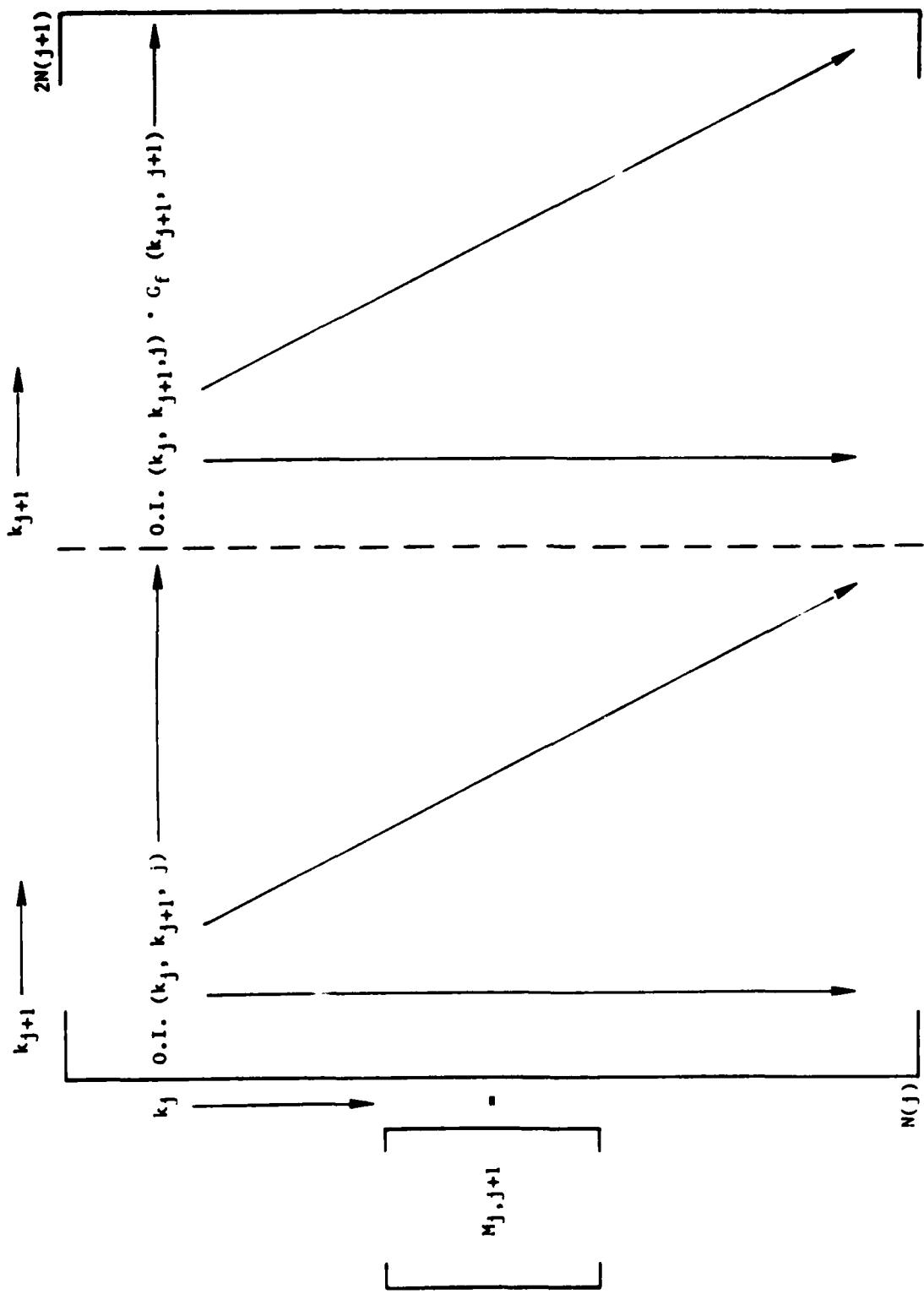
Figure A-5. Equation (A12a).

$$b_j = \left[-F'_s(k_j, j) + \sum_{k_{j+1}=1}^{N(j+1)} \left\{ B'_s(k_{j+1}, j+1) \cdot O.I. \, (k_j, k_{j+1}, j) \right\} \right]_{N(j)}$$

Figure A-6. Equation (A12a).
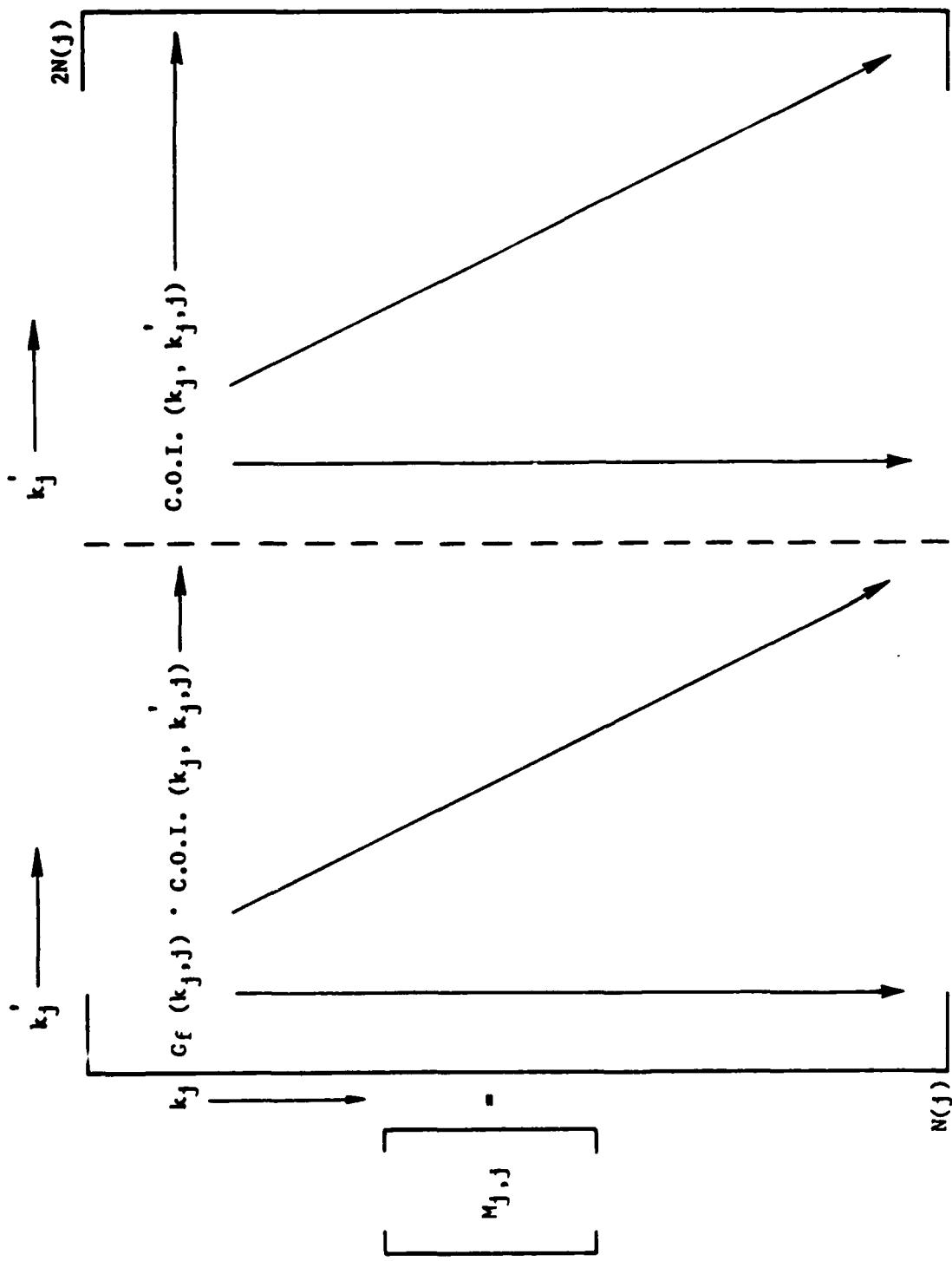
Figure A-7. Equation (A12b).

k_j'

C.O.I. (k_j, k_j', j)

$2N(j)$

k_j'

$G_f (k_j, j) \cdot$ C.O.I. (k_j, k_j', j)

$k_j \longrightarrow$

$M_{j,j}$

$N(j)$

53
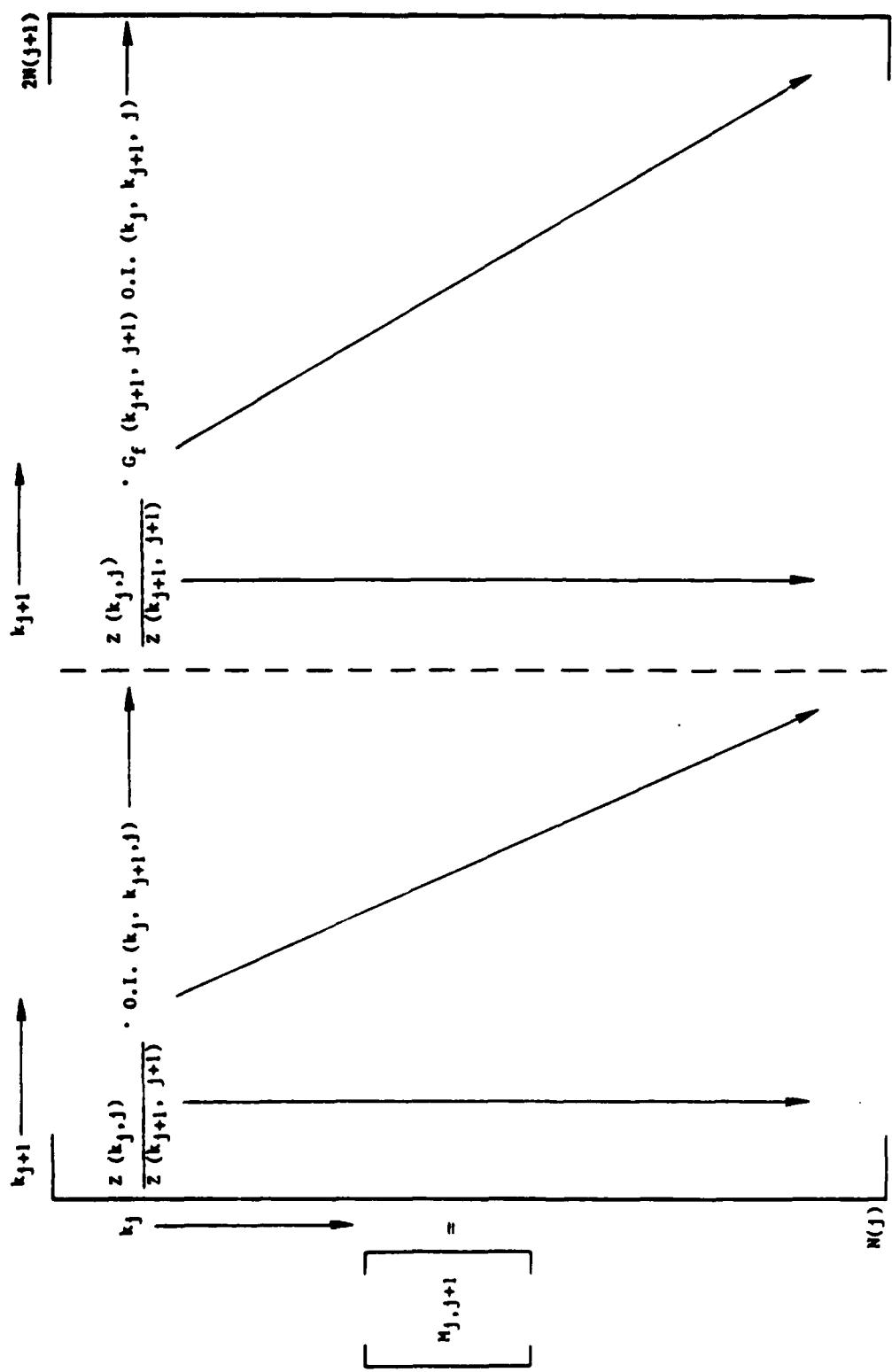
Figure A-8. Equation (A12b).

54

$$b_j = \left[-F_s'(k_j, j) \cdot \sum_{k_j=1}^{N(j)} \text{C.O.I.}(k_j, k',) - z(k_j, j) \cdot \sum_{k_{j+1}=1}^{N(j+1)} \left\{ B_s'(k_{j+1}, j+1) \cdot \frac{\text{O.I.}(k_j, k_{j+1}, j)}{z(k_{j+1}, j+1)} \right\}_{N(j)} \right]$$

Figure A-9. Equation (A12b).
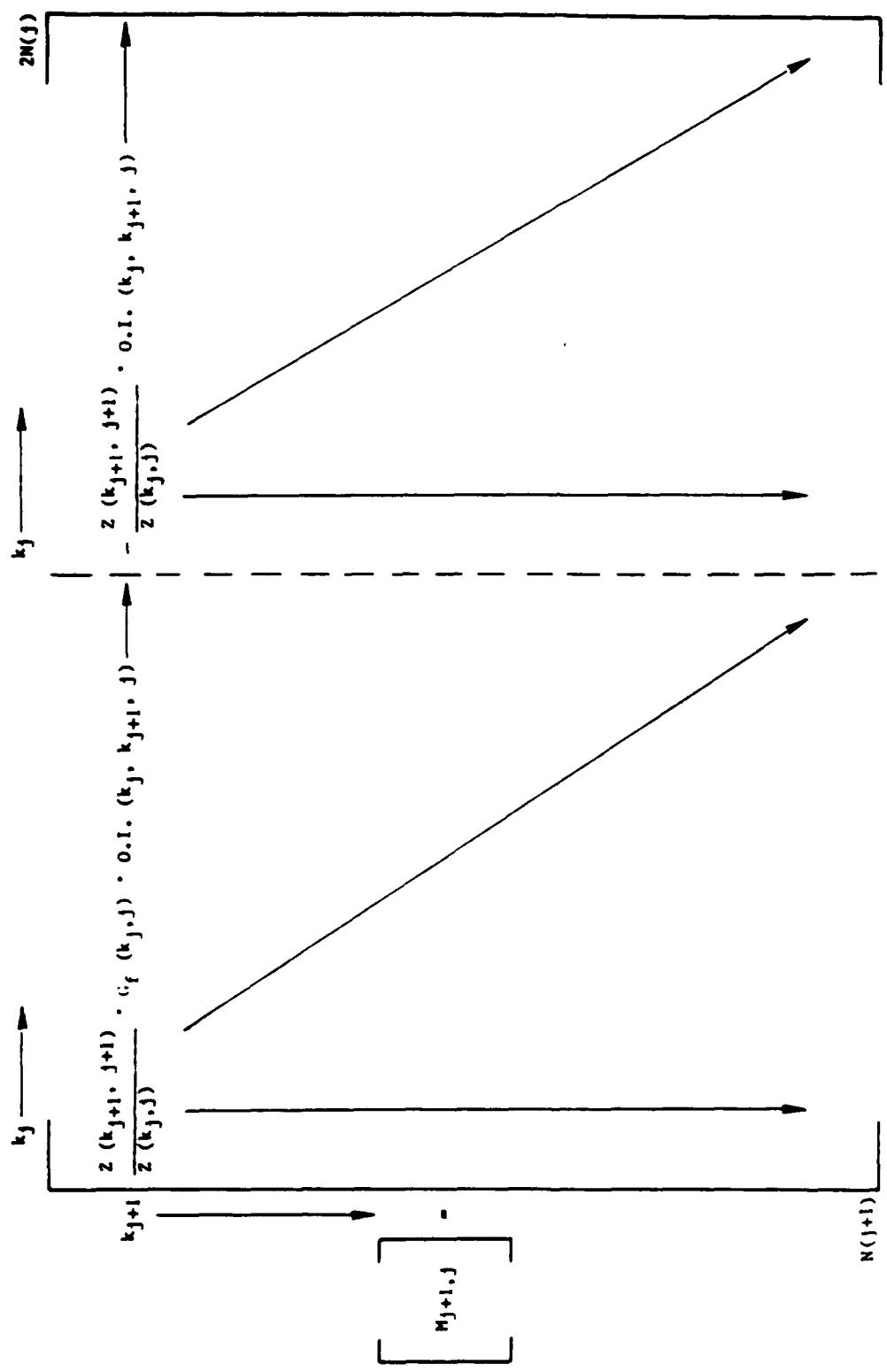
Figure A-10. Equation (A13a).
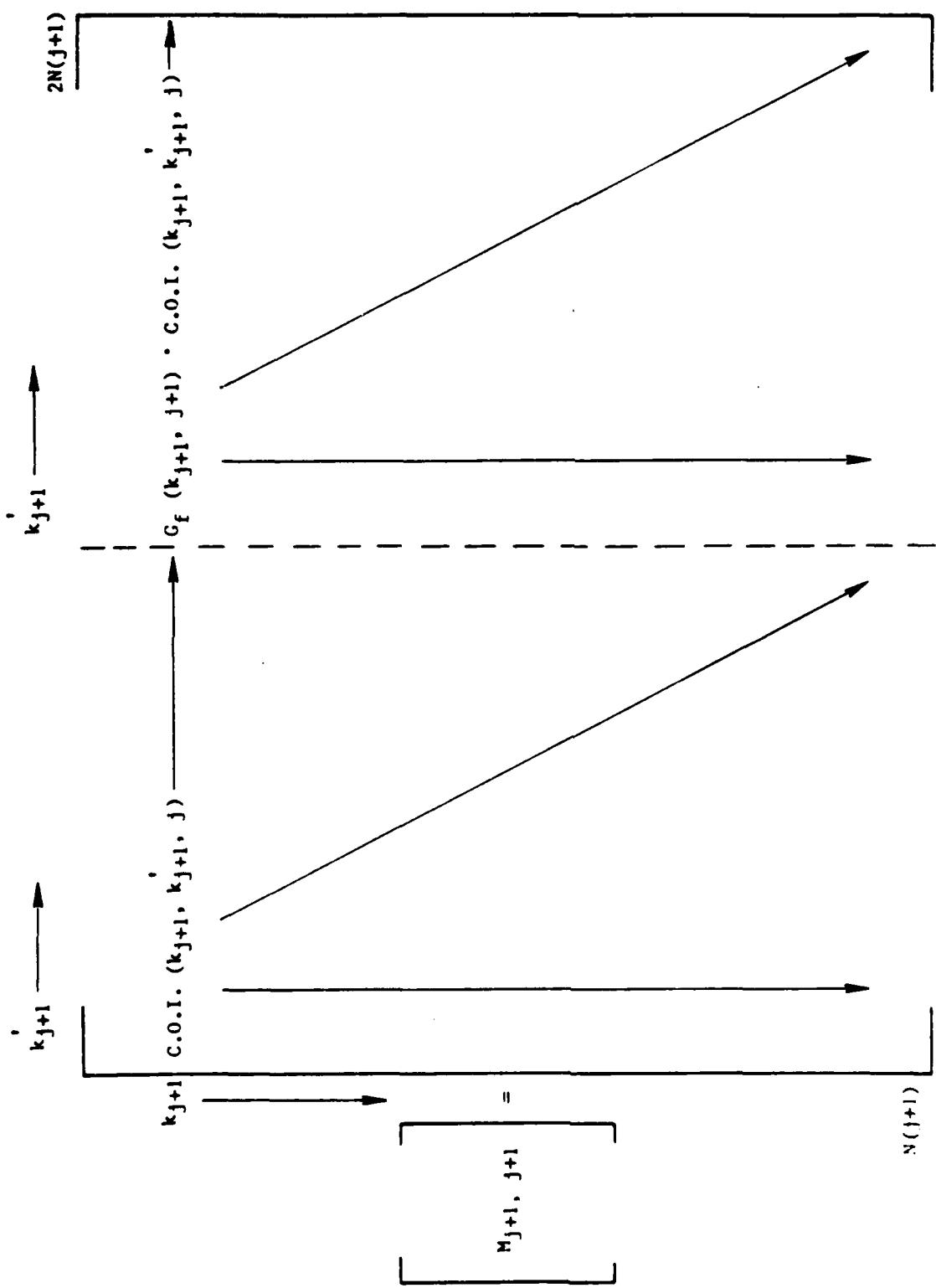
Figure A-11. Equation (A13a).

57

$$
b_{j+1} = \left[-\sum_{k_j=1}^{N(j)} \left\{ F_s'(k_j, j) \cdot \frac{Z(k_{j+1}, j+1)}{Z(k_j, j)} \cdot O.I.(k_j, k_{j+1}, j) \right\} - B_s'(k_{j+1}, j+1) \cdot \sum_{k_{j+1}'=1}^{N(j+1)} C.O.I.(k_{j+1}, k_{j+1}', j) \right]_{k_{j+1}=1}^{N(j+1)}
$$

Figure A-12. Equation (A13a).

58
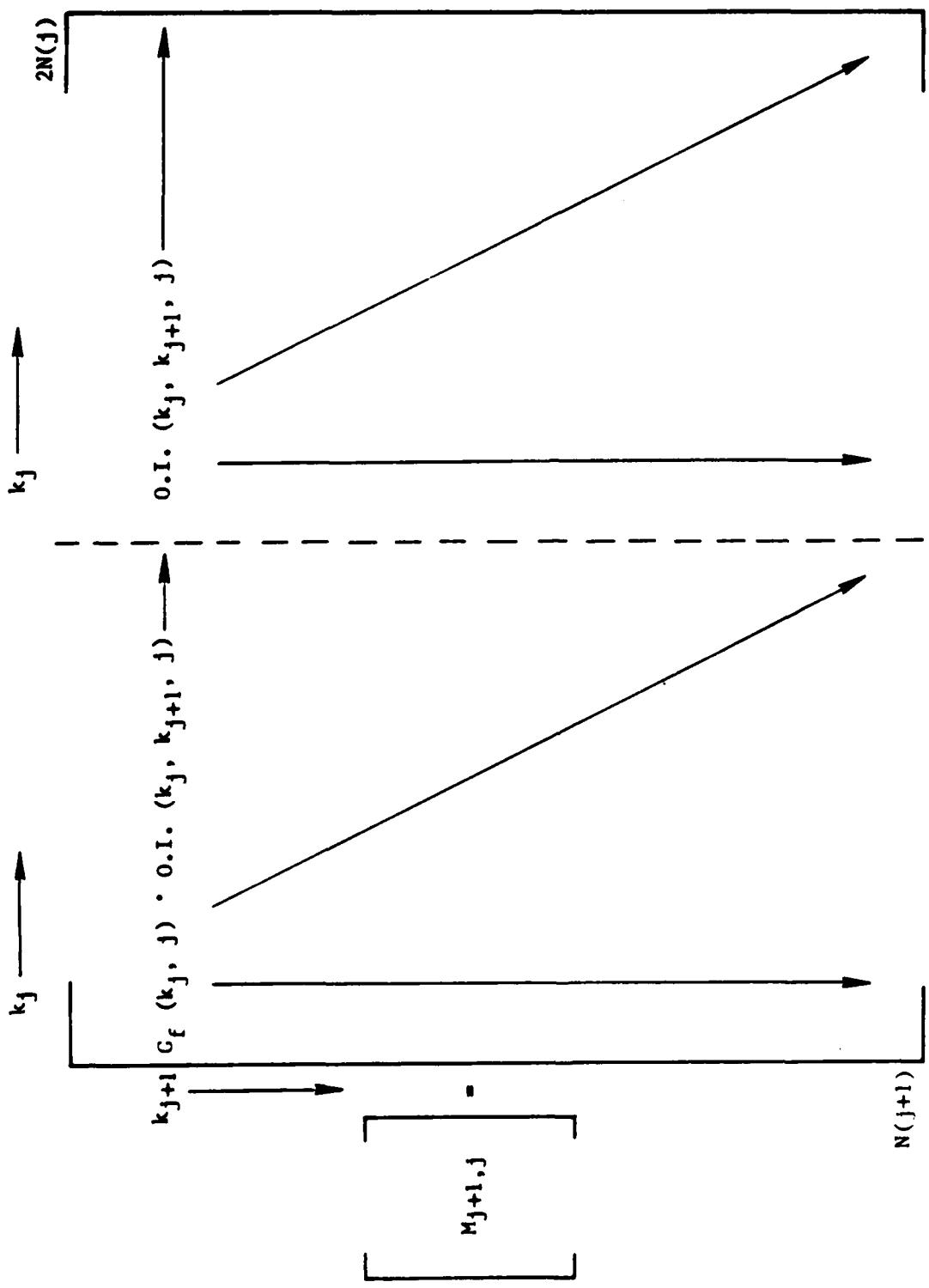
Figure A-13. Equation (A13b).
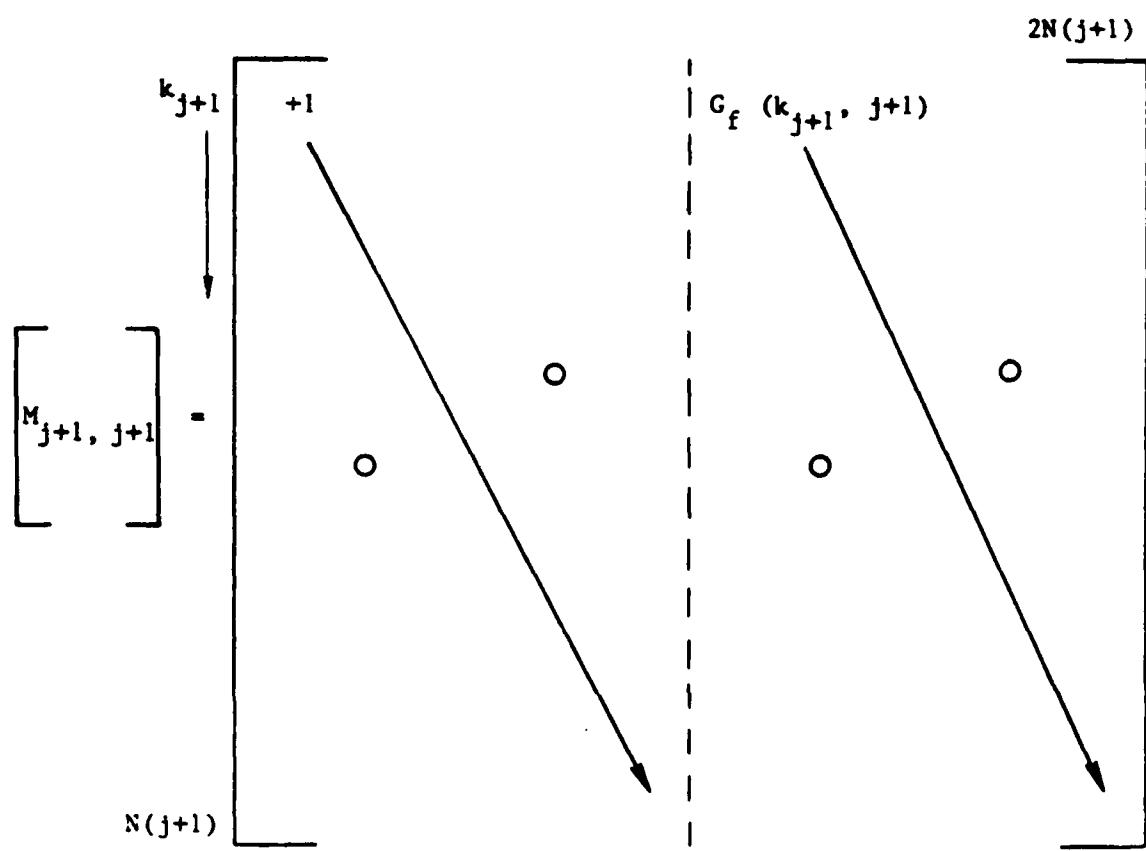
Figure A-14. Equation (A13b).

$$b_{j+1} = k_{j+1} \longrightarrow \left[-\sum_{k_j=1}^{N(j)} \left\{ F'_s(k_j, j) \cdot O.T.(k_j, k_{j+1}, j) \right\} + B'_s(k_{j+1}, j+1) \right]_{N(j+1)}$$

Figure A-15. Equation (A13b).

61
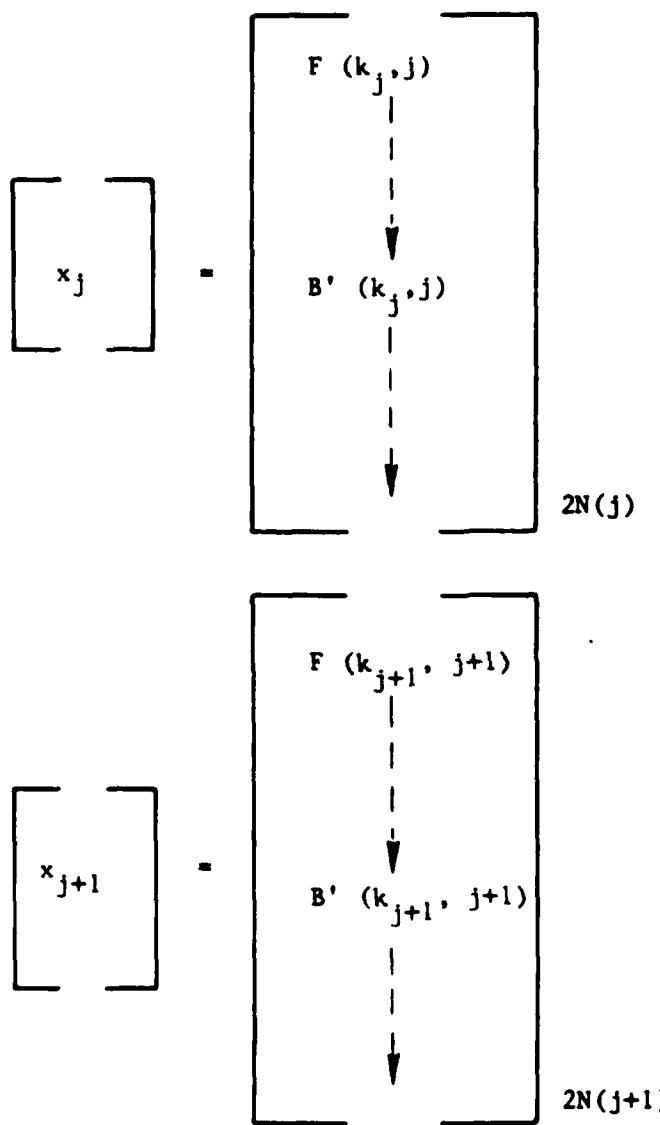
Figure A-16. Solution Subvectors.

$$
\begin{bmatrix}
M_{1,1} & -M_{1,2} \\
M_{2,1} & M_{2,2}
\end{bmatrix}
\begin{bmatrix}
x_1 \\
x_2
\end{bmatrix}
=
\begin{bmatrix}
b_1 \\
b_2
\end{bmatrix}
$$

Figure A-17. Single Junction Matrix.

$$
\begin{bmatrix}
\begin{bmatrix} M_{1,1} \end{bmatrix}^{2N(1)}_{N(1)} & \begin{bmatrix} -M_{1,2} \end{bmatrix}^{2N(2)}_{N(1)} & \Phi & \Phi \\
\begin{bmatrix} M_{2,1} \end{bmatrix}^{2N(1)}_{N(2)} & \begin{bmatrix} -M_{2,2} \end{bmatrix}^{2N(2)}_{N(2)} & \Phi & \Phi \\
\Phi & \begin{bmatrix} M_{3,2} \end{bmatrix}^{2N(2)}_{N(2)} & \begin{bmatrix} -M_{3,3} \end{bmatrix}^{2N(3)}_{N(2)} & \\
\Phi & \begin{bmatrix} M_{4,2} \end{bmatrix}^{2N(2)}_{N(3)} & \begin{bmatrix} -M_{4,3} \end{bmatrix}^{2N(3)}_{N(3)} &
\end{bmatrix}
\begin{bmatrix}
\begin{bmatrix} x_1 \end{bmatrix}^{2N(1)} \\
\begin{bmatrix} x_2 \end{bmatrix}^{2N(2)} \\
\begin{bmatrix} x_3 \end{bmatrix}^{2N(3)}
\end{bmatrix}
=
\begin{bmatrix}
\begin{bmatrix} b_1 \end{bmatrix}^{N(1)} \\
\begin{bmatrix} b_2 \end{bmatrix}^{N(2)} \\
\begin{bmatrix} b_3 \end{bmatrix}^{N(2)} \\
\begin{bmatrix} b_4 \end{bmatrix}^{N(3)}
\end{bmatrix}
$$

Figure A-18. Two Junctions Matrix.
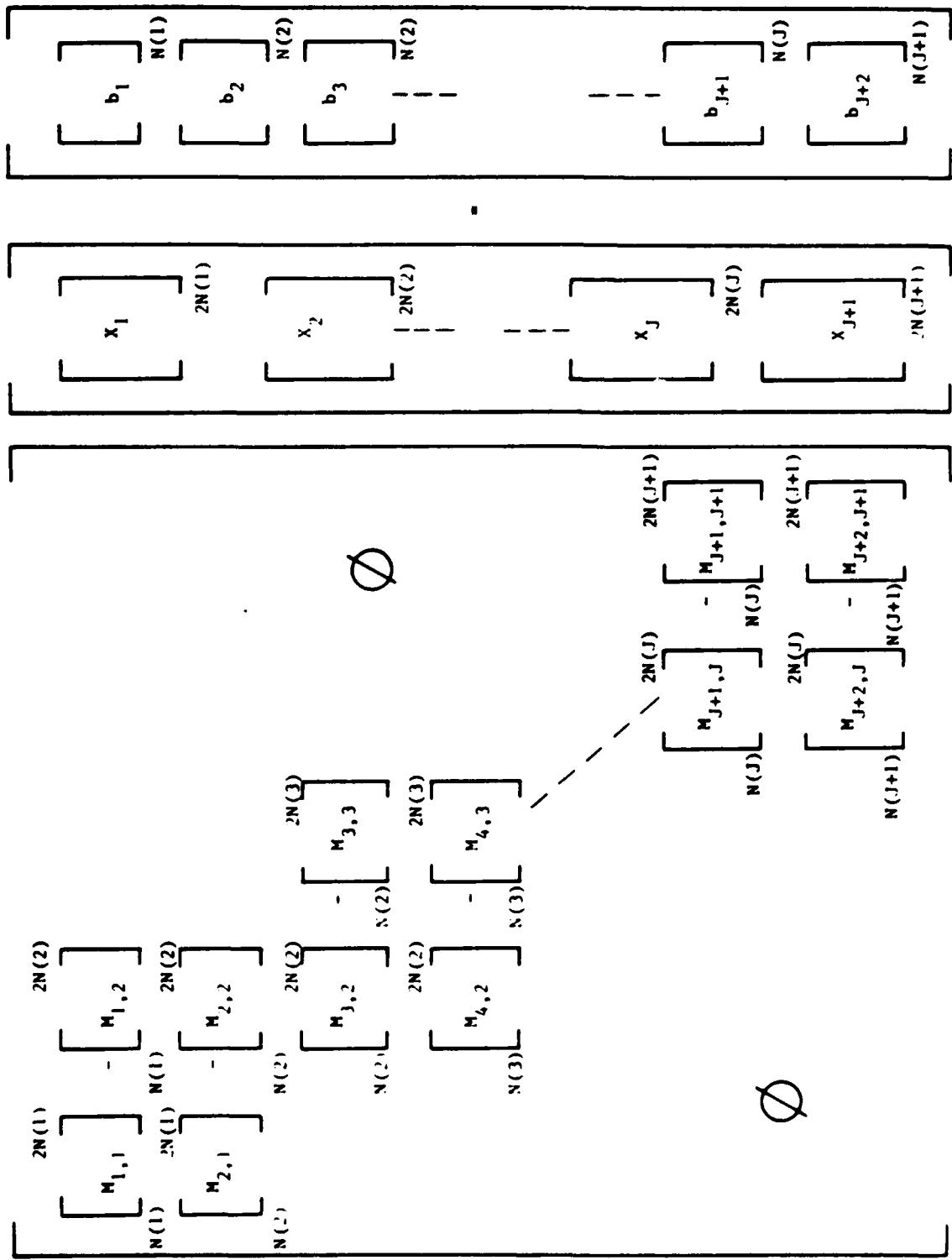
Figure A-19. J Junctions Matrix.

65

faster to the correct solutions as the number of modes per region is increased for junctions that have most of the conducting wall on the left side. Similarly one would expect the solutions to equations (A-12b) and (A-13b) to converge more rapidly to the right answers for junctions with most of the conducting wall on the right side of the boundary. Therefore, it would seem reasonable to make a linear combination of equations (A-12a), (A-13a) and (A-12b), (A-13b) where each term is weighted by the relative area of the conducting wall on each side.

Thus,

$$
\begin{aligned}
\omega_\ell * M_a \; \overline{x} &= \omega_\ell * \overline{b}_a \\
\omega_r * M_b \; \overline{x} &= \omega_r * \overline{b}_b
\end{aligned}
\tag{A-16}
$$

Where ω_ℓ and ω_r are defined by:

$$
\omega_\ell = \frac{\text{area of left wall}}{\text{area of left wall} + \text{area of right wall}}
$$

$$
\omega_r = \frac{\text{area of right wall}}{\text{area of left wall} + \text{area of right wall}}
\tag{A-17}
$$

After combining, it yields:

$$
\left\{ \omega_\ell * M_a + \omega_r * M_b \right\} \; \overline{x} = \omega_\ell * \overline{b}_a + \omega_r * \overline{b}_b
\tag{A-18}
$$

Where the submatrices and subvectors of (A-18) are shown in Figures A-20 through A-26 for a single junction.

The backward mode reflection coefficient for the first region that generates a forward going wave in the first region (not a source term) is normally defined for a given problem. Similarly, the forward mode reflection coefficient for the last region that generates a backward going wave in that last section is also a known quantity.

66
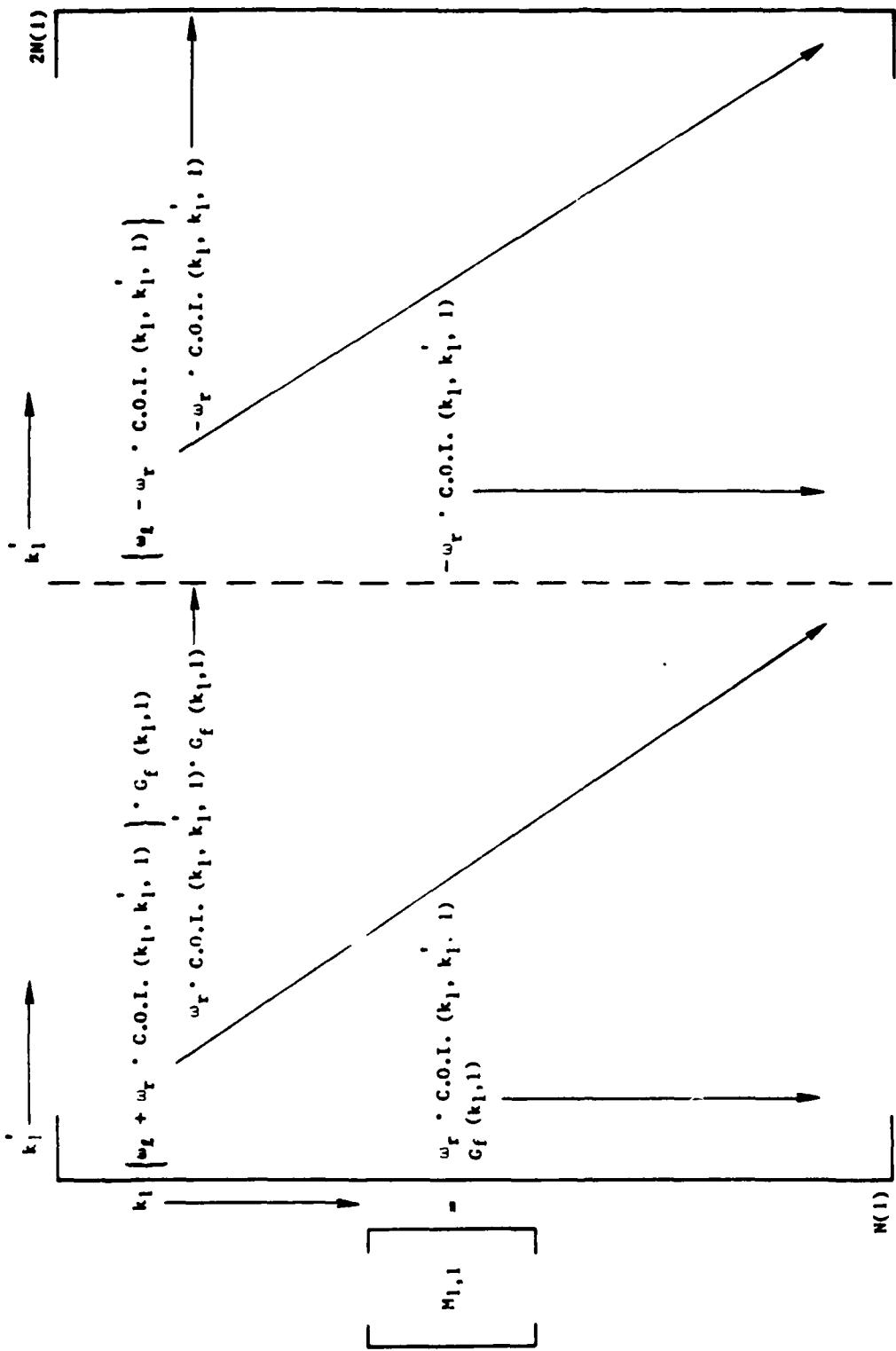
Figure A-20. Combined Equation (A12a + A12b).
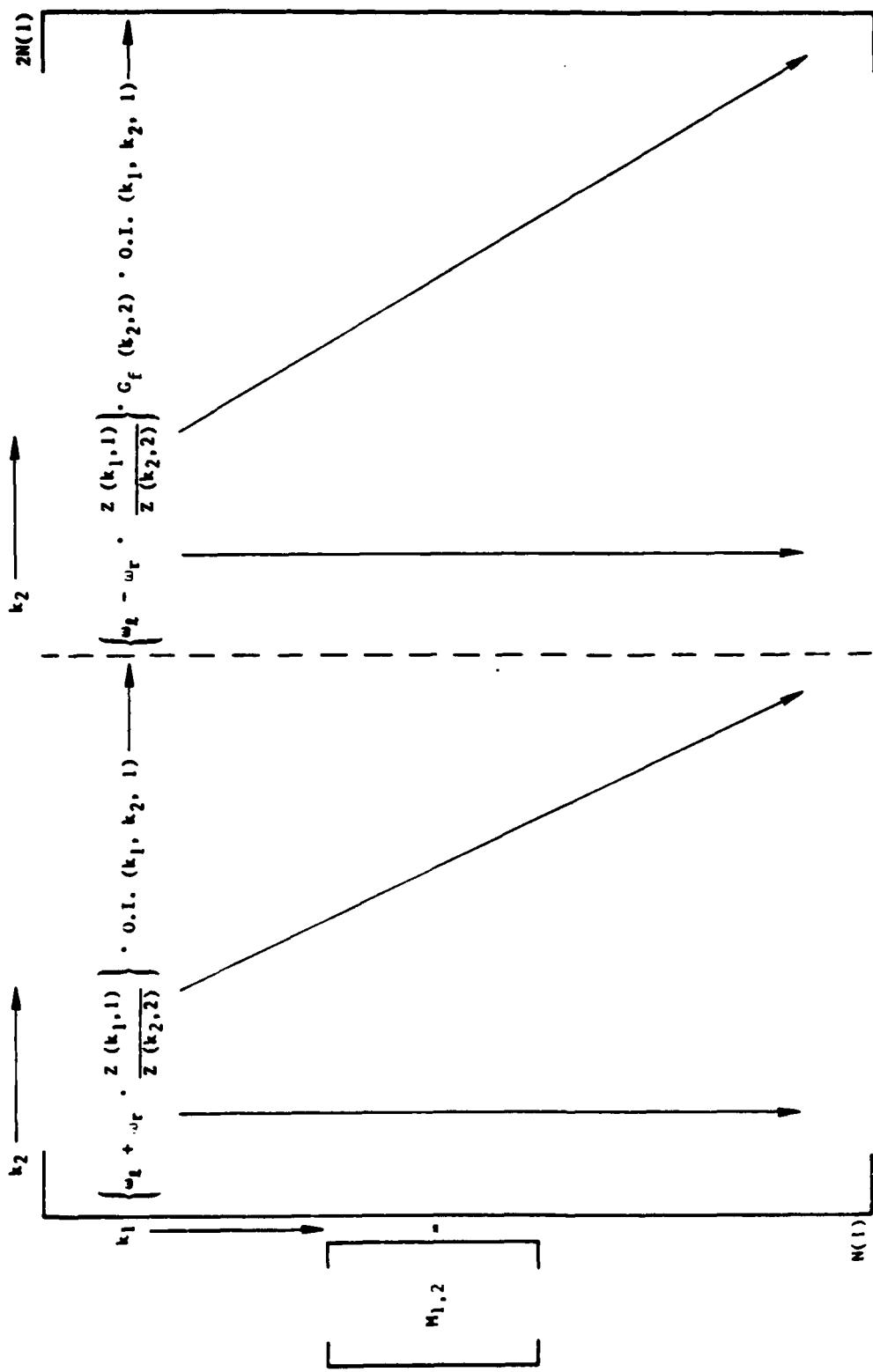
Figure A-21. Combined Equation (A12a + A12b).
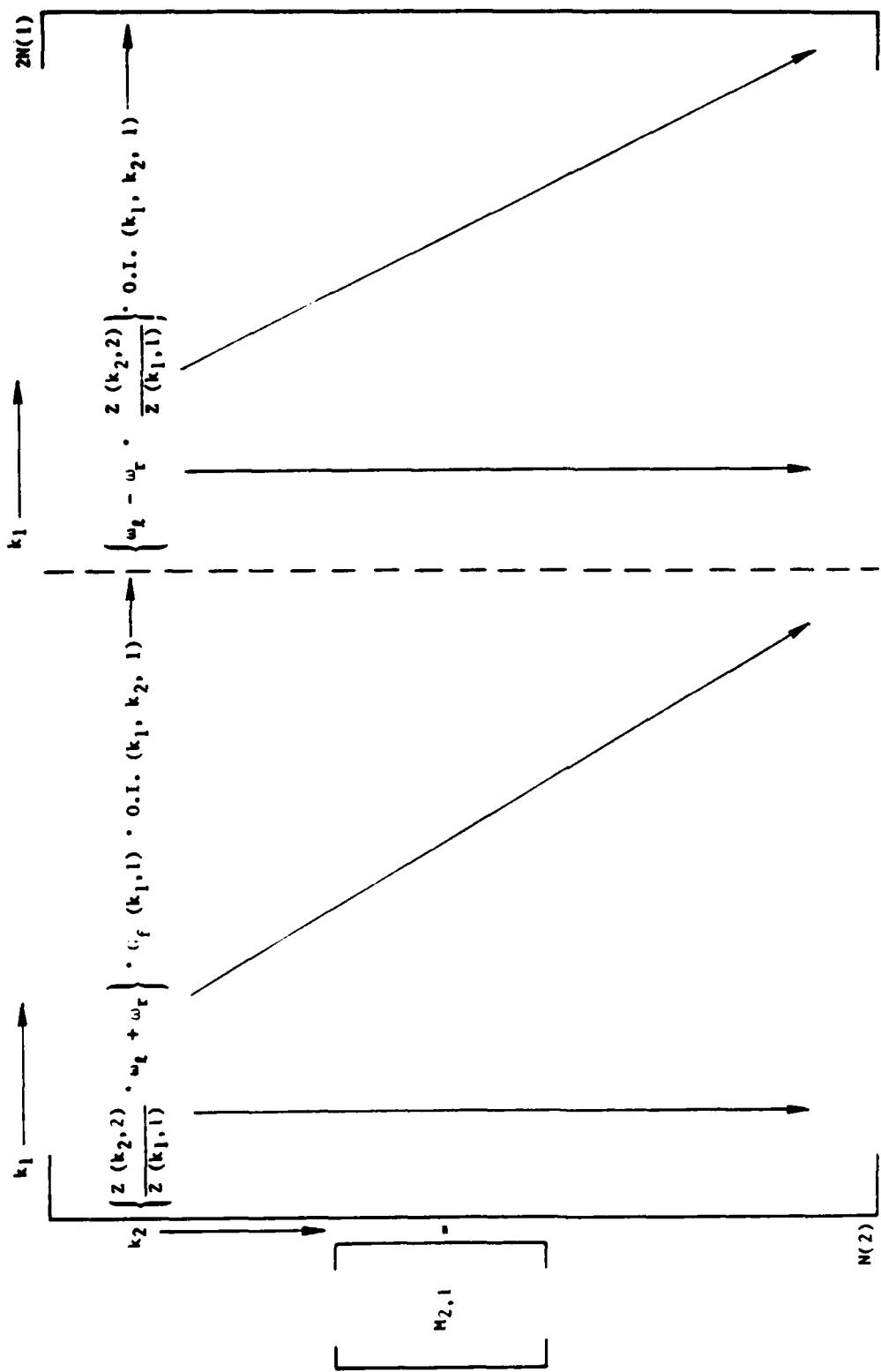
Figure A-22. Combined Equation (A13a + A13b).
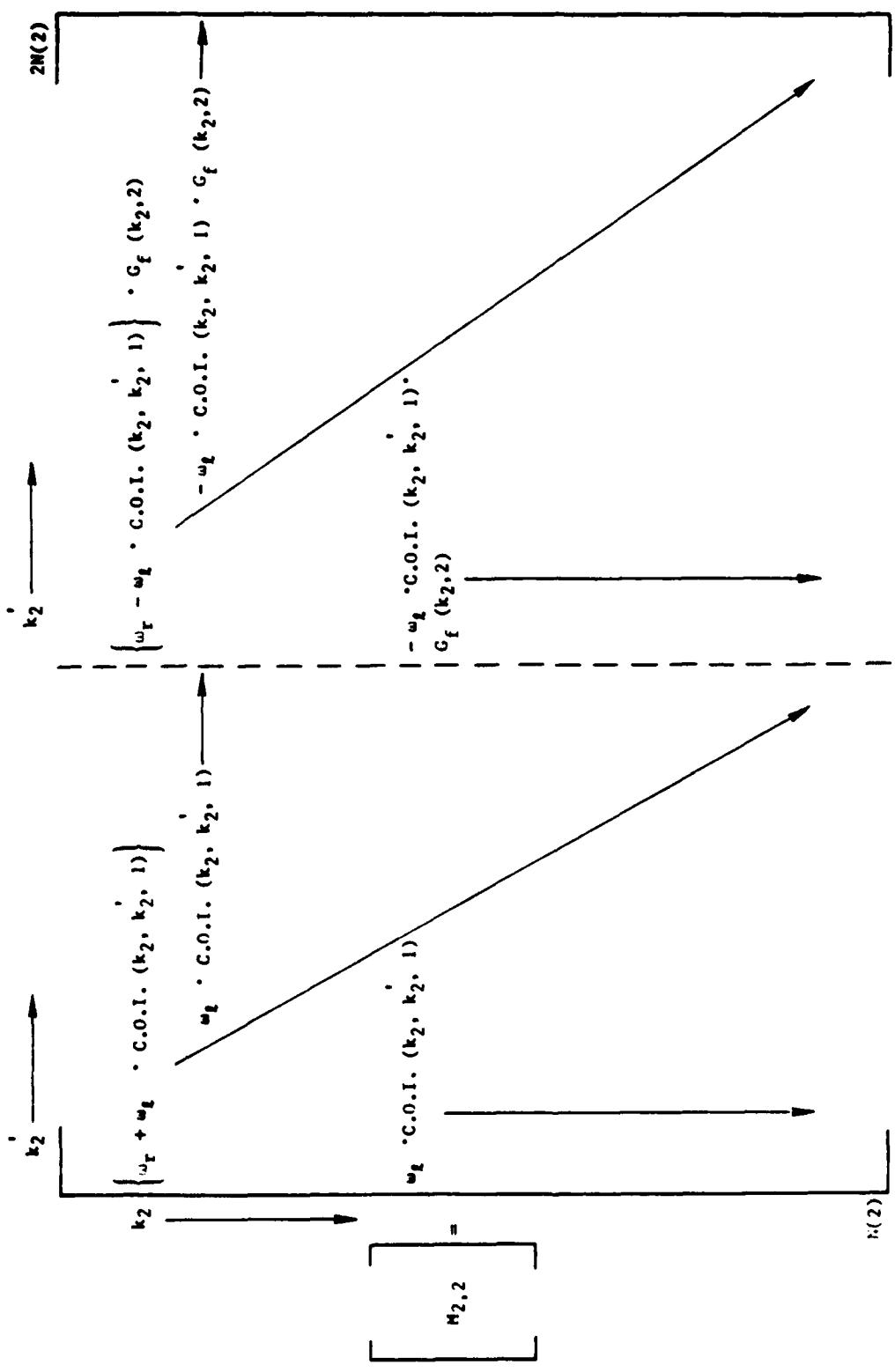
Figure A-23. Combined Equation (A13a + A13b).

$$\mathbf{b} = \begin{Bmatrix} -F_0^i(k_1, 1) \cdot \left\{ \left[u_\ell + u_r \sum_{k_1'=1}^{N(1)} C.O.I. (k_1, k_1', 1) \right] + \sum_{k_2=1}^{N(2)} \left[B_m^i (k_2, 2) \cdot O.I. (k_1, k_2, 1) \right] \cdot \left[u_\ell - u_r \frac{Z(k_1, 1)}{\sum_{k_2=1}^{N(2)} Z(k_2, 2)} \right] \right\} \end{Bmatrix}_{N(1)}$$

$$k_1 \longrightarrow$$
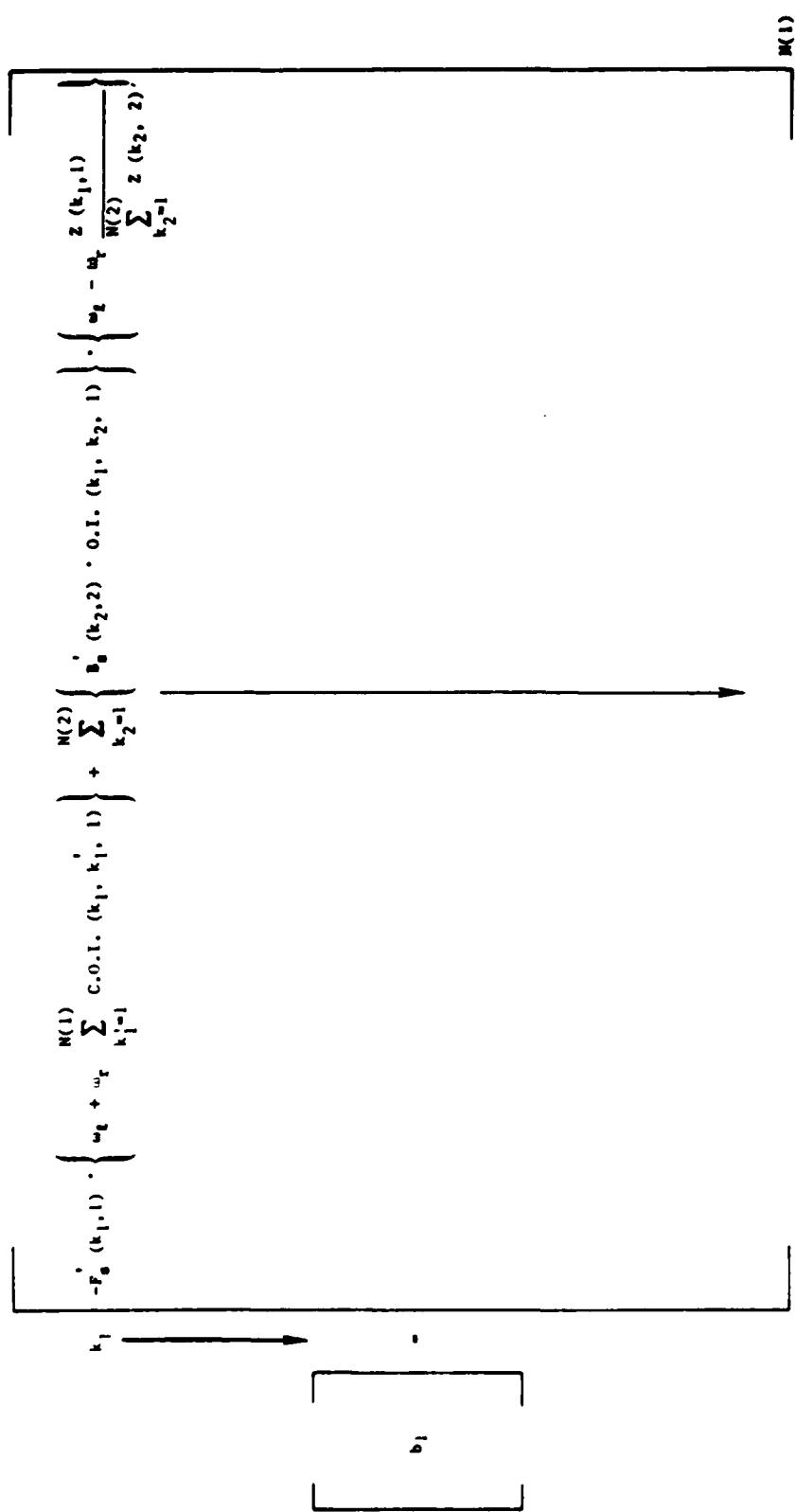
Figure A-24. Known Subvector.

71

$$b_2 \quad \left[-\sum_{k_1=1}^{N(1)} \left\{ F_s'(k_1,1) \cdot \text{O.I.}(k_1, k_2, 1) \right\} \cdot \left\{ \frac{z(k_2,2)}{\sum\limits_{k_1=1}^{N(1)} z(k_1,1)} \cdot w_2 + w_r \right\} + B_s'(k_2,2) \cdot \left\{ w_r - \sum_{k_2'=1}^{N(2)} \text{C.O.I.}(k_2, k_2', 1) \cdot w_2 \right\} \right] \quad N(2)$$
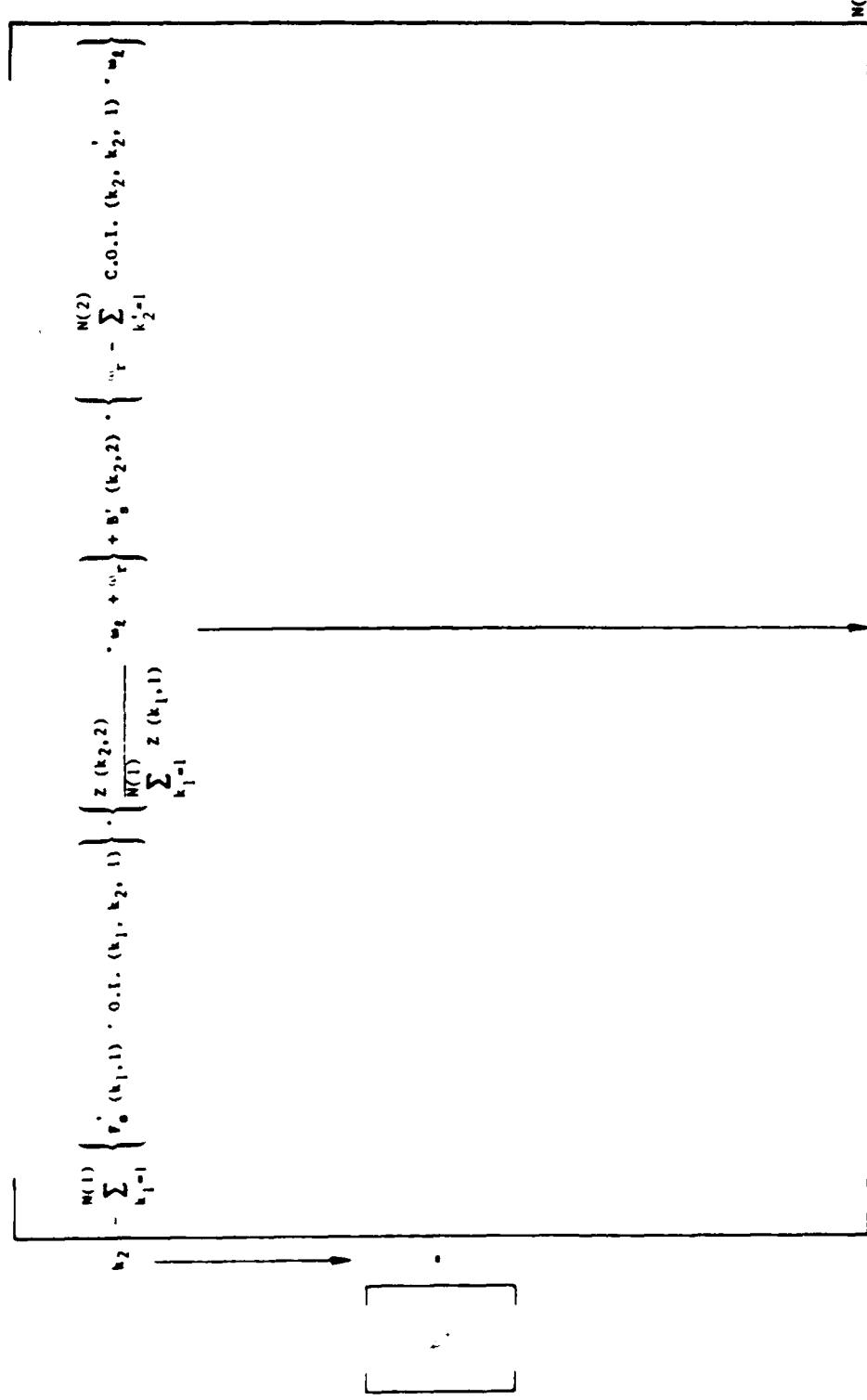
Figure A-25. Known Subvector.

$$
\begin{bmatrix} x_1 \end{bmatrix} = \begin{bmatrix} F\ (1,1) \\ F\ (2,1) \\ F\ (3,1) \\ | \\ | \\ | \\ F\ (N(1),1) \\ B'\ (1,1) \\ B'\ (2,1) \\ B'\ (3,1) \\ | \\ | \\ | \\ | \\ B'\ (N(1),1) \end{bmatrix}_{2N(1)} ;\quad \begin{bmatrix} x_2 \end{bmatrix} = \begin{bmatrix} F\ (1,2) \\ F\ (2,2) \\ F\ (3,2) \\ | \\ | \\ | \\ F\ (N(2),2) \\ B'\ (1,2) \\ B'\ (2,2) \\ B'\ (3,2) \\ | \\ | \\ | \\ | \\ B'\ (N(2),2) \end{bmatrix}_{2N(2)}
$$

Figure A-26.   Solution Subvectors.

This is equivalent to defining the input and output termination of the problem. Therefore, the structure of the matrix equation for J junctions (J+1 regions) is modified as shown in Figure A-27; where the modified submatrices and solution subvectors are shown in Figures A-28 through A-32.
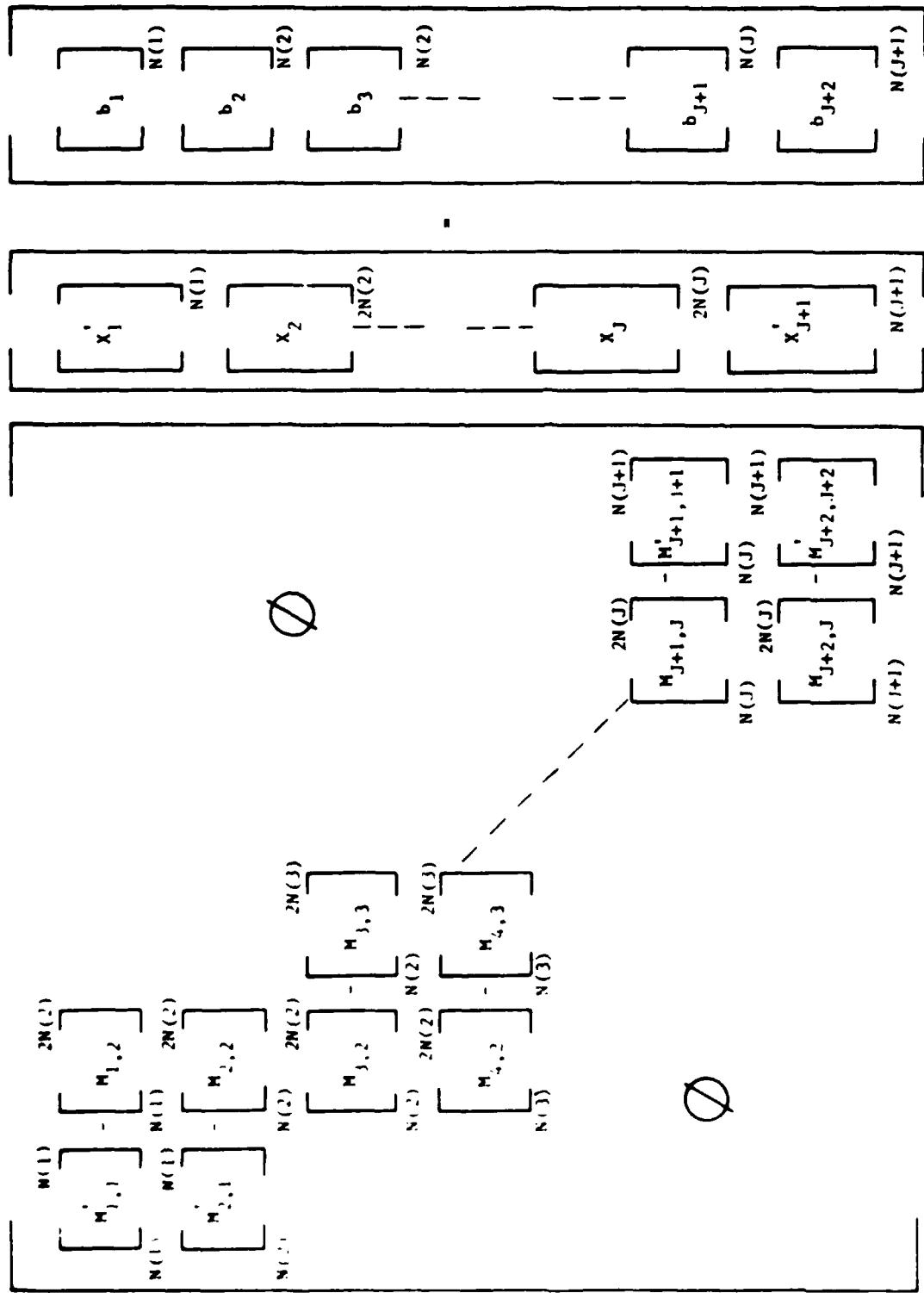
Figure A-27. Modified J Junctions Matrix.

Choose $F(k_1,1) = VRI(k_1,1) \cdot B'(k_1,1) \cdot G_f(k_1,1)$

Figure A-28. Modified First Region Submatrix.

Choose $F(k_1,1) = VRI(k_1,1) \cdot B'(k_1,1) \cdot G_f(k_1,1)$

$$\left\{\left[\left[\frac{Z(k_2,2)}{Z(k_1,1)} \cdot \omega_\ell + \omega_r\right] \cdot G_f^2(k_1,1) \cdot VRI(k_1,1) + \left[\omega_\ell - \omega_r \cdot \frac{Z(k_2,2)}{Z(k_1,1)}\right]\right]\right\} \quad O.I.\ (k_1,k_2,1) \longrightarrow$$

N(1)

k_1

k_2

N(2)

$M_{2,1}$
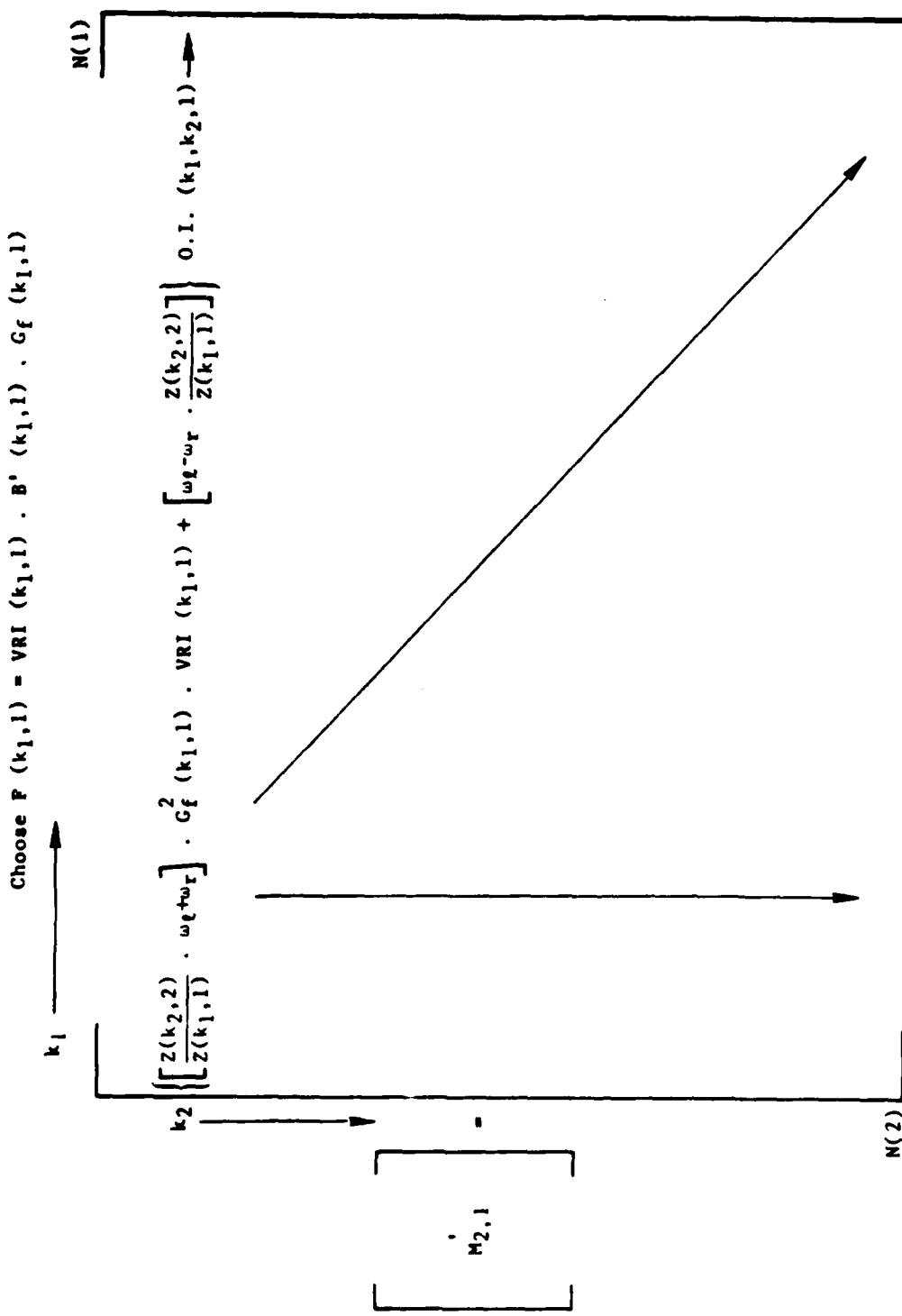
Figure A-29. Modified First Region Submatrix.

77

Choose $B' (k_{j+1}, J+1) = VRO (k_{j+1}, J+1) \cdot F (k_{j+1}, J+1) \cdot G_f (k_{j+1}, J+1)$

$0.1. (k_j, k_{j+1}, J) \cdot \left[\left[\left\{ 1 + VRO (k_{j+1}, J+1) \cdot C_f^2 (k_{j+1}, J+1) \right\} \cdot u_g + \left\{ 1 - VRO (k_{j+1}, J+1) \cdot C_f^2 (k_{j+1}, J+1) \right\} \cdot \frac{z (k_j, J)}{z (k_{j+1}, J+1)} \cdot u_g \right. \right.$

k_{j+1}

$M(J+1)$

k_j

$M(J)$

$u_{j+1, J+1}$
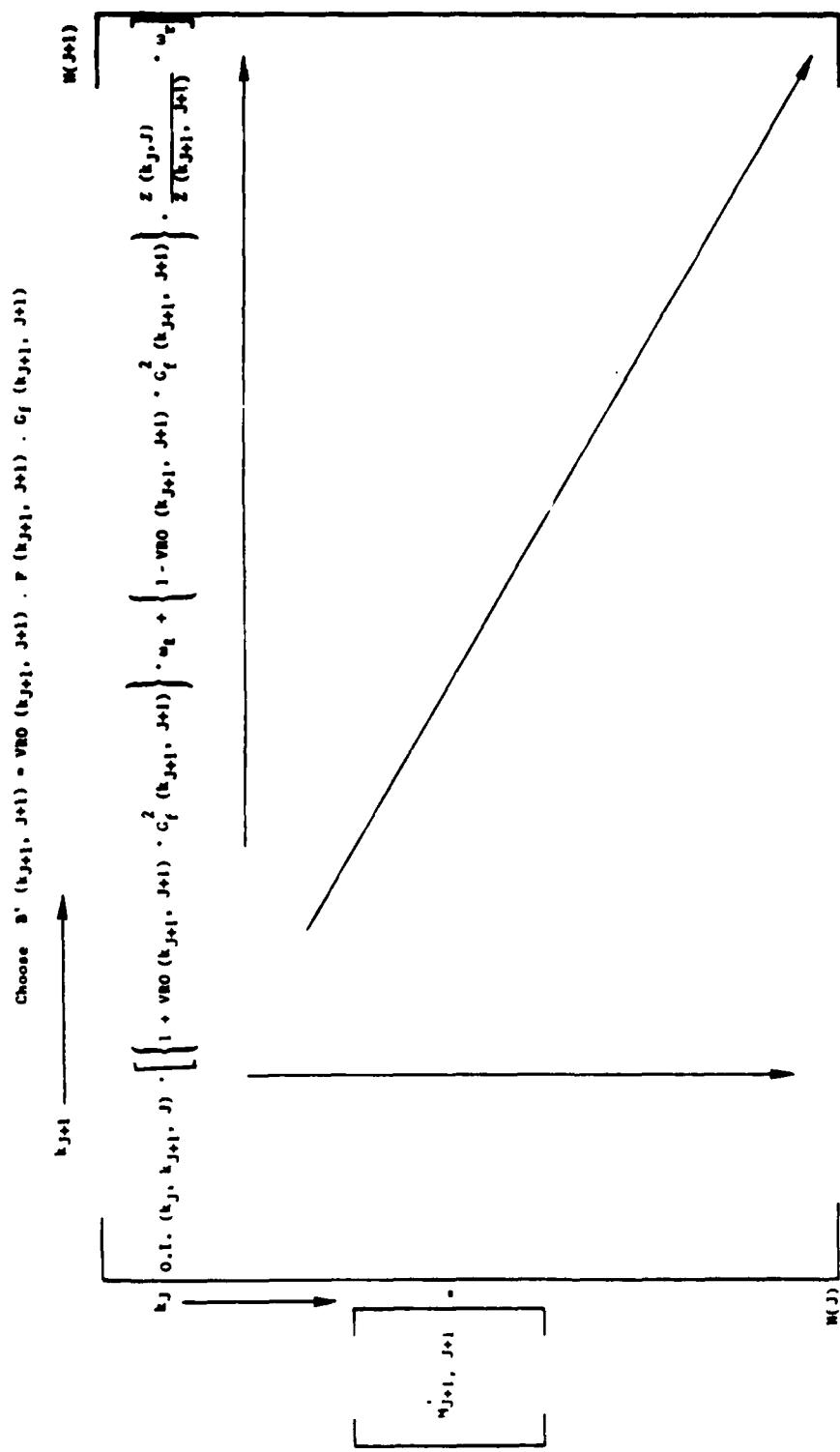
Figure A-30. Modified L ;t Region Submatrix.

Choose $B'(k_{J+1}, J+1) = VRO(k_{J+1}, J+1) \cdot F(k_{J+1}, J+1) \cdot G_f(k_{J+1}, J+1)$

$\left[1 + VRO(k_{J+1}, J+1)\right] \cdot \omega_r + \left[\left[1 - VRO(k_{J+1}, J+1) \cdot G_f^2(k_{J+1}, J+1)\right] \cdot C.O.I.(k_{J+1}, k_{J+1}, J)\right] \cdot \omega_\ell$

$\left[1 - VRO(k_{J+1}, J+1) \cdot G_f^2(k_{J+1}, J+1)\right] \cdot C.O.I.(k_{J+1}, k_{J+1}, J+1) \cdot \omega_\ell$

$\left[1 - VRO(k_{J+1}, J+1) \cdot G_f^2(k_{J+1}, J+1)\right] \cdot C.O.I.(k_{J+1}, k_{J+1}, J) \cdot \omega_\ell$

$M_{J+2, J+1}$

k_{J+1}

$N(J+1)$

$M(J+1)$
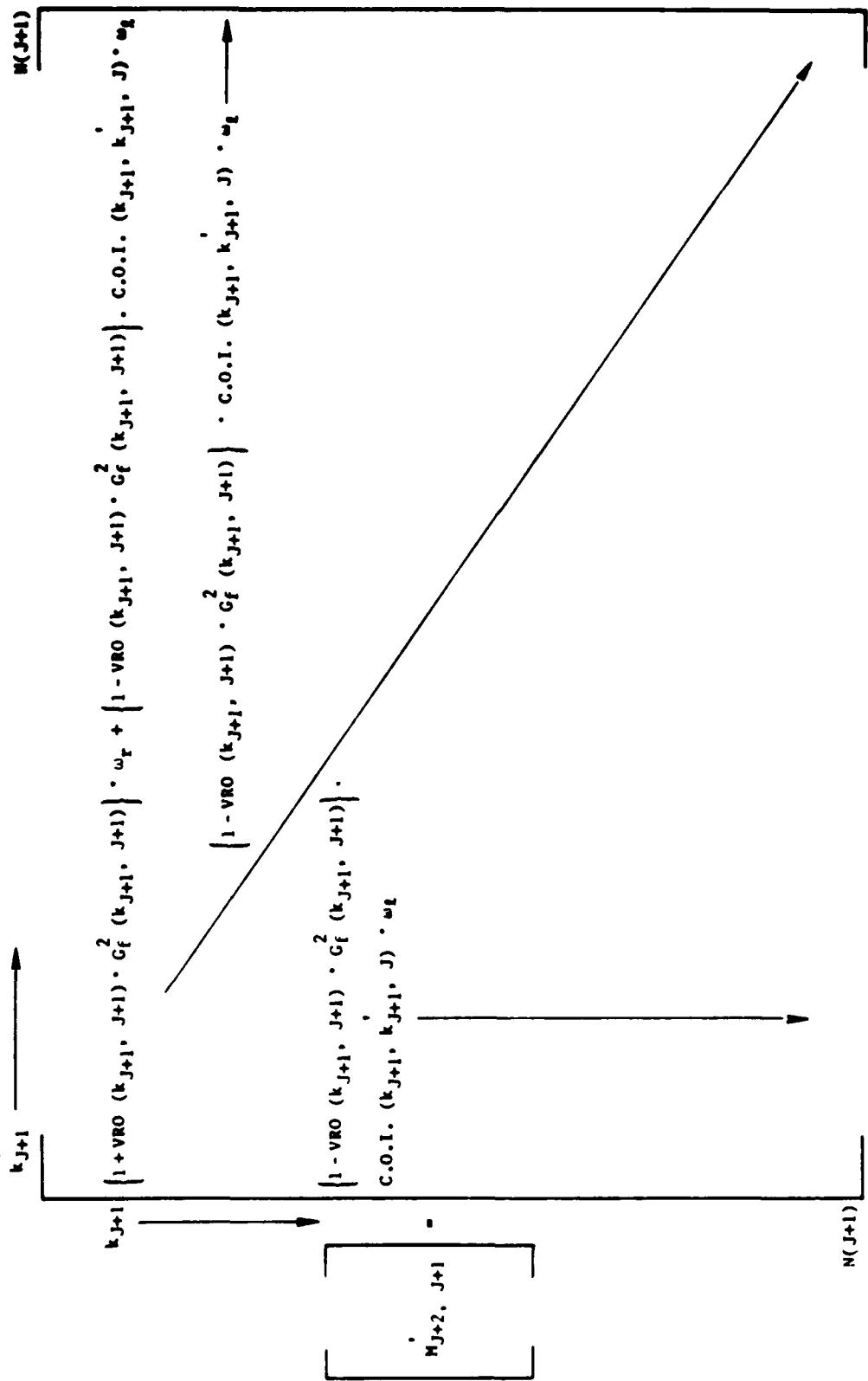
Figure A-31. Modified Last Region Submatrix.
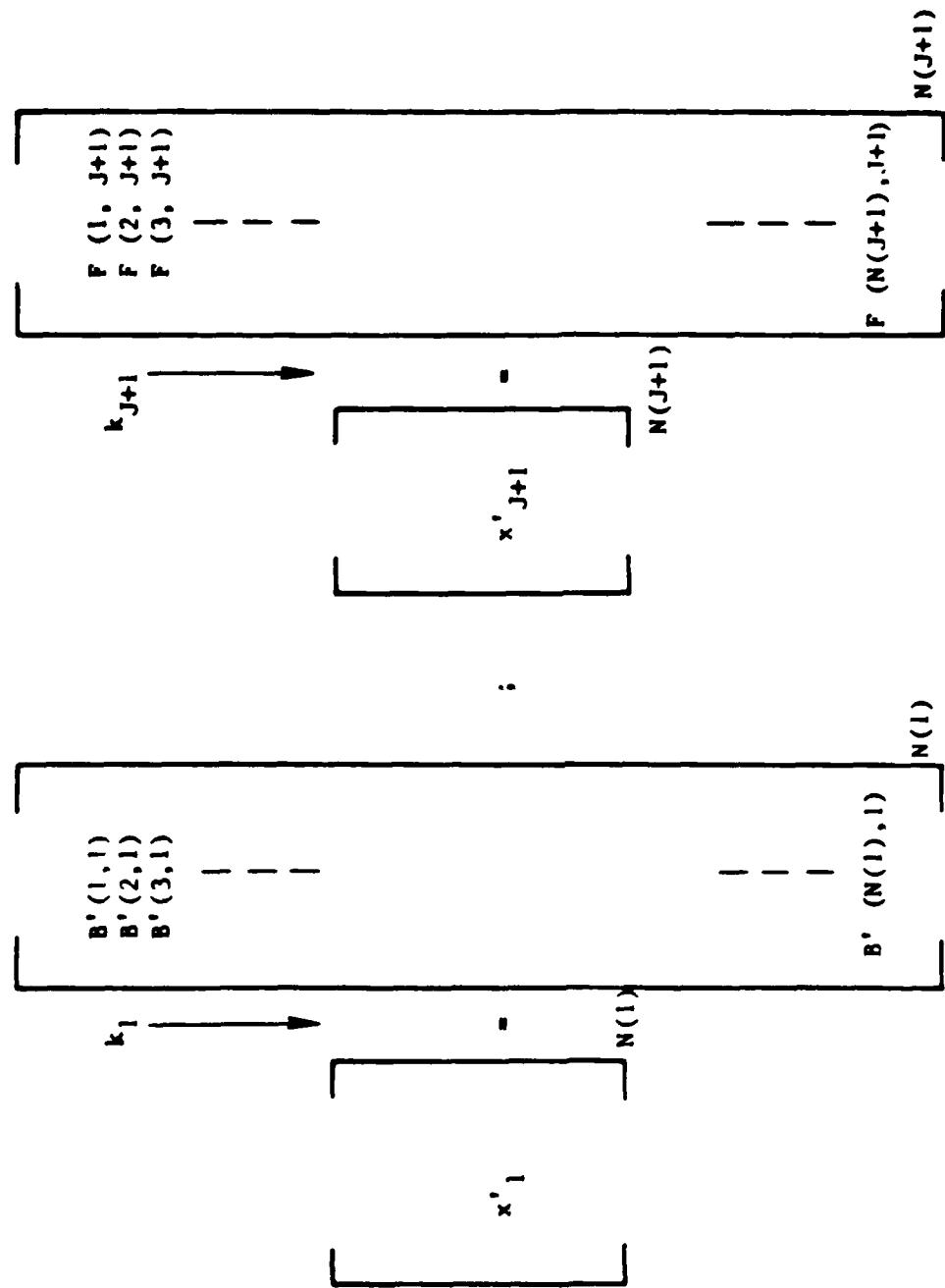
Figure A-32. Modified First and Last Region Solution Subvectors.

Appendix B: <u>Derivation of the Self-Overlap Integrals for Symmetrical</u>
<u>Modes of Circular and Coaxial Geometries On-Axis Transition</u>

The criteria for the convergence check established in Chapter III
requires a knowledge of the values of the self-overlap integrals of
every mode accounted for at the junction. The area of integration is
always the common cross-sectional aperture. The self-overlap integral
for any mode in the smaller guide is trivially unity. Therefore, only
the self-overlap integral for a mode in the larger guide over the
common aperture is derived.

The S.O.I. for any mode k_j in the larger cross section guide j
is defined by

$$S.O.I. (k_j,j) = \iint_{A(j,j+1)} \overline{e} (k_j, j) \cdot \overline{e} (k_j, j) \, ds \qquad (B-1)$$

The closed form solutions of the self-overlap integrals for the
symmetrical (m=0) modes on-axis transition are derived below for
various waveguide geometries.

B.1. <u>Circular to Circular Transition</u>

The longitudinal view of the transition is depicted in
Figure B-1. From the Appendix C, the TE mode vector function in
guide j with k_j representing m = 0 and arbitrary n is given by:

$$\overline{e}^{TE} (k_j,j) = \sqrt{\frac{1}{\pi}} \; \frac{J_0' (x_{on}' \cdot \frac{r}{a_j})}{a_j \cdot J_0 (x_{on}')} \cdot \hat{r}_0 \qquad (B-2)$$

Where n = 1, 2, 3, ... and x_{on}' is the nth zero of J_0'

81
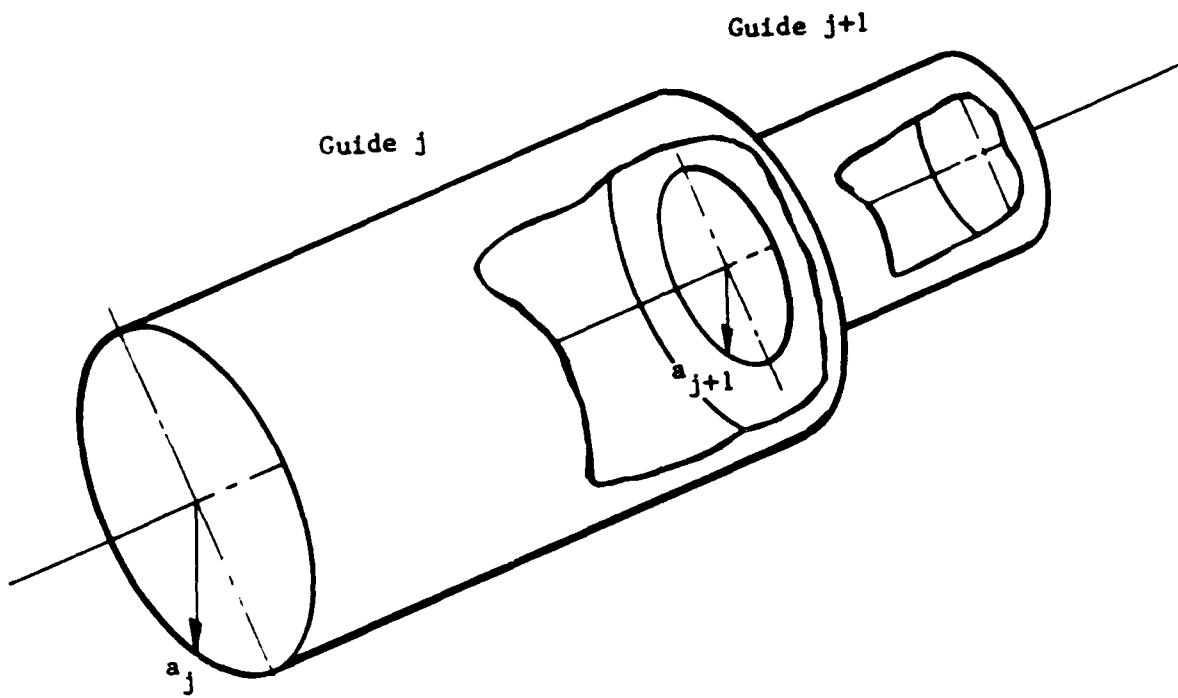
Figure B-1. Longitudinal View of Circular to Circular Transition.

Substitution of (B-2) into (B-1) yields:

$$\text{S.O.I. } (k_j,j) = \int_0^{2\pi} \int_0^{a_{j+1}} \left\{ \sqrt{\frac{1}{\pi}} \cdot \frac{J_0'\left(x_{on}' \cdot \frac{r}{a_j}\right)}{a_j \cdot J_0\left(x_{on}'\right)} \right\}^2 \cdot r dr \, d\psi \quad (B-3)$$

Application of the derivative formula of Bessel function:

$$J_0'(x) = - J_1(x)$$

And with the use of the integrals of Bessel functions formula (4) on page 255 in Reference 2, (B-3) becomes

$$\text{S.O.I. } (k_j,j) = \left(\frac{a_{j+1}}{a_j}\right)^2 \cdot \frac{\left\{ J_1^2\left(x_{on}' \frac{a_{j+1}}{a_j}\right) - J_0\left(x_{on}' \frac{a_{j+1}}{a_j}\right) \cdot J_2\left(x_{on}' \frac{a_{j+1}}{a_j}\right) \right\}}{J_0^2\left(x_{on}'\right)} \quad (B-4)$$

For TM mode with k_j representing $m=0$ and arbitrary n, the vector mode function is:

$$\overline{e}^{TM}(k_j,j) = - \sqrt{\frac{1}{\pi}} \cdot \frac{J_0'\left(x_{on} \cdot \frac{r}{a_j}\right)}{a_j \cdot J_1(x_{on})} \cdot \hat{r}_0 \quad (B-5)$$

Where x_{on} is the nth zero of J_0

Substitution of (B-5) into (B-1) gives:

$$\text{S.O.I. } (k_j,j) = \int_0^{2\pi} \int_0^{a_{j+1}} \left\{ - \sqrt{\frac{1}{\pi}} \frac{J_0'\left(x_{on} \cdot \frac{r}{a_j}\right)}{a_j \cdot J_1(x_{on})} \right\}^2 \cdot r \, dr \, d\psi \quad (B-6)$$

Evaluating the integration yields:

$$\text{S.O.I. } (k_j,j) = \left(\frac{a_{j+1}}{a_j}\right)^2 \cdot \frac{J_1^2\left(x_{on} \frac{a_{j+1}}{a_j}\right) - J_0\left(x_{on} \frac{a_{j+1}}{a_j}\right) \cdot J_2\left(x_{on} \frac{a_{j+1}}{a_j}\right)}{J_1^2(x_{on})} \quad (B-7)$$

B.2. Coaxial to Coaxial Transition

The type of transition (one-sided boundary) as shown in Figure B-2 is valid for the derivations below. For the case of k_j representing $m=0$ and arbitrary n, the TE mode vector function is:

$$\bar{e}^{TE}(k_j,j) = \frac{x'_{on}}{b_j} \cdot \frac{\sqrt{\pi}}{2} \frac{J'_o\left(x'_{on}\frac{r}{b_j}\right) \cdot N'_o(x'_{on}) - N'_o\left(x'_{on}\cdot\frac{r}{b_j}\right) \cdot J'_o(x'_{on})}{\left\{\dfrac{J_o^{'2}(x'_{on})}{J_o^{'2}\left(x'_{on}\frac{a_j}{b_j}\right)} - 1\right\}^{1/2}} \cdots \qquad (B-8)$$

Substituting (B-8) into (B-1) and collecting terms yields:

$$S.O.I.(k_j,j) = \left(\frac{x'_{on}}{b_j}\right)^2 \frac{\dfrac{\pi^2}{2}}{\left\{\dfrac{J_o^{'2}(x'_{on})}{J_o^{'2}\left(x'_{on}\frac{a_j}{b_j}\right)} - 1\right\}} \cdot \int_{b_{j+1}}^{a_{j+1}} \left\{J'_o\left(x'_{on}\frac{r}{b_j}\right)\cdot \right.$$

$$\left. N'_o(x'_{on}) - N'_o\left(x'_{on}\frac{r}{b_j}\right) \cdot J'_o(x'_{on})\right\}^2 \cdot r\,dr \qquad (B-9)$$

Evaluating the integral yields:

$$S.O.I.(k_j,j) = \frac{\pi^2}{4\left\{\dfrac{J_o^{'2}(x'_{on})}{J_o^{'2}\left(x'_{on}\cdot\frac{a_j}{b_j}\right)} - 1\right\}} \left\{\left(\frac{x'_{on}}{b_j}\cdot a_{j+1}\right)^2 \cdot \left[\left\{J_1\left(x'_{on}\cdot\frac{a_{j+1}}{b_j}\right)\right.\right.\right.$$

$$\left.\cdot N_1(x'_{on}) - N_1\left(x'_{on}\cdot\frac{a_{j+1}}{b_j}\right)\cdot J_1(x'_{on})\right\}^2 - \left\{N_o\left(x'_{on}\cdot\frac{a_{j+1}}{b_j}\right)\cdot J_1(x'_{on}) - \right.$$
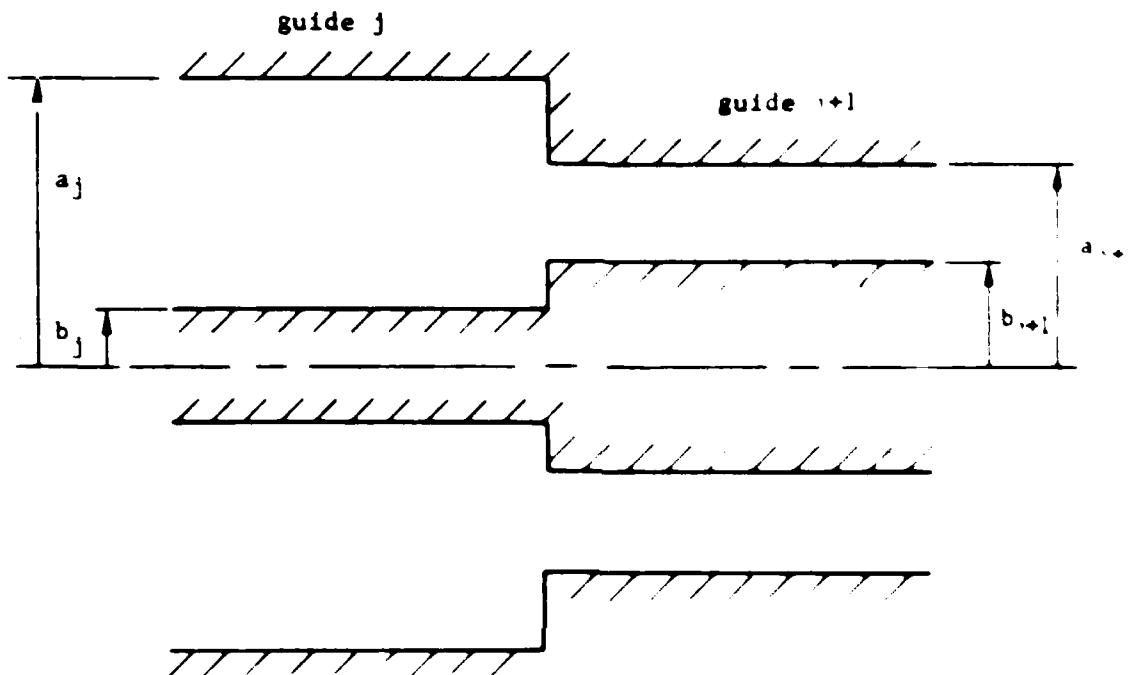
Figure B-2. One-Sided Boundary Coaxial to Coaxial Transition.

$$J_0 \left(x'_{on} \cdot \frac{a_{j+1}}{b_j} \right) \cdot N_1 (x'_{on}) \right\} \cdot \left\{ N_2 \left(x'_{on} \frac{a_{j+1}}{b_j} \right) \cdot J_1 (x'_{on}) - J_2 \left(x'_{on} \cdot \frac{a_{j+1}}{b_j} \right) \right.$$

$$\left. \cdot N_1 (x'_{on}) \right\} \right] - \left(\frac{x'_{on}}{b_j} \cdot b_{j+1} \right)^2 \cdot \left[\left\{ J_1 \left(x'_{on} \cdot \frac{b_{j+1}}{b_j} \right) \cdot N_1 (x'_{on}) - \right. \right.$$

$$N_1 \left(x'_{on} \cdot \frac{b_{j+1}}{b_j} \right) \cdot J_1 (x'_{on}) \right\}^2 - \left\{ N_0 \left(x'_{on} \cdot \frac{b_{j+1}}{b_j} \right) \cdot J_1 (x'_{on}) - \right.$$

$$J_0 \left(x'_{on} \cdot \frac{b_{j+1}}{b_j} \right) \cdot N_1 (x'_{on}) \right\} \cdot \left\{ N_2 \left(x'_{on} \cdot \frac{b_{j+1}}{b_j} \right) \cdot J_1 (x'_{on}) - \right.$$

$$J_2 \left(x'_{on} \cdot \frac{b_{j+1}}{b_j} \right) \cdot N_1 (x'_{on}) \right\} \right] \right\} \qquad \text{(B-10)}$$

For TM mode with k_j representing $m=0$ and arbitrary n, the vector mode function is:

$$\bar{e}^{TM} (k_j, j) = \frac{x_{on}}{b_j} \sqrt{\frac{\pi}{2}} \; \frac{J'_0 \left(x_{on} \frac{r}{b_j} \right) \cdot N_0 (x_{on}) - N'_0 \left(x_{on} \frac{r}{b_j} \right) \cdot J_0 (x_{on})}{\left\{ \dfrac{J_0^2 (x_{on})}{J_0^2 \left(x_{on} \cdot \frac{a_j}{b_j} \right)} - 1 \right\}^{1/2}} \cdot \hat{r}_o \qquad \text{(B-11)}$$

Substitution (B-11) into (B-1) gives:

$$\text{S.O.I. } (k_j, j) = \int_0^{2\pi} \int_{b_{j+1}}^{a_{j+1}} \left\{ \frac{x_{on}}{b_j} \cdot \sqrt{\frac{\pi}{2}} \cdot \right.$$

$$\left. \frac{J'_0 \left(x_{on} \frac{r}{b_j} \right) \cdot N_0 (x_{on}) - N'_0 \left(x_{on} \cdot \frac{r}{b_j} \right) \cdot J_0 (x_{on})}{\left\{ \dfrac{J_0^2 (x_{on})}{J_0^2 \left(x_{on} \cdot \frac{a_j}{b_j} \right)} - 1 \right\}^{1/2}} \right\} \cdot \quad \dots \dots$$

Evaluating the integration yields:

$$\text{S.O.I. } (k_j, j) = \frac{\pi^2}{4\left\{\dfrac{J_o^2 (x_{on})}{J_o^2 \left(x_{on} \dfrac{a_j}{b_j}\right)} - 1\right\}} \cdot \left\{\left(x_{on} \cdot \frac{a_{j+1}}{b_j}\right)^2 \left[\left\{N_1 \left(x_{on} \cdot \frac{a_{j+1}}{b_j}\right) \cdot \right.\right.\right.$$

$$J_o (x_{on}) - J_1 \left(x_{on} \cdot \frac{a_{j+1}}{b_j}\right) \cdot N_o (x_{on})\right\}^2 - \left\{N_o \left(x_{on} \cdot \frac{a_{j+1}}{b_j}\right) \cdot J_o (x_{on}) - \right.$$

$$J_o \left(x_{on} \cdot \frac{a_{j+1}}{b_j}\right) \cdot N_o (x_{on})\right\} \cdot \left\{N_2 \left(x_{on} \cdot \frac{a_{j+1}}{b_j}\right) \cdot J_o (x_{on}) - J_2 \left(x_{on} \cdot \frac{a_{j+1}}{b_j}\right) \right.$$

$$N_o (x_{on})\right\}\right] - \left(x_{on} \cdot \frac{b_{j+1}}{b_j}\right)^2 \left[\left\{N_1 \left(x_{on} \cdot \frac{b_{j+1}}{b_j}\right) \cdot J_o (x_{on}) - J_1 \left(x_{on} \cdot \frac{b_{j+1}}{b_j}\right) \right.\right.$$

$$N_o (x_{on})\right\}^2 - \left\{N_o \left(x_{on} \cdot \frac{b_{j+1}}{b_j}\right) \cdot J_o (x_{on}) - J_o \left(x_{on} \cdot \frac{b_{j+1}}{b_j}\right) \cdot N_o (x_{on})\right\} \cdot$$

$$\left\{N_2 \left(x_{on} \cdot \frac{b_{j+1}}{b_j}\right) \cdot J_o (x_{on}) - J_2 \left(x_{on} \cdot \frac{b_{j+1}}{b_j}\right) \cdot N_o (x_{on})\right\}\right]\right\} \qquad (B-13)$$

For TEM mode with k_j representing $m=0$ and $n=0$, the vector mode function is:

$$\bar{e}^{\text{TEM}} (k_j, j) = \frac{-1}{r \cdot \sqrt{2\pi \ln \left(\dfrac{a_j}{b_j}\right)}} \cdot \hat{r}_o \qquad (B-14)$$

Equation (B-1) becomes:

$$\text{S.O.I. } (k_j, j) = \int_0^{2\pi} \int_{b_{j+1}}^{a_{j+1}} \left\{\frac{-1}{r \cdot \sqrt{2\pi \ln \left(\dfrac{a_j}{b_j}\right)}}\right\}^2 r \, dr \, d\psi \qquad (B-15)$$

87

Evaluating the integration yields:

$$\text{S.O.I. } (k_j, j) = \frac{\ln \left(\dfrac{a_{j+1}}{b_{j+1}}\right)}{\ln \left(\dfrac{a_j}{b_j}\right)} \tag{B-16}$$

B.3.   Circular to Coaxial Transition

The derivation below is valid for a smaller coaxial guide totally embedded inside a larger circular waveguide. Such a transition is depicted in Figure B-3.

With k_j representing $m=0$ and arbitrary n, the vector mode functions for a circular guide are given in (B-2) and (B-5) above. Performing the integration over the annular aperture yields expressions of S.O.I. For TE mode:

$$\text{S.O.I. } (k_j, j) = \frac{1}{J_0^2 (x'_{on})} \cdot \left\{ \left(\frac{a_{j+1}}{a_j}\right)^2 \left[J_1^2 \left(x'_{on} \cdot \frac{a_{j+1}}{a_j}\right) - J_0 \left(x'_{on} \cdot \frac{a_{j+1}}{a_j}\right) \right. \right.$$
$$\left. \cdot J_2 \left(x'_{on} \cdot \frac{a_{j+1}}{a_j}\right) \right] - \left(\frac{b_{j+1}}{b_j}\right)^2 \cdot \left[J_1^2 \left(x'_{on} \cdot \frac{b_{j+1}}{a_j}\right) - J_0 \left(x'_{on} \cdot \frac{b_{j+1}}{a_j}\right) \cdot \right.$$
$$\left. \left. J_2 \left(x'_{on} \cdot \frac{b_{j+1}}{a_j}\right) \right] \right\} \tag{B-17}$$

Where x'_{on} is the nth zero of J'_0
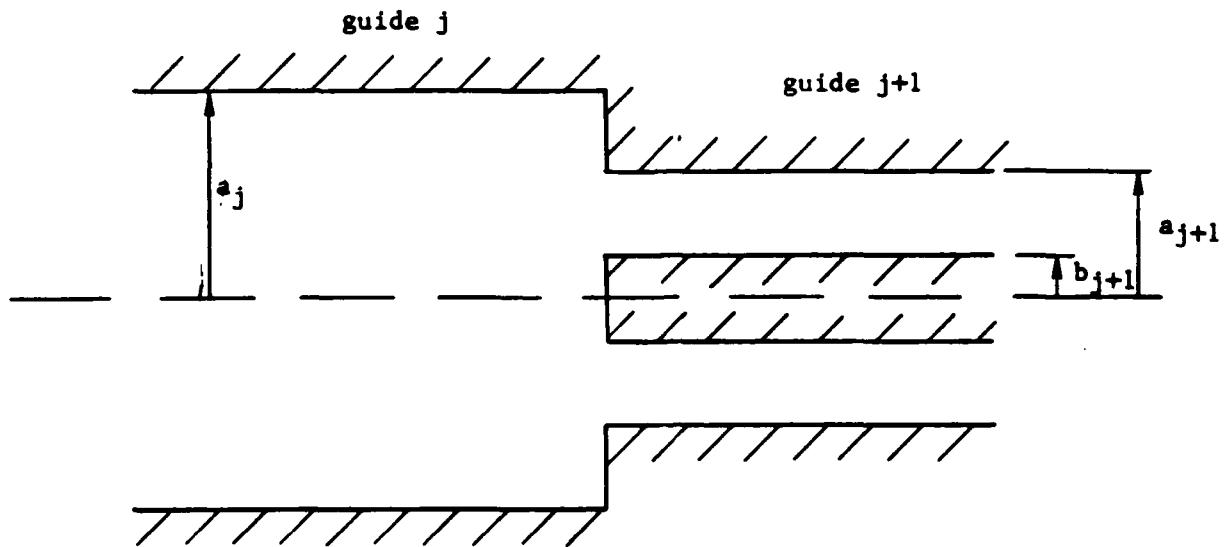
Figure B-3. One-Sided Boundary Circular to Coaxial Transition.

For TM mode:

$$\text{S.O.I.}(k_j, j) = \frac{1}{J_1^2(x_{on})} \cdot \left\{ \left(\frac{a_{j+1}}{a_j}\right)^2 \cdot \left[J_1^2\left(x_{on} \cdot \frac{a_{j+1}}{a_j}\right) - J_0\left(x_{on} \cdot \frac{a_{j+1}}{a_j}\right) \cdot \right. \right.$$

$$\left. J_2\left(x_{on} \cdot \frac{a_{j+1}}{a_j}\right)\right] - \left(\frac{b_{j+1}}{b_j}\right)^2 \cdot \left[J_1^2\left(x_{on} \cdot \frac{b_{j+1}}{a_j}\right) - J_0\left(x_{on} \cdot \frac{b_{j+1}}{a_j}\right) \cdot \right.$$

$$\left. \left. J_2\left(x_{on} \cdot \frac{b_{j+1}}{a_j}\right)\right]\right\} \tag{B-18}$$

Where x_{on} is the nth zero of J_0.

All the above integrals are evaluated with the aid of the integrals of Bessel functions formula (4) on page 255 in Reference 2.

Appendix C: Vector Mode Functions for TE, TM, and TEM Mode for Rectangular, Circular, and Coaxial Geometries

The transverse fields for the rectangular, circular, and coaxial waveguides are derived in Reference 3. The formulas for the TE, TM, and TEM modes are given below. The origin of the coordinates have been moved to the center of the guide from the lower left hand corner for the rectangular waveguide modes. The vector mode functions are represented by

$$\overline{e}_{mn}^{TM} \equiv \text{TM mode vector function}$$

$$\overline{e}_{mn}^{TE} \equiv \text{TE mode vector function}$$

$$\overline{e}_{00}^{TEM} \equiv \text{TEM mode vector function (coaxial guide only)}$$

For a rectangular waveguide, the cross section view is depicted in Figure C-1.
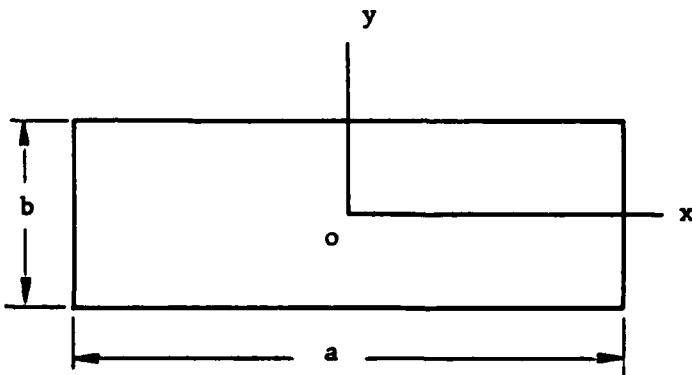

Figure C-1. Cross Section View of a Rectangular Waveguide.

The TM, and TE vector mode functions for a rectangular waveguide are given by

$$\overline{e}_{mn}^{TM} = \frac{-\frac{2}{\pi}}{\sqrt{m^2 \frac{b}{a} + n^2 \frac{a}{b}}} \left\{ \left[\frac{m\pi}{a} \cos \frac{m\pi}{a} \left(x + \frac{a}{2}\right) \cdot \sin \frac{n\pi}{b} \left(y + \frac{b}{2}\right) \right] \cdot \hat{x}_0 \right.$$

$$\left. + \left[\frac{n\pi}{b} \sin \frac{m\pi}{a} \left(x + \frac{a}{2}\right) \cdot \cos \frac{n\pi}{b} \left(y + \frac{b}{2}\right) \right] \cdot \hat{y}_0 \right\} \quad (C-1)$$

$$\overline{e}_{mn}^{TE} = \frac{\sqrt{\frac{\varepsilon_m \varepsilon_n}{\pi}}}{\sqrt{m^2 \frac{b}{a} + n^2 \frac{a}{b}}} \left\{ \left[\frac{n\pi}{b} \cos \frac{m\pi}{a} \left(x + \frac{a}{2}\right) \cdot \sin \frac{n\pi}{b} \left(y + \frac{b}{2}\right) \right] \cdot \hat{x}_0 \right.$$

$$\left. - \left[\frac{m\pi}{a} \sin \frac{m\pi}{a} \left(x + \frac{a}{2}\right) \cdot \cos \frac{n\pi}{b} \left(y + \frac{b}{2}\right) \right] \cdot \hat{y}_0 \right\} \quad (C-2)$$

Where $\hat{x}_0$, $\hat{y}_0$ are unit vectors along x and y – axis respectively

$m, n = 0, 1, 2, 3, \ldots$, mode $m = n = 0$ excluded

$$\varepsilon_m = \begin{cases} 1 \text{ if } m = 0 \\ 2 \text{ if } m \neq 0 \end{cases}$$

Figure C-2 illustrates the cross section view of a circular waveguide.
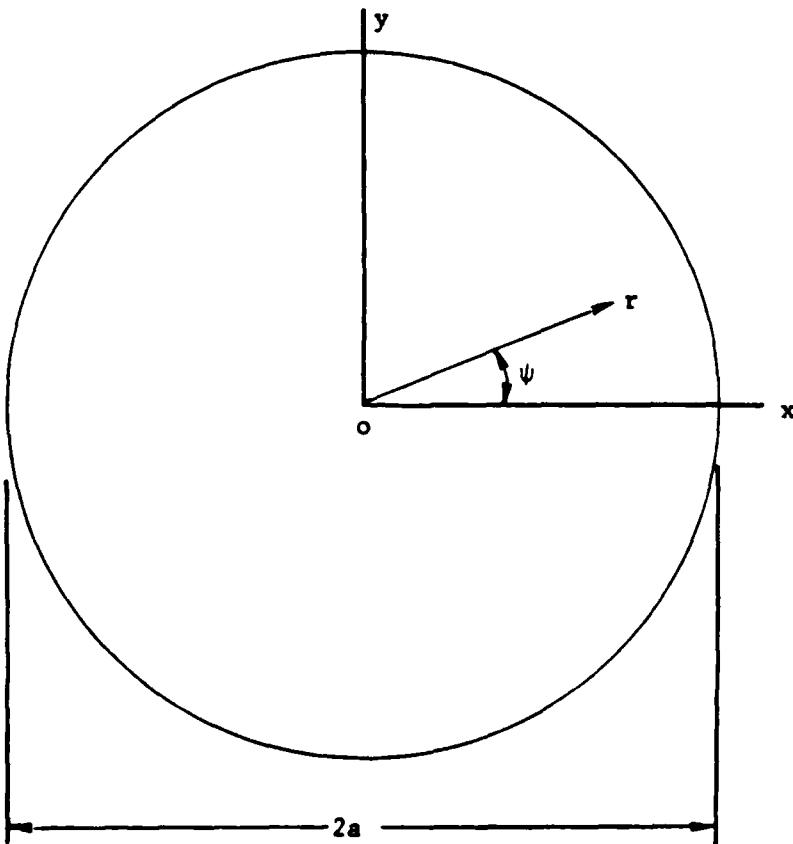
Figure C-2.   Cross Section View of a Circular Waveguide.

92

The TM mode vector function for a circular waveguide is:

$$\overline{e}_{mn}^{TM} = \frac{-\sqrt{\frac{\varepsilon_m}{\pi}}}{J_{m+1}(x_{mn})} \left\{ \left[\frac{1}{a} \cdot J_m'\left(x_{mn} \cdot \frac{r}{a}\right) \cdot \begin{bmatrix} \cos \\ \sin \end{bmatrix} m\psi \right] \cdot \hat{r}_o + \right.$$

$$\left. \left[\frac{m}{r \cdot x_{mn}} \cdot J_m\left(x_{mn} \cdot \frac{r}{a}\right) \cdot \begin{bmatrix} -\sin \\ \cos \end{bmatrix} m\psi \right] \cdot \hat{\psi}_o \right\} \quad (C-3)$$

The TE mode vector function for a circular waveguide is:

$$\overline{e}_{mn}^{TE} = \sqrt{\frac{\varepsilon_m}{\pi (x_{mn}'^2 - m^2)}} \cdot \frac{1}{J_m(x_{mn}')} \cdot \left\{ \left[\frac{m}{r} \cdot J_m\left(x_{mn}' \cdot \frac{r}{a}\right) \cdot \begin{bmatrix} \sin \\ -\cos \end{bmatrix} m\psi \right] \cdot \hat{r}_o \right.$$

$$\left. + \left[\frac{x_{mn}'}{a} \cdot J_m'\left(x_{mn}' \cdot \frac{r}{a}\right) \cdot \begin{bmatrix} \cos \\ \sin \end{bmatrix} m\psi \right] \cdot \hat{\psi}_o \right\} \quad (C-4)$$

Where $\hat{r}_o$, $\hat{\psi}_o$ are unit vectors along r and ψ directions

$$m \quad = \quad 0, 1, 2, \ldots$$

$$n \quad = \quad 1, 2, 3, \ldots$$

x_{mn} = nth non-vanishing root of the mth – order Bessel

function $J_m(x_{mn}) = 0$

x_{mn}' = nth non-vanishing root of the derivative of the mth –

order Bessel function $J_m'(x_{mn}') = 0$

$$\varepsilon_m \quad = \begin{cases} 1 & \text{if } m = 0 \\ 2 & \text{if } m \neq 0 \end{cases}$$

For a coaxial waveguide, the cross section view is shown in Figure C-3.

93
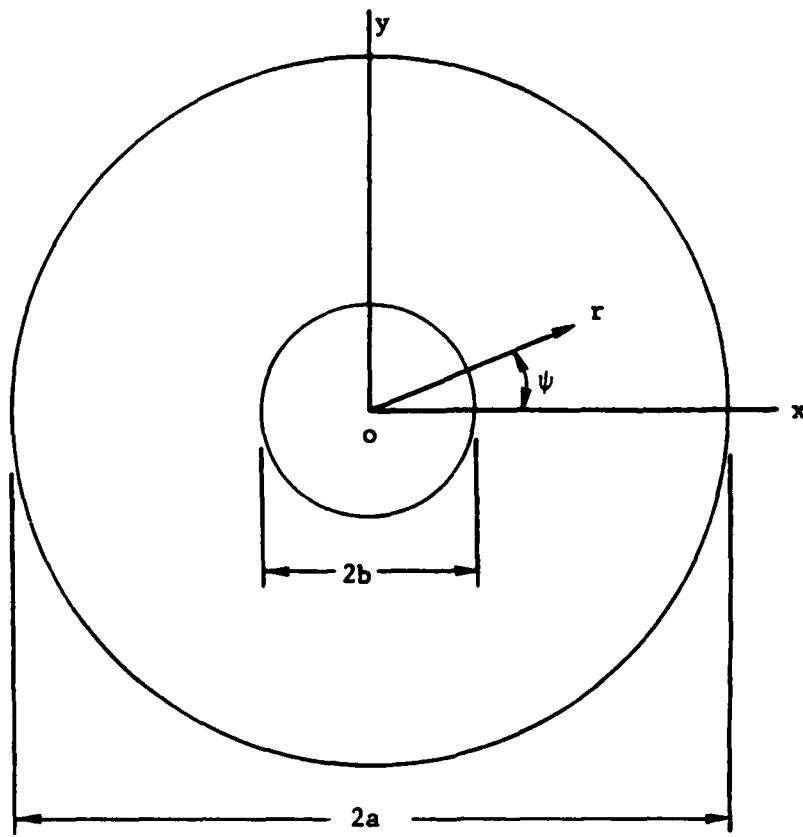
Figure C-3. Cross Section View of a Coaxial Waveguide.

The TM mode vector function for a coaxial waveguide is:

$$\bar{e}_{mn}^{TM} = -\frac{\sqrt{\pi\epsilon_m}}{2} \cdot \left\{ \left[\frac{x_{mn}}{b} \frac{J_m'\left(x_{mn} \cdot \frac{r}{b}\right) N_m(x_{mn}) - N_m'\left(x_{mn} \cdot \frac{r}{b}\right) J_m(x_{mn})}{\left(\dfrac{J_m^2(x_{mn})}{J_m^2(C\, x_{mn})} - 1\right)^{1/2}} \cdot \right. \right.$$

$$\left. \begin{bmatrix} \cos \\ \sin \end{bmatrix} m\psi \right] \cdot \hat{r}_o + \left[\frac{m}{b} \frac{J_m\left(x_{mn} \cdot \frac{r}{b}\right) N_m(x_{mn}) - N_m\left(x_{mn} \cdot \frac{r}{b}\right) J_m(x_{mn})}{\left(\dfrac{J_m^2(x_{mn})}{J_m^2(C\, x_{mn})} - 1\right)^{1/2}} \cdot \right.$$

$$\left. \left. \begin{bmatrix} -\sin \\ \cos \end{bmatrix} m\psi \right] \cdot \hat{\psi}_o \right\} \qquad (C-5)$$

The TE mode vector function for a coaxial waveguide is:

$$\bar{e}_{mn}^{TE} = \frac{\sqrt{\pi\epsilon_m}}{2} \cdot \left\{ \left[-\frac{m}{r} \frac{J_m\left(x_{mn}' \cdot \frac{r}{b}\right) N_m'(x_{mn}') - N_m\left(x_{mn}' \cdot \frac{r}{b}\right) J_m'(x_{mn}')}{\left(\left\{\dfrac{J_m'(x_{mn}')}{J_m'(C\, x_{mn}')}\right\}^2 \left\{1 - \left(\dfrac{m}{C\, x_{mn}'}\right)^2\right\} - \left\{1 - \left(\dfrac{m}{x_{mn}'}\right)^2\right\}\right)^{1/2}} \cdot \right. \right.$$

$$\left. \begin{bmatrix} -\sin \\ \cos \end{bmatrix} m\psi \right] \cdot \hat{r}_o + \left[\frac{x_{mn}'}{b} \frac{J_m'\left(x_{mn}' \cdot \frac{r}{b}\right) N_m'(x_{mn}') - N_m'\left(x_{mn}' \cdot \frac{r}{b}\right) J_m'(x_{mn}')}{\left(\left\{\dfrac{J_m'(x_{mn}')}{J_m'(C\, x_{mn}')}\right\}^2 \left\{1 - \left(\dfrac{m}{C\, x_{mn}'}\right)^2\right\} - \left\{1 - \left(\dfrac{m}{x_{mn}'}\right)^2\right\}\right)^{1/2}} \cdot \right.$$

$$\left. \left. \begin{bmatrix} \cos \\ \sin \end{bmatrix} m\psi \right] \cdot \hat{\psi}_o \right\} \qquad (C-6)$$

95

And the TEM mode vector function is:

$$\bar{e}_{oo}^{TEM} = -\frac{1}{r \cdot \sqrt{2\pi \, \ln\left(\frac{a}{b}\right)}} \cdot \hat{r}_o \qquad\qquad (C-7)$$

Where $\hat{r}_o$, $\hat{\psi}_o$ are unit vectors along r and ψ directions

$m = 0, 1, 2, 3, \ldots$

$n = 1, 2, 3, \ldots$

$C = \dfrac{a}{b}$

x_{mn} = nth non-vanishing root of the mth – order Bessel– Neumann combination.

$x_{mn}^{\prime}$ = nth non-vanishing root of the derivative of the mth – order Bessel–Neumann combination

$$\varepsilon_m = \begin{cases} 1 & \text{if } m = 0 \\ 2 & \text{if } m \neq 0 \end{cases}$$

BIBLIOGRAPHY

1. Clarricoats, P.J.B.; Slinn, K.R.: "Numerical Solution of Waveguide - Discontinuity Problems," Proc. I.E.E., pp. 878-886 Vol. 114, No. 7, July 1967.

2. Luke, Y.L.: <u>Integrals of Bessel Functions</u>, McGraw-Hill, Inc., 1962.

3. Marcuvitz, N.: Waveguide Handbook, Boston Technical Publishers, Inc., 1964.

4. Mielke, T.A.: Solution of the Generalized Waveguide Discontinuity Problem, Engineer Thesis, Stanford University, Stanford, California, (to be Published).

5. Palevsky, A. (Private Communication).

6. IMSL Incorporated, 7500 Bellaire Blvd., 6th Floor, Houston, Texas 77036.

LIST OF SYMBOLS

$A(j, j+1)$ — Common cross-sectional area at the junction j between regions j and $j+1$

a_j, a_{j+1} — Outer radius of circular to coaxial waveguides j and $j+1$

$a(k_{j+1}, j+1)$ — Weighting factor of each excited mode k_{j+1} region $j+1$

b_j, b_{j+1} — Inner radius of coaxial waveguides j and $j+1$

$b(k_j, j)$ — Weighting factor of each reflected mode k_j region j

$B(k,j)$ — Backward mode k of $\vec{E}$ field magnitude defined at input plane of region j

$B'(k,j)$ — Backward mode k of $\vec{E}$ field magnitude defined at output plane of region j ($= B(k,j) \cdot G_b(k,j)$)

$B_s(k,j)$ — Component of backward mode k of $\vec{E}$ field magnitude defined at distance $d(k,j)$ from input plane of region j due to source terms

$B'_s(k,j)$ — Component of backward mode k of $\vec{E}$ field magnitude defined at input plane of region j due to source terms $= B_s(k,j) \cdot G_{bs}(k,j)$

$C.O.I.(k_j, k'_j, j)$ — Cross-overlap integral of mode k_j to mode k'_j in the same region j left to junction j. The integration is evaluated over the common cross-sectional area of regions j and $j+1$

$$= \iint_{A(j,\ j+1)} \overline{e}(k_j,j) \cdot \overline{e}(k'_j,j)\ ds$$

$C.O.I.(k_{j+1}, k'_{j+1}, j)$ — Cross-overlaop integral of mode k_{j+1} to mode k'_{j+1} in the same region $j+1$ right to junction j. The integration is evaluated over the common cross-sectional area of regions j and $j+1$

$$= \iint_{A(j,\ j+1)} \overline{e}(k_{j+1}, j+1) \cdot \overline{e}(k'_{j+1}, j+1)\ ds$$

|	
cs (j)	Cross-sectional area of region j
d (k,j)	Distance of the location of excited source mode k from input plane of region j
$\overline{e}$ (k,j)	Vector mode function of mode k region j transverse $\vec{E}$ field pattern
$\overline{e}^{TM}$ (k$_j$,j)	TM mode vector function of mode k$_j$ region j transverse $\vec{E}$ field pattern
$\overline{e}^{TE}$ (k$_j$,j)	TE mode vector function of mode k$_j$ region j transverse $\vec{E}$ field pattern
$\overline{e}^{TEM}$ (k$_j$,j)	TEM mode vector function of mode k$_j$ region j transverse $\vec{E}$ and $\vec{H}$ fields pattern
$\vec{E}_t$ (j), $\vec{E}_t'$ (j)	Total input and output transverse electric fields representation of guide j
E_r (k$_j$, j, r)	The radial dependent part of the radial electric field magnitude of mode k$_j$ in region j
E_ψ (k$_j$, j, r)	The radial dependent part of the azimuthal electric field magnitude of mode k$_j$ in region j
F (k,j)	Forward mode k of $\vec{E}$ field magnitude defined at input plane of region j
F' (k,j)	Forward mode k of $\vec{E}$ field magnitude defined at output plane of region j (= F (k,j) · G$_f$ (k,j))
F$_s$ (k,j)	Component of forward mode k of $\vec{E}$ field magnitude defined at distance d (k,j) from the input plane of region j due to source terms
F$_s'$ (k,j)	Component of forward mode k of $\vec{E}$ field magnitude defined at the output plane of region j due to source terms = F$_s$ (k,j) · G$_{fs}$ (k,j)

G_b (k,j)   Backward propagation term of mode k region j
$= \exp\{+\gamma\ (k,j)\cdot \ell\ (j)\}$

G_f (k,j)   Forward propagation term of mode k region j
$= \exp\{-\gamma\ (k,j)\cdot \ell\ (j)\}$

G_{bs} (k,j)   Backward propagation term of source mode k at distance d (k,j) from the input plane of region j
$= \exp\{-\gamma\ (k,j)\cdot d\ (k,j)\}$

G_{fs} (k,j)   Forward propagation term of source mode k at distance d (k,j) from the input plane of region j
$= \exp\{-\gamma\ (k,j)\cdot [\ell\ (j) - d\ (k,j)]\}$

$\overline{h}$ (k,j)   Vector mode function of mode k region j transverse $\vec{H}$ field pattern

$\vec{H}_t$ (j), $\vec{H}_t'$ (j)   Total input and output transverse magnetic fields representation of guide j

J   Number of regions

j   Index number of jth region

(k,j)   Index number of kth mode in region j

ℓ (j)   Length of region j

m   Azimuthal mode number

n   Radial mode number

N (j), N (j+1)   Total number of modes considered in regions j and j+1

O.I. (k_j, k_{j+1}, j)   Overlap integral of mode k_j in region j left to junction j to mode k_{j+1} in region j+1 right to junction j. The integration is evaluated over the common cross-sectional area of regions j and j+1

$$= \iint_{A(j,\ j+1)} \overline{e}\ (k_j,\ j)\cdot \overline{e}\ (k_{j+1},\ j+1)\ ds$$

100

$P(k_j, k_{j+1}, \psi)$ Integral of the product of the polarization

terms $= \int_0^{2\pi} P_r(k_j, k_{j+1}, \psi) \cdot d\psi = \int_0^{2\pi}$

$P_\psi(k_j, k_{j+1}, \psi) \cdot d\psi$

$P_r(k_j, k_{j+1}, \psi)$ Product of the polarization terms $= p(k_j, j, \psi) \cdot p(k_{j+1}, j+1, \psi)$

$P_\psi(k_j, k_{j+1}, \psi)$ Product of the polarization terms $= q(k_j, j, \psi) \cdot q(k_{j+1}, j+1, \psi)$

$p(k_j, j, \psi)$ Polarization term of the azimuthal dependent part of mode k_j in region j for radial electric field component

$q(k_j, j, \psi)$ Polarization term of the azimuthal dependent part of mode k_j in region j for azimuthal electric field component

VRI (k,j) Input voltage reflection coefficient of mode k in region j (only valid for the first region)

VRO (k,j) Output voltage reflection coefficient of mode k in region j (only valid for the last region)

x_{lower}, x_{upper} Lower and upper limits of horizontal end points

$y(x)_{lower}, y(x)_{upper}$ Lower and upper limits of vertical end points

$Z(k, j)$ Mode k region j wave impedance

Δx x-shift between waveguide centers at the junction

Δy y-shift between waveguide centers at the junction

$\Delta \theta$ Angular rotation of the secondary axes relative to main frame axes performed after Δx and Δy

$\gamma(k, j)$ Propagation constant of mode k region j

END

5-87

DTIC